A STUDY OF α/ß BOUNDARIES IN A Zr-2.5 wt% Nb ALLOY

By

WENZHENG ZHANG, M.E.

A Thesis

Submitted to the School of Graduate Studies

in Partial Fulfilment of the Requirements

for the Degree

Doctor of Philosophy

McMaster University

A STUDY OF α/ß BOUNDARIES IN A Zr-2.5 wt% Nb ALLOY

DOCTOR OF PHILOSOPHY (1991) McMASTER UNIVERSITY

(Materials Science and Engineering) Hamilton, Ontario

TITLE: A Study of α/ß Boundaries in a Zr-2.5 wt% Nb Alloy

AUTHOR: Wenzheng Zhang M.E. (Beijing University of Iron and Steel Technology)

SUPERVISOR: Professor G.R. Purdy

NUMBER OF PAGES: xv, 198

ABSTRACT

The crystallography and the interfacial structure of interphase boundaries in a Zr-2.5 wt% Nb alloy have been studied by transmission electron microscopy (TEM), and the results compared with the predictions of a model developed in this work. The α phase (HCP), when precipitated from ß (BCC), usually forms as intragranular plates. The habit plane of an α plate is characterized by the regularly spaced dislocations, parallel to the long axis of the α plate. These dislocations, about 10nm apart, have a Burgers vector [0 1 0] with respect to ß phase. The orientation relationship between α and ß phases was found to deviate slightly from the ideal Burgers orientation relationship. Based on the O-lattice and invariant line analysis a geometrical model has been further developed. The cell structure of O-lattice, which is the key information in predicting the configuration of the interfacial dislocations, has been constructed by a simple calculation made in reciprocal space of the O-lattice. This is expected to improve the general application of the existing O-lattice model. The plane of the least lattice mismatch, determined by the O-lattice plane of the smallest spacing, is consistent

with the observed habit plane. The optimum orientation relationship suggested based on the analysis of mismatch in the habit plane is shown to deviate slightly from the Burgers orientation, which is supported by experimental evidence. The analysis also indicated that the misfit in the habit plane could be accommodated completely by a set of $[0\ 1\ 0]_{\beta}$ dislocations of ~10nm in spacing, lying along the invariant line, in agreement with the experimental observations.

ACKNOWLEDGMENTS

I would like to express my sincere gratitude to my supervisor Dr. G.R. Purdy, for his continuing guidance, support, and encouragement throughout the project, which made this thesis possible.

I am grateful to the technical staff of Department of Materials Science and Engineering and the Institute for Materials Research for the technical assistance, in particular to Mr. F. Pearson, and Mr J.M. Hudak in electron microscope lab. The gratitude is extended to my fellow graduate students, especially to Ms. G. Julien and Ms. J. Luo and Mr. M. Dynna, in Department of Materials Science and Engineering for friendly help, and to Dr. H.P. Dai, Mr. W.G. Chen, and Mr. X.P. Huang in Department of Electrical Engineering for useful discussions on linear algebra.

I also wish to express my thanks, in particular to:

Dr. H.I. Aaronson of Carnegie-Mellon University, for his recommendation, which introduced this precious study opportunity to me.

Dr. Weatherly, for valuable comments during the course

of this investigation and criticism of the manuscript.

Dr. Z.S. Basinski, for stimulating discussions, and critical review of the manuscript. The additional review by Mrs. Basinski is highly appreciated.

Dr. Y.P. Lin of Bell Northern Research, for excellent advice about techniques of TEM and careful review of the main part of the manuscript.

Dr. V. Perovic of Ontario Hydro Research, for providing the alloy and making very helpful suggestions regarding experimental work.

Dr. A. Perovic, for kindly offering the constant help in various aspects, especially providing proof read most of the manuscript.

Dr. C.P. Luo of South China Institute of Technology, for useful suggestion in the initial stage of this program.

Mrs. P. Monger and Ms. M. Van der Wel, for the assistance in computer technicalities.

I acknowledge, with thanks, the financial support of the University scholarship of C.W. Sherman Graduate Scholarship, and scholarship provided by the Department of Materials Science and Engineering.

I am deeply indebted to my parents, my teachers, and

many people of my country, for their encouragement and support that has enabled me to pursue graduate study at McMaster.

Finally I wish to thank my husband, Baogang, for his love, understanding, help, and encouragement over the course of this study.

TABLE OF CONTENTS

APPENDIX

LIST OF FIGURES

LIST OF TABLES

CHAPTER 1

INTRODUCTION

The structure of interfaces formed by solid state phase transformations is a subject of considerable experimental and theoretical interest, for the ultimate goal of this subject is a full understanding of the nature of phase transformations and microstructure-property relationships. The interfaces between precipitates and matrix have been of particular interest, since they are the dominant interfaces in many important engineering alloys and their formation reactions can be controlled with relative ease. While a large number of investigations has concerned interfaces between FCC and BCC crystals because of the technological importance of steels and brasses, interest has been recently extended to the interfaces between HCP and BCC phases due to the emergence of Ti and Zr based alloys as engineering materials. Recently, some interesting structures of HCP/BCC boundaries were observed in a Zr-2.5 wt% Nb alloy (Perovic and Weatherly, 1988). The principal interfacial dislocations were shown to lie along an invariant line. A comprehensive investigation was felt essential to further rationalize these observations. For this purpose, a Zr-2.5 wt% Nb alloy was chosen for study.

The geometrical approach has been an essential step in the analysis of the interfacial structure in terms of misfit in a boundary. This has led to a measure of success in studies of grain boundaries. Gleiter (1983) noted that geometrical models were also applicable to interfaces between crystals of different structure, but of the same type of bonding. The interfaces in the present study belong to such a case. Therefore, a geometrical approach was adopted in this work.

Among various geometrical models, the O-lattice theory developed by Bollmann (1970) is the most general. The O-lattice theory, together with other geometrical models, is reviewed in Chapter 2. Essentially, the O-lattice procedure predicts the possible configuration and Burgers vectors of interfacial dislocations within an arbitrary boundary. It therefore provides a very useful device for the investigation of semicoherent boundaries. To predict the configuration of dislocations it is necessary to construct the cell structure in an O-lattice, since the lines of intersection between the boundary and the cell walls are interpreted as dislocation lines.

However, except for simple cases of grain boundaries and a few cases of interphase boundaries (Bollmann, 1974a and Solenthaler, 1988), cell structures have been widely adopted in an oversimplified form, perhaps because there was no simple

method available to solve for the cell structure. Thus, as indicated by Ecob and Ralph (1981), the description of interfacial dislocations becomes a function of the initial choice of the crystal lattice unit cell. Nevertheless, the true cell structure as defined by Bollmann (1970) should not depend on such a choice. In order to describe dislocations properly it is necessary to clarify the physical representations of lines produced by different descriptions, and to develop a simple method to solve the cell structure. This is provided in Chapter 3, where the reciprocal space of the O-lattice is explored.

Dahmen and Westmacott (1981) have noted the important role of invariant lines in precipitation transformations. Since then, invariant lines have been claimed to exist in many precipitation systems including the alloy studied in the present work (Perovic and Weatherly, 1988). The concept of the invariant line would be useful for understanding the orientation relationship between precipitates and matrix, and the direction of interfacial dislocation lines. When dealing with the Burgers vectors of the dislocations and the habit plane, additional concepts must be involved. Generally, invariant lines are not equivalent to a line O-lattice (O-line). Bollmann (1970) has suggested a projection translation to deal with such a case. It was realized in this work that a certain amount of tolerance should be given in calculations

due to the uncertainty or the true scattering in experimental measurements. Specifically, the tolerance was applied in two aspects in this study: firstly, to allow for small, physically insignificant, departures from the true invariance, and secondly, to let orientation relationship vary within a narrow range. Corresponding to these two aspects, ideas of effective invariant line and optimum orientation relationship are proposed in Chapter 3. In addition, the properties of invariant line strain are summarized, and on this basis the interfacial misfit is analyzed.

Chapter 4 describes the experimental procedures. Experimental observations are presented in Chapter 5. The results are discussed in Chapter 6 together with the predictions of the geometrical model. Agreements are reached on the orientation relationship, the geometry of the habit plane and the structure in the habit plane, including the direction, the spacing, and the Burgers vector of the dislocations. The conclusions are presented in Chapter 7. Further work is needed for a better understanding of the interfacial structures in boundaries other than the habit plane.

CHAPTER 2

LITERATURE REVIEW

—— Geometrical Approaches to Interface Structures

Two crystals meeting at a boundary can have differences in orientation, structure, composition, and types of bonding. Geometrical models of interfacial structure only take into account the differences in orientation and structure, and assume that the interfacial configuration having the lowest free energy is represented by that having the "best" geometrical fit. The predictive power of geometrical models is therefore limited to cases in which the interfacial energy varies monotonically with the degree of geometrical fit. In a review on geometric criteria for low interfacial energy, Sutton and Balluffi (1987) indicated that various best-fit geometrical models could apply for certain types of interfaces, but there is no general geometrical criterion valid for all types of interfaces. Gleiter (1983) noted that geometrical models were successful when applied to interfaces between crystals of the same type of bonding, but

controversial results were obtained for phase boundaries between crystals of different types of bonding. For the former cases, the best-fit geometrical criterion can then serve as a useful guide to understand the structure of the interphase boundaries.

2.1 Dislocation Model for the Low Angle Grain Boundaries

A dislocation model for a "surface of misfit" was introduced by Burgers (1939). For a symmetrical low angle tilt boundary, the spacing of the dislocation lines in the boundary is

$$h = \frac{|\mathbf{b}|}{\theta} \qquad (2.1)$$

where θ is the angle between the two grains, and $\mathbf{b}$ is the Burgers vector.

The hypothesis of dislocations at low angle grain boundaries has been confirmed by the lattice image though the detailed description of the boundary structure could be more complicated than that predicted by this simple model (for example, see Krakow and Smith 1987).

2.2 Frank's Formula for the General Grain Boundaries

Using an extension of this simple grain boundary model, Frank (1950) studied a pair of like lattices in arbitrary orientation, by rotating through appropriate angles α_1 and α_2 about axes $\mathbf{l}_1$ and $\mathbf{l}_2$ respectively. The expression for total Burgers vector, $\mathbf{b}$, of dislocations lying in the boundary and crossed by any vector $\mathbf{r}$ in the boundary is given by the following formula:

$$\begin{aligned}\mathbf{b} = \mathbf{r} \times (\mathbf{l}_1 \sin\alpha_1 - \mathbf{l}_2 \sin\alpha_2) - \mathbf{r} (\cos\alpha_1 - \cos\alpha_2) \\ - \mathbf{l}_1 (1 - \cos\alpha_1) (\mathbf{l}_1 \cdot \mathbf{r}) \\ + \mathbf{l}_2 (1 - \cos\alpha_2) (\mathbf{l}_2 \cdot \mathbf{r}) \end{aligned} \qquad (2.2)$$

2.3 Dislocation Theory of Interfaces

Bilby et al. (1964) further developed the analysis of Frank and proposed a general theory of surface dislocations, which they expressed in a matrix notation. The net Burgers vector, $\mathfrak{b}$, of dislocations which are cut by an arbitrary vector $\mathbf{r}$ in a general grain boundary separating the lattice (+) and lattice (-) is

$$\mathbf{b} = (\mathbf{R}^{-1} - \mathbf{I})\mathbf{r} \qquad (2.3)$$

where $\mathbf{R}$ is a matrix of the rotation, by which the (+) lattice is generated from the (-) reference lattice, and $\mathbf{I}$ is a (3 ×

3) unit matrix (**I** will be taken to have the same meaning in the rest of this thesis). Equations (2.2) and (2.3) are actually equivalent expressions.

For general boundaries the resultant Burgers vector can be expressed as:

$$\mathbf{b} = (\mathbf{A}^{-1} - \mathbf{I})\mathbf{r} \qquad (2.4)$$

where **A** is the deformation which transforms the reference lattice (+) from the lattice (-).

Expression (2.4) has become the basic formula for the further study of the geometry of interfacial dislocations. Knowles and Smith (1982) applied this formula to FCC/BCC interfaces. Without considering the accommodation of misfit by discrete dislocations, they were able to explain the preferred FCC/BCC interfaces found in the Cu-Cr system (Hall, et al. 1972) on the basis of the minimum or near-minimum net Burgers-vector contents.

2.4 Epitaxial Dislocations

Starting from the theory of surface dislocations, Sargent and Purdy (1975) analyzed epitaxial interfaces with the Burgers vectors specified as the lattice translation

vectors of either the matrix or the particle. If the misfit at the interface is accommodated by a network of several sets of dislocations, expression (2.4) becomes:

$$\mathbf{b} = \sum_i (\mathbf{N}_i \cdot \mathbf{r})\mathbf{b}_i = (\mathbf{A}^{-1} - \mathbf{I})\mathbf{r}, \qquad (2.5)$$

where $\mathbf{b}_i$ is the Burgers vector of the ith set of dislocations and $\mathbf{N}_i$ is defined as a vector lying in the interface, normal to the ith set of dislocation lines, given in the form

$$\mathbf{N}_i = \frac{\mathbf{n} \times \boldsymbol{\delta}_i}{d_i} , \qquad (2.6)$$

where $\mathbf{n}$ is a unit vector normal to the boundary, $\boldsymbol{\delta}_i$ and d_i are respectively the line vector and the spacing of the dislocations with Burgers vector $\mathbf{b}_i$.

Knowles (1982) modified the above formulae by introducing a reciprocal Burgers vector notation. In his analysis the (+) lattice was chosen as the reference lattice, and equation (2.5) was written in the form

$$\mathbf{b} = \sum_i (\mathbf{N}_i \cdot \mathbf{r})\mathbf{b}_i = (\mathbf{I} - \mathbf{A}^{-1})\mathbf{r}, \qquad (2.7)$$

where $\mathbf{A}$ is the deformation carrying the reference lattice (+) into the (-) lattice. The boundaries were assumed to consist of three sets of dislocations with non-coplanar Burgers vectors, b_i, (i=1,2,3). With a matrix $\mathbf{T}$ defined as:

$$\mathbf{T} = \mathbf{I} - \mathbf{A}^{-1} \tag{2.8}$$

Knowles gave the following description of the dislocation geometry of the interface. The spacing of dislocations with Burgers vector $\mathbf{b}_i$ is

$$d_i = \frac{1}{|\mathbf{T}^T\mathbf{b}_i^* \times \mathbf{n}|} \tag{2.9a}$$

where $\mathbf{b}_i^*$ is a reciprocal Burgers vector defined by:

$$\mathbf{b}_i^* = \frac{\mathbf{b}_j \times \mathbf{b}_k}{\mathbf{b}_i \cdot \mathbf{b}_j \times \mathbf{b}_k}\ , \tag{2.9b}$$

$\mathbf{b}_j^*$ and $\mathbf{b}_k^*$ can be defined in a similar way, the superscript T denotes a transposition and will be taken to have the same meaning in the rest of this thesis. The line vector of the dislocations with Burgers vector $\mathbf{b}_i$ becomes

$$\boldsymbol{\delta}_i \ /\!/\ \mathbf{T}^T\mathbf{b}_i^* \times \mathbf{n}. \tag{2.10}$$

With this method of calculation of the dislocation geometry, Knowles (1982) attempted to predict the structure of the interfaces of all orientations, instead of simply applying the analysis to epitaxial interfaces of a particular orientation as originally suggested by Sargent and Purdy (1975).

2.5 O-Lattice Theory of Crystalline Interfaces

Bollmann (1970) developed a general theory of interface dislocations by introducing the idea of an O-lattice. The idea of O-lattice provides a very important device for study of interfacial structures. On this basis, periodic misfit instead of the net Burgers vector of total dislocations can be analyzed. Due to its close relevance to the present study, Bollmann's O-lattice theory will be explained in somewhat more detail in the balance of this Section.

2.5.1 O-lattice Concept

An O-lattice is a fictitious three dimensional lattice. The lattice points (O-points) are the positions of the best matching of two interpenetrating point lattices (lattice 1 and lattice 2). (A two-dimension O-lattice is provided in Figure 3.2a and c). It has been shown that each of these O-points is an origin for transformation between lattices 1 and 2, which is therefore called O(origin)-point. At an O-point the lattices 1 and 2 have the same internal coordinates, which can be expressed as:

$$\mathbf{A}\,\mathbf{x}_1 = \mathbf{x}_1 + \mathbf{b}_1 = \mathbf{X}^O, \qquad (2.11)$$

where $\mathbf{X}^O$ is an O-lattice vector which defines an O-point, and $\mathbf{A}$ is the transformation matrix, $\mathbf{b}_1$ is a lattice translation vector in the reference lattice 1, and $\mathbf{x}_1$ can be any vector in lattice 1. Eliminating $\mathbf{x}_1$ from (2.11) gives the basic equation for solving the O-lattice:

$$\mathbf{b}_1 = (\mathbf{I} - \mathbf{A}^{-1})\ \mathbf{X}^O, \qquad (2.12a)$$

or

$$\mathbf{b}_1 = \mathbf{T}\ \mathbf{X}^O, \qquad (2.12b)$$

where $\mathbf{T}$ is defined as

$$\mathbf{T} = \mathbf{I} - \mathbf{A}^{-1}. \qquad (2.13)$$

The basic equation for O-lattice calculations has a form similar to that in the continuum theory of dislocations (referred to equations (2.4) or (2.7)), but now the Burgers vector is confined to be a lattice translation vector. The O-vectors defined by equation (2.12) are not necessarily relatively short lattice translation vectors in O-lattice. $\mathbf{b}_1$ and $\mathbf{X}^O$ still keep the same meaning as in the continuum theory of interfacial dislocations, i.e. $\mathbf{b}_1$ is the displacement between the lattices 1 and 2 in the distance from the origin point to the O-point defined by $\mathbf{X}^O$.

Equation (2.12) has three types of solutions, depending on the rank of **T**. The solutions, or the 'O-elements' are O-points, O-lines, and O-planes respectively corresponding to the rank = 3, 2, 1. Only the most general case, rank = 3, will be reviewed in this Section; the case rank = 2 will be reviewed Section 2.8.

2.5.2 The Construction of O-Lattice Cell Structure

In the O-lattice, the region where lattices 1 and 2 match badly forms a cell structure, in which each O-point is enclosed by a cell. The cell wall can be defined in such a way that the relative displacement within a given cell with respect to the O-point inside the cell is smaller than it is with respect to any other O-points. In the faces of cells, i.e. the locations of the worst matching, the relative displacement has the same value with respect to the two closest O-points on the opposite sides of the cell wall.

Thus, the location of the cell wall should satisfy the following condition

$$|\mathbf{b}|^2 - |\mathbf{b} - \mathbf{b}_1|^2 = 0 \qquad (2.14)$$

or

$$(\mathbf{b}_1^T\ \mathbf{G}\ \mathbf{T})\mathbf{x} - (1/2)(\mathbf{b}_1^T\ \mathbf{G}\ \mathbf{b}_1) = 0$$

where G is the metric tensor, $\mathbf{b}_1$ is the displacement between the two closest O-points separated by the cell wall; **b** is the displacement defined as

$$\mathbf{b} = \mathbf{x} - \mathbf{A}^{-1}\mathbf{x}, \qquad (2.15)$$

and **x** is a vector variable. The locus of points **x** defines the surface of the cell wall corresponding to the displacement $\mathbf{b}_1$. No simple method has been suggested to solve equation (2.14), except for one particular solution given as $\mathbf{x} = 1/2\ \mathbf{X}^{O}$. In general, the orientation of the cell wall depends on the choice of the reference lattice.

2.5.3 The Dislocation Description of Interfacial Structures

If the O-lattice cell is significantly large compared with the unit cell in the reference lattice, the intersections of the boundary between the two lattices with the cell walls are considered as the starting point for atomic relaxation. Each line of the intersection can be interpreted as a dislocation, into which the lattice misfits are concentrated. The Burgers vector of the dislocation is the displacement associated with the cell wall intersected by the boundary at the dislocation.

Given the information of the orientation relationship between the lattices, the interfacial orientation, and the lattice parameters of both lattices, a dislocation description of interfacial structure can be predicted by this model. The models reviewed in the last Section require additional information, either the line directions or Burgers vectors of the dislocations.

It is important to note that in applications of O-lattice theory (Bollmann and Nissen, 1968), the cell structure was not constructed as originally suggested. Instead, the cell structure was simplified to be the unit cell of the O-lattice which is defined by any three O-lattice vectors (defined in (2.12)). Such a simplification has been followed in other applications of O-lattice (see, for example, Hall et al. 1986). Although O-lattice cell structures have been illustrated in a few references (for example, see Bollmann 1974 (a), Solenthaler 1989), no details have been provided as to how these structures were constructed.

2.5.4 The Choice of Low Energy Interface

Bollmann (1974 b) suggested that a boundary of low energy should be oriented so as to pass through as many O-elements as possible. Consequently, the possible boundaries are considered to lie parallel to a face of the O-lattice unit

cell. Provided the bad-matching cell walls take the shape of the unit cell of the O-lattice, the boundary will be parallel to one of the cell walls, and hence it will consist of two sets of dislocations. In fact, this description in terms of a simplified cell structure provides the same geometry of interfacial dislocation as that suggested by Knowles' model (1982), shown in equations (2.9, 2.10).

Starting from this configuration of dislocations at the interface, Bollmann and Nissen (1968) introduced a geometrical parameter, P:

$$P = (|\mathbf{b}_1|/d_1)^2 + (|\mathbf{b}_2|/d_2)^2. \qquad (2.16)$$

where $\mathbf{b}_1$ and $\mathbf{b}_2$ are the Burgers vectors of the dislocations, and d_1 is defined by:

$$d_1 = |\mathbf{X}^O{}_1 \times \mathbf{X}^O{}_2/|\mathbf{X}^O{}_2|\ |, \qquad (2.17)$$

d_2 is given in similar form, and $\mathbf{X}^O{}_1$ and $\mathbf{X}^O{}_2$ are the O-lattice vectors associated with $\mathbf{b}_1$ and $\mathbf{b}_2$ respectively. A small value of P means good fit in the boundary, so it is assumed to be a rough indication of the boundary energy. Hence, an interface with minimum P is desired.

This prediction, however, as Ecob and Ralph (1981) pointed out, has considerable uncertainty as to the initial choice of the crystal lattice unit cell. Hall et al. (1986) further developed the above model by extending the choice of the unit cell of the reference lattice, e.g. the FCC lattice. O-lattice unit cells of different sizes and shapes were generated by combinations of three non-coplanar FCC lattice vectors of <1 1 0> family, and seven boundaries resulted from the cross product of each pair of the six O-lattice vectors. The most favoured interface was selected among the seven, using the minimum P criterion defined in equation (2.16).

However, the interface with the minimum P may not usually be the one containing the densest O-lattice points, which is also a criterion for a low energy boundary as noted in Section 2.5.4. Ecob and Ralph (1981) indicated that the optimum incoherent boundary (without relaxation to a dislocation structure), will pass through the maximum number of O-elements, while the optimum semi-coherent boundary (with dislocations taking up the misfit) will contain a minimum density of lines of intersection with the cell walls.

2.5.5 The Selection of Transformation Matrix A

The transformation matrix **A** depends on the orientation relationship of the two crystals. However, even for a given

orientation, as noted by Bilby et al. (1964), two grains can be generated by different rotations due to the symmetry of the crystal structure. Bollmann (1970) suggested that the matrix **A** in equation (2.12) should be selected as the transformation by which the nearest neighbours in both lattices are related. With such an **A**, the determinant $|\mathbf{I} - \mathbf{A}^{-1}|$, corresponding to the ratio of the volume of the unit cell of reference lattice to the O-lattice unit cell, has the smallest value.

In addition to the above consideration, there are other cases where the matrix **A** should be carefully selected, due to the choices of orientation relationships. One is the case of coincidence-site-lattice (CSL), which is to be reviewed in the next Section. Another is the case of an interphase boundary generated by a phase transformation or vapour deposition in such a manner that there is a fixed, or a narrow range of, orientation relationships between the phases. Many attempts have been made to predict such a kind of orientation relationship. For non-martensitic transformations, the favourable orientation relationships could be selected as the one with the minimum interfacial energy. In Bollmann and Nissen's work (1968), the orientation relationship was determined by the minimum value of the P parameter. Another well accepted energetic criterion for adoption of an orientation relationship is the presence of an invariant line between the phases (Dahmen, 1982). It was found that

conditions associated with the minimisation of geometrical parameters P (or R, a parameter similar to P and proposed by Ecob and Ralph (1981)), could be consistent with that corresponding to the presence of an invariant lines (Ecob, 1985).

2.6 CSL/DSC Lattice Model

A coincident site lattice (CSL) is constructed in a similar way to the O-lattice. It is a special type of O-lattice: each O-point is also a lattice point of both real lattices. A general O-lattice may consist fully, partially, or scarcely at all, of CSL points.

The boundary with the densest CSL before relaxation is assumed to be of low energy, corresponding to the cusps in the energy vs misorientation curve for the grain boundaries (Balluffi, et al. 1982). The bad-matching regions with a relatively short wavelength periodicity may not be pictured as crystal lattice dislocations, or primary dislocations termed by Bollmann (1970). The degree of fit for this periodic coherent boundary is evaluated differently from that for the semi-coherent boundaries, where the bad-matching regions are concentrated on the core of the primary dislocations. In this model, the regions of 'fit' are the patches where partial lattice matching across the boundary is achieved (Balluffi et

al., 1982). To conserve the pattern of 'fit', a network of dislocations is suggested, formed to compensate for the deviations from the high density CSL orientation. Such new networks are denoted as networks of secondary dislocations. The Burgers vectors of the secondary dislocations are defined within the framework of the "complete pattern shift lattice" or DSC-lattice* (Bollmann, 1970), since this lattice is composed of all translation vectors of lattice 2 with respect to lattice 1, which conserve the atomic pattern of the interpenetrating lattices. The secondary dislocations are related to the "O-lattice of second order" by a formula analogous to equation (2.12) (Bollmann, 1970). The transformation matrix in this formula depends on the deviation of the real orientation from the CSL orientation.

A large body of experimental evidence has been reported to confirm the secondary relaxations occurring at high-angle grain boundaries near coincidence orientations (see, for example, Mader et al., 1987). However, the two grains joined at a boundary generally tend to translate slightly with respect to each other, in order to allow the boundary to relax to a true minimum energy configuration. It has been shown by computer simulations of the atomic structure of grain boundaries that, in general, atoms do not occupy

---

* D stands for displacement, S for shift, and C for complete.

coincidence sites in the lowest energy structure (Pond and Vitek, 1977).

The CSL/DSC model has also been applied to interphase boundaries. An O-lattice rarely contains CSL points if the lattices 1 and 2 have different crystal structures. Bonnet and Durand (1975) introduced the concept of the near-coincidence lattice. The lattice is formed by identifying a pair of cells in the lattices 1 and 2, which almost match each other in shape and size. This model is especially useful for studying interfaces, where the lattice mismatch is so large that the primary relaxation has no physical reality (see, for example, Knowles and Goodhew, 1983). The model has been applied to interfaces, for which the observed line defect structure cannot be rationalized on the basis of dislocations with lattice vectors of either adjoining lattice (see, for example, Forwood and Clarebrough, 1989). Due to the lack of uniqueness in defining the near-coincidence-lattice cells as the reference state the predictions of this model can be ambiguous even when taken in conjunction with the experimental results (Forwood and Clarebrough, 1989).

2.7 Plane Matching Model

The plane matching model was introduced to explain the line structures of grain boundaries with misorientations far

from coincidence relationships (Pumphrey, 1972). It has been suggested that the periodic lines observed in a grain boundary result from the mismatch of the low index atom planes across the boundary, provided at least one set of such planes in each grain adjoining the boundary is nearly parallel. This suggestion is supported by the systematic study of specially prepared plane matching bicrystals with controlled misorientations (Schindler et al., 1979). As pointed out by Schindler et al. (1979), there is considerable evidence for a one dimensional relaxation, i.e. the relaxation which improves the degree of alignment of lattice planes.

The plane matching model has been used to study interphase boundaries. The straight parallel lines observed in FCC/BCC interphase boundaries in brass were interpreted as the dislocations accommodating the mismatch of the {1 1 1} planes of FCC lattice with their counterparts in the BCC lattice, namely the {1 1 0} planes (Bäro and Gleiter, 1973). The same approach has been applied by Luo and Weatherly (1988) in the study of FCC/BCC interfaces in a Ni-Cr alloy. They found that the contrast of the dislocations with various reflections and their spacing could be better explained, if the Burgers vector of the dislocation was chosen to be normal to the close-packed conjugate planes and to have a magnitude equal to the plane spacing, than if it is assumed to be a lattice translation vector. Bollmann (1974 a) considered the plane matching model

to be a one-dimensional approximation to a three-dimensional problem. Using this approximation, Bollmann (1974 a) derived the geometry of the line structure and showed that it was equivalent to the result of the plane matching model (Pumphrey, 1972).

2.8 Interfaces Containing Invariant Lines

Based on a literature survey on the orientation relationships observed in many precipitation systems, Dahmen (1982) hypothesized that the precipitate and matrix tend to be related by an invariant line strain whereby the precipitate dimensions tend to be inverse to the directional mismatch and the habit plane of the precipitate contains the invariant line. With this invariant line analysis, Dahmen (1982) was able to rationalize the orientation relations and the morphologies of precipitates in some BCC/FCC and BCC/HCP systems.

The necessary condition for an invariant line strain is that one principal strain should be either zero, or have the opposite sign from the other two (Christian, 1975). Under this condition, there will be a cone of vectors which remain unchanged in length (unextended cone). Any vector in the cone can be made an invariant line by adding a suitable rotation.

There could be many ways of producing invariant lines as well as many choices of invariant lines for the same transformation system (Dahmen and Westmacott, 1981). A simple way to obtain the invariant line is to consider it in two dimensions; namely, through a small rotation around the normal to the close-packed planes from the principal distortion (Dahmen, 1982, and Aaronson et al., 1983). The magnitude of the rotation depends on the lattice parameter ratio. For those systems deviating from the parallelism of close-packed planes, Dahmen (1982) suggested another rotation axis to be used, which may lead to the smallest total rotation. Taking the loss of coherency into account, Dahmen and Westmacott (1981) postulated that the invariant line of a semicoherent precipitate is determined by the intersection of the cone of unextended lines with the slip planes of the matrix.

Luo and Weatherly (1987) noted that the observed invariant line may not lie in the close-packed planes as would be predicted by the two-dimensional model. They have developed a method to solve the invariant line problem in three-dimensions. The potential invariant lines can be obtained by intersecting the initial cone of the unextended lines with the final (or transformed) cone of unextended lines. The intersection is determined from the rotation due to the observed (or assumed) orientation relationship. A true invariant line is obtained if the intersection line is also

unrotated. The habit plane is determined by the invariant line and an unrotated line as suggested by Ryder and Pitsch (1966). This three-dimensional invariant line model was compared with the O-lattice method further developed by Hall et al. (1986). The habit plane and the growth direction of precipitate predicted by both theories were in good agreement with their experimental observations (Luo and Weatherly, 1987), although the principles for choosing the habit plane are different in the two approaches. Despite the success of the invariant line model from continuum approach in rationalizing several observations, the model sheds no light on the nature of the strain field associated with the discrete defect lines (Luo and Weatherly, 1988).

A true invariant line can be a solution of the O-lattice (equation 1.12), when the rank of $(\mathbf{I} - \mathbf{A}^{-1})$ is two. Bollmann (1970) has shown how to solve this two dimensional O-lattice problem mathematically. It is known from linear algebraic theory that we cannot always find solutions to equation (2.12) if the rank of $(\mathbf{I} - \mathbf{A}^{-1})$ is two. In order to solve the equation, $\mathbf{b}_1$ must be confined to a plane (b-subspace). Such b-subspace may not contain sufficient useful Burgers vectors. Bollmann assumed the Burgers vectors in the reference lattice to be projected onto the b-subspace. Finally the O-lattice (O-lines) may be solved by a complicated non-homogeneous transformation.

2.9 Structural Ledge Model

The idea of structural ledges was proposed by Hall et al. (1972) to solve the problem of the poor lattice matching of the two close packed planes from lattices 1 and 2, which are in near parallel orientation. In this model, the two planes are overlapped so as to build a two dimensional O-lattice. Due to a shift of the lattice planes in the sequence of both lattices 1 and 2, there is a relative shift with respect to each O-lattice plane in three dimensions. The boundary was supposed to be stepped so that it would pass through as many good matching patches as possible. These steps on the boundary were termed "structural ledges", and were considered to be composed of one, two, or three layers of atoms (Rigsbee and Aaronson, 1979). According to this model, the boundary will contain dense O-points disregarding what Burgers vectors may associated with the assumed line defects separating the O-points; this aspect of the model has been criticized by Ecob and Ralph (1981).

In his recent work, Furuhara (1989) further developed the structural ledge model in a study of HCP/BCC interfaces. A graphical technique was used to search for the near-coherent patches not only on the single pair of parallel close-packed planes, but also on other parallel conjugate planes from the two lattices. As suggested by Dahmen (1987), the structural

ledges were chosen to step down along the invariant line, so that another set of misfit dislocations at the interface can be eliminated. In addition, the misfit dislocations in this model were constructed according to the simplified O-lattice model (Bollmann and Nissen, 1968) to avoid the drawback discussed earlier in defining the Burgers vectors associated with the defects. The broad interface predicted by the modified structural ledge model has been shown to be close to the experimental measurements in a Ti-Cr alloy.

CHAPTER 3

AN O-LATTICE CALCULATION FOR INTERFACIAL STRUCTURES

The O-lattice concept suggested by Bollmann (1970) is adopted to assess the three-dimensional mismatch between two crystals. In this Chapter, a model will be developed as extension of the O-lattice procedure. The main modification is in the following aspects:

Firstly, a method for solving the O-lattice cell structure will be provided. An analysis will also be made of the physical representation of the planes corresponding to the faces of the unit cell of the O-lattice, which has often been taken as a simplified cell of "poor matching". The physical difference between the faces of these unit cells and the real cells will therefore be clarified.

Secondly, the habit plane is defined as the smallest-spacing O-lattice plane which is related to a close-packed plane of reference lattice. It will be shown that this plane

is defined in reciprocal space by a simple form and can be measured directly in diffraction patterns.

Thirdly, by introducing the idea of an effective invariant line, the O-lattice theory can be applied, (with the rank of **T** kept to three), to interfaces between two lattices which are related by the invariant line strain. Based on the analysis of the mismatch in the habit plane, it is found that the plausible orientation relationships will correspond to the existence of at least a one-dimensional O-lattice, i.e. an O-line, in an invariant line strain transformation.

Finally, the criterion for the formation of the dislocations corresponding to the lines of intersection of the O-lattice cell wall with a boundary is judged by the spacing of these lines rather than the ratio of the volume of the unit cell of the O-lattice to that of the reference lattice as suggested by Bollmann (1970).

3.1 Basic Ideas

According to the O-lattice model (Bollmann 1970), the configuration of mismatch in an interface of any orientation can be provided by the O-lattice calculation. Such a configuration is regarded as a starting point for analyzing the interfacial structures. It is a purely geometrical

approach, and has some limitations. The following assumptions are implicit in the calculation:

(1) The orientation relationship between the precipitate and the matrix is governed predominantly by minimizing the interfacial energy in the system.

(2) The best match between the two lattices is realized in the habit plane, which is the major part of the boundary connecting the precipitate and the matrix. The habit plane represents a minimum interfacial energy state and has a fixed orientation.

(3) When the periodicity of the misfit strain in an interface is considerably larger than the atomic spacing, the strain will be highly localized and will be taken up by discrete dislocations.

(4) The locations of the dislocations are centred at the region of the poorest matching before relaxation. The misfit dislocations may be associated with steps.

The precipitate system of interest in the present study is a Zr-2.5 wt% Nb alloy (for reasons see Chapter 4). On cooling from high temperatures, a HCP structured phase, α, is precipitated from a ß phase having a BCC structure. This

transformation can be written as:

$$\mathbf{x}_\alpha = \mathbf{A}\ \mathbf{x}_\beta, \qquad (3.1)$$

where $\mathbf{x}_\alpha$ and $\mathbf{x}_\beta$ are any vectors in the HCP and BCC structures, respectively. In fact the transformation of BCC into HCP involves a change of lattice from BCC to simple hexagonal. Take BCC as the reference lattice. Based on the O-lattice theory, an O-point is defined by equation:

$$\mathbf{b}_\beta = (\mathbf{I} - \mathbf{A}^{-1})\ \mathbf{X}^0, \qquad (3.2a)$$

or

$$\mathbf{b}_\beta = \mathbf{T}\ \mathbf{X}^0, \qquad (3.2b)$$

where $\mathbf{T}$ is defined as

$$\mathbf{T} = \mathbf{I} - \mathbf{A}^{-1}. \qquad (3.3)$$

Strictly speaking, $\mathbf{X}^0$ is an O-lattice vector which defines an O-point, and then $\mathbf{b}_\beta$, should be a BCC lattice translation vector which is correlated to a translation vector in the hexagonal lattice. However, according to this definition some of $\mathbf{b}_\beta$ (larger than Burgers vectors of BCC) are not the primitive lattice vectors, due to the corresponding large translation vectors in hexagonal lattice (refer to Figure 3.3). It is noted that the BCC structure tends to have a one-

to-one atomic correspondence with respect to HCP structure, for there are two atoms associated with each hexagonal lattice point in the HCP structure. Since we are more interested in the misfit between atoms than that between lattices, an alternative choice is to define $\mathbf{b}_\beta$ as a primitive translation vector in BCC lattice. Then an $\mathbf{X}^0$ defines a point of the best atomic matching, but may not define the point of another Origin though we may still call it an O-point for convenience*. With such a choice, $\mathbf{X}^0$ is an O-lattice vector, but it may not be an O-lattice translation vector. This is because the vector, $\mathbf{b}_\alpha$, correlated to the $\mathbf{b}_\beta$, may not be a translation vector in the hexagonal lattice. Generally, if there is an atom in the origin, then $2\mathbf{b}_\alpha$ will define another atom, but $\mathbf{b}_\alpha$ may not define one. Due to the one-to-one correspondence of atoms in the two structure, we could assume that a small shift of atoms, which is possible in a interface, may bring an atom to the position defined by $\mathbf{b}_\alpha$. Consequently, the O-lattice (or pseudo-O-lattice) defined in (3.2) may provide the periodicity of the misfit between α and ß. Therefore, $\mathbf{b}_\beta$ will be defined as the primitive vector. For convenience, $\mathbf{b}_\beta$ is given by one of the column vectors in the following expression:**

---

* Because the same equation is used (3.2 vs 2.12), the formulae developed in this Chapter do not lose their generality.

** Each vector in (3.4) corresponds to a face of the Wigner-Seitz cell of BCC lattice.

$$[\mathbf{b}_{B1}\cdots\mathbf{b}_{B7}] = a_B \begin{bmatrix} \frac{1}{2} & \frac{1}{2} & \frac{1}{2} & -\frac{1}{2} & 1 & 0 & 0 \\ \frac{1}{2} & \frac{1}{2} & -\frac{1}{2} & \frac{1}{2} & 0 & 1 & 0 \\ \frac{1}{2} & -\frac{1}{2} & \frac{1}{2} & \frac{1}{2} & 0 & 0 & 1 \end{bmatrix}, \qquad (3.4)$$

where a_B is the lattice parameter of the BCC phase.

3.2 Mismatch of Lattice Points

Bollmann (1970) defined the regions of the poorest matching as cell walls, due to the resemblance of these regions around each O-point to a cell structure.* Such a cell structure can be obtained by solving equation (2.14). However, the cell structure obtained by solving this equation has not been reported in the literature. As indicated by Bollmann, these cells are related to the Wigner-Seitz cells of the reference lattice by an imaging operation. (To distinguish the cells of the poorest matching region from the Wigner-Seitz cells, the former is here after termed the O-cell.) It will be shown that the O-cell structure can be easily solved by such an imaging operation.

---

* An example of formation of a cell structure in the two-dimensional O-lattice by a rotation is given in Figure 3.2 (a), where two point lattices of the same structure, the (110) plane of BCC lattice, are rotated with respect to each other by 8°. The least-matching regions are defined as cell walls.

It is convenient to conduct this operation in reciprocal space, since the operation is related planes. Provided **T** is invertible, the equation (3.2b) becomes:

$$\mathbf{X}^0 = \mathbf{T}^{-1}\ \mathbf{b}_\beta, \qquad (3.5)$$

The corresponding translation in reciprocal space is (Christian, 1975):

$$\mathbf{X}^{0*} = \mathbf{T}^{\intercal}\ \mathbf{b}_\beta^*$$

or

$$(\mathbf{X}^{0*})^{\intercal} = (\mathbf{b}_\beta^*)^{\intercal}\ \mathbf{T}, \qquad (3.6)$$

where $\mathbf{b}_\beta^*$ and $\mathbf{X}^{0*}$ are reciprocal vectors in the BCC lattice and O-lattice, respectively.

The Wigner-Seitz cell for a BCC lattice is a "truncated octahedron" (Ashcroft and Mermin, 1976) with six square faces perpendicularly bisecting <1 0 0> type vectors and eight regular hexagon faces perpendicularly bisecting <1 1 1> type vectors. Therefore the reciprocal vectors, $\mathbf{WS}_i^*$, representing the face normals of the Wigner-Seitz cell will be in the same directions as $\mathbf{b}_{\beta i}$ in (3.4), but with inverse magnitude, as given in the form of a column vector in the following expression:

$$[\mathbf{WS}_1^* \cdots \mathbf{WS}_7^*] = \frac{1}{a_\beta} \begin{bmatrix} \frac{2}{3} & \frac{2}{3} & \frac{2}{3} & -\frac{2}{3} & 1 & 0 & 0 \\ \frac{2}{3} & \frac{2}{3} & -\frac{2}{3} & \frac{2}{3} & 0 & 1 & 0 \\ \frac{2}{3} & -\frac{2}{3} & \frac{2}{3} & \frac{2}{3} & 0 & 0 & 1 \end{bmatrix} \qquad (3.7)$$

From (3.6), the reciprocal vectors, $\mathbf{OC}_i^*$, representing the O-cell walls will be:

$$\mathbf{OC}_i^* = \mathbf{T}^T \mathbf{WS}_i^*, \qquad (3.8)$$

The direction of $\mathbf{OC}_i^*$ gives the normals to the O-cell walls and the inverse of the magnitude of $\mathbf{OC}_i^*$ gives the spacings between pairs of walls. Seven pairs of O-cell walls enveloping an O-point form one cell; the whole cell structure of O-lattice can be constructed by translating this O-cell repeatedly in the O-lattice space.

Given a normal to an interface, the dislocations in the interface are determined by the lines of intersection of the cell walls with the boundary. Taking $\mathbf{bdy}^*$ as a unit reciprocal vector normal to a boundary, the directions of the lines of intersection are determined by

$$\mathbf{D}_i = \mathbf{OC}_i^* \times \mathbf{bdy}^*, \qquad (3.9)$$

It can be seen from Figure 3.1 that the spacing of lines of intersection, i.e. the spacing of dislocations is simply:

$$ds_i = 1/|\mathbf{D}_i| = 1/(|\mathbf{oc}_i^*|\sin\theta). \qquad (3.10)$$

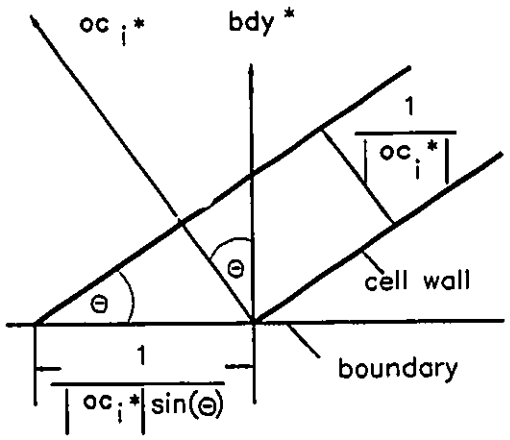

Fig. 3.1 The spacing of the lines of intersection of the cell walls with a boundary.

3.3 Mismatch of Lattice Planes and the Determination of the Habit Plane

It has been reported that some defect lines observed at interphase boundaries can be explained as the result of the mismatch of low index planes. (For example, see Bäro and Gleiter (1973), and Luo and Weatherly, (1988)). In these studies, as well as in the plane matching model first suggested by Pumphrey (1972), only one set of mismatching planes was taken into account.

Here, the three-dimensional mismatch of all planes, especially low index planes, will be analyzed. As we know, moiré fringes are formed by superposition of two grid structures having a similar period. When two sets of planes interpenetrate, there are regions of perfect match and regions in which the planes match particularly badly. If we view the pattern of interpenetrating planes along the zone axis of the two sets of planes, we see the poorly matched regions as moiré fringes, which, if extended to the viewing direction, are also a set of planes. Such a situation is demonstrated in Figure 3.2b. In the right part of the Figure 3.2b the formation of moiré fringes from two sets of slightly misoriented (8°) lines is illustrated. When three pairs of misoriented lines are plotted, three set of fringes are formed. The pattern shown in the left-hand portion of Figure 3.2b is due to the three sets of moiré fringes interweaving with each other. The lines in Figure 3.2b have been drawn according to the lattice vectors in Figure 3.2a. They could be considered as the lines of intersection of {1 1 0} type of planes in (1 1 0).

Moiré fringes often form in the TEM due to double diffraction of planes from two crystals. It has been shown by Hirsch et al. (1977) that the moiré fringes in TEM image are perpendicular to Δg, defined by:

$$\Delta g = g_{\beta} - g_{\alpha} \qquad (3.11)$$

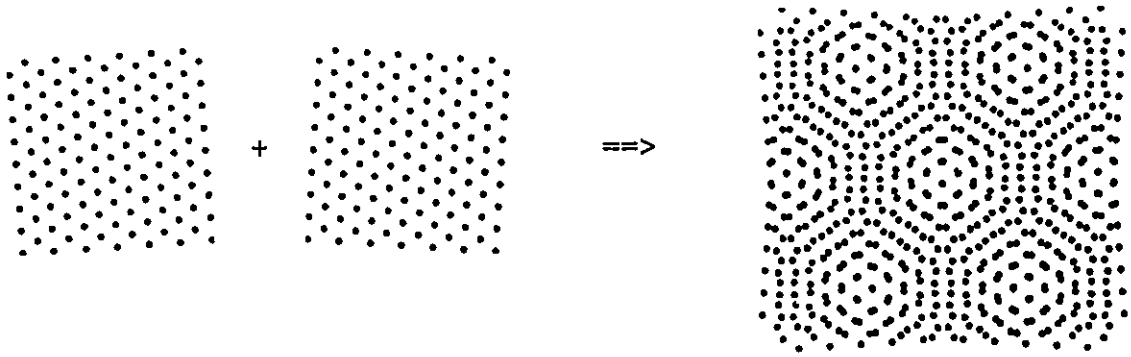

(a)

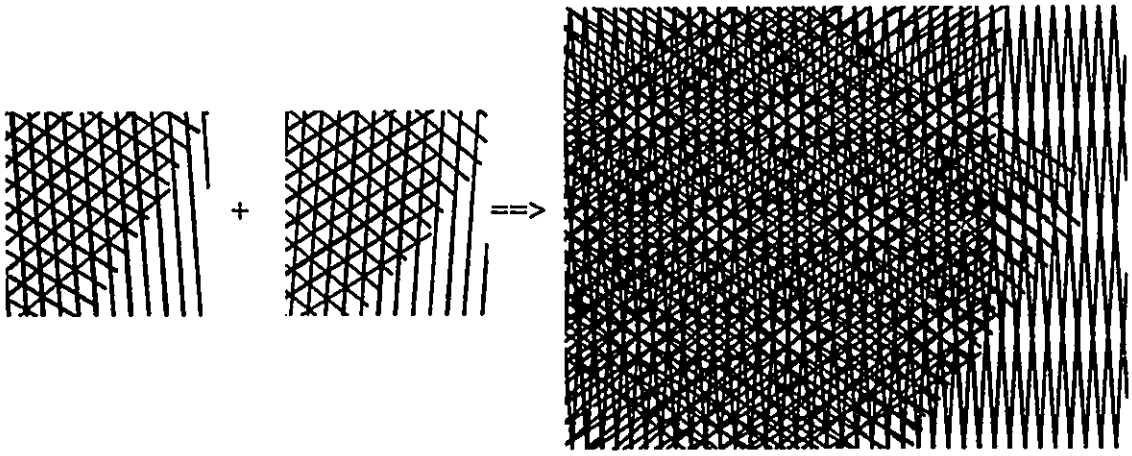

(b)

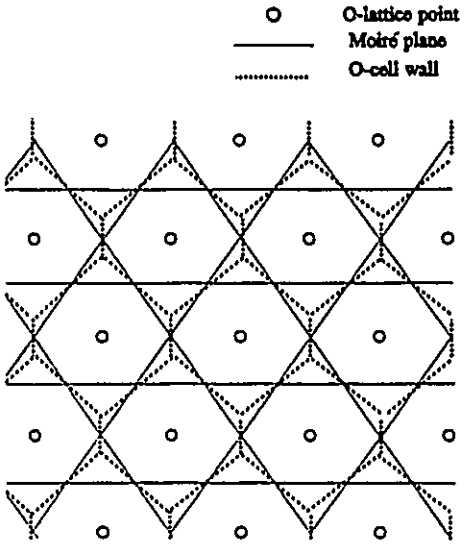

(c)

Fig. 3.2 An illustration of the formation of O-cell walls due to the mismatch of lattice points (a); formation of "moiré planes" related to the mismatch of lattice planes (b); locations of O-cell walls and "moiré planes", refer to the O-points (c).

where g_α and g_β are the reciprocal vectors representing the planes, involved in the double diffraction from the two crystals. The inverse magnitude of Δg gives the fringe spacing. Equation (3.11) gives the general formula for the geometry of the moiré pattern. Let $\mathbf{b}_{\beta i}^*$ be the reciprocal vector representing a set of low index planes in the reference BCC lattice in the form of a column vector in the following expression:

$$[\mathbf{b}_{\beta 1}^* \cdots \mathbf{b}_{\beta 11}^*] = \frac{1}{a_\beta} \begin{bmatrix} 1 & 1 & 1 & 1 & 0 & 0 & 2 & 0 & 0 \\ 1 & -1 & 0 & 0 & 1 & 1 & 0 & 2 & 0 \\ 0 & 0 & -1 & 1 & 1 & -1 & 0 & 0 & 2 \end{bmatrix}. \qquad (3.12)$$

From the definition of equation (3.1) and the relationship between the transformation in real and reciprocal space (Christian, 1975), planes transformed from planes $\mathbf{b}_{\beta i}^*$ can be given as:

$$(\mathbf{b}_{\alpha i}^*)^T = (\mathbf{b}_{\beta i}^*)^T \mathbf{A}^{-1}. \qquad (3.13)$$

If we define

$$g_\beta = (\mathbf{b}_{\beta i}^*)^T \qquad (3.14, a)$$

and

$$g_\alpha = (\mathbf{b}_{\alpha i}^*)^T, \qquad (3.14, b)$$

then the transpose of (3.11) can be written as

$$\mathbf{OP}_i^* = \mathbf{b}_{\beta i}^* - \mathbf{b}_{\alpha i}^*, \qquad (3.15)$$

where $\mathbf{OP}_i^*$ is the transpose of $\Delta\mathbf{g}$. Just as $\mathbf{b}_{\beta i}^*$ and $\mathbf{b}_{\alpha i}^*$ represent planes in α and β lattices, $\mathbf{OP}_i^*$ also represents a set of planes in three dimensions, the planes of the most poorly matching. Due to the similarity of these planes to the two-dimensional moiré fringes, the term "moiré planes" will be used to refer to these planes.

Besides defining the geometry of the plane of poorly matching $\mathbf{OP}_i^*$ also carries another important message for interfacial study: A plane in the O-lattice containing at least two O-lattice vectors defined by equation (3.2) can also be defined by a vector $\mathbf{OP}_i^*$. By transposing the vectors in (3.15) and combining with (3.13), we have:

$$\begin{aligned}(\mathbf{OP}_i^*)^T &= (\mathbf{b}_{\beta i}^*)^T - (\mathbf{b}_{\beta i}^*)^T \mathbf{A}^{-1} \\ &= (\mathbf{b}_{\beta i}^*)^T (\mathbf{I} - \mathbf{A}^{-1}) \\ &= (\mathbf{b}_{\beta i}^*)^T \mathbf{T}. \end{aligned} \qquad (3.16)$$

because

$$\mathbf{T} = (\mathbf{I} - \mathbf{A}^{-1}).$$

In fact the relationship in (3.16) is identical to that in (3.6), and hence

$$\mathbf{OP}_i^* = \mathbf{X}^{O*}. \qquad (3.17)$$

Namely, $\mathbf{OP}_i^*$ represents a set of planes in the O-lattice. Since the transformation in (3.5) is a homogeneous deformation of space, lines which are originally coplanar, remain coplanar. Consider a vector $\mathbf{b}_{\beta i}^*$ defined by

$$\mathbf{b}_{\beta i}^* = \frac{\mathbf{b}_{\beta j} \times \mathbf{b}_{\beta k}}{\mathbf{b}_{\beta i} \cdot \mathbf{b}_{\beta j} \times \mathbf{b}_{\beta k}} , \qquad (3.18)$$

where $\mathbf{b}_{\beta i}$, $\mathbf{b}_{\beta j}$ and $\mathbf{b}_{\beta k}$ are three non-coplanar lattice translation vectors. By definition, $\mathbf{b}_{\beta j}$ and $\mathbf{b}_{\beta k}$ are in a plane determined by $\mathbf{b}_{\beta i}^*$. The plane in the O-lattice transformed from $\mathbf{b}_{\beta i}^*$, i.e. $\mathbf{OP}_i^*$, will contain $\mathbf{X}^O_j$ and $\mathbf{X}^O_k$ which are transformed from $\mathbf{b}_{\beta j}$ and $\mathbf{b}_{\beta k}$, respectively. Therefore the following relationship holds

$$\mathbf{OP}_i^* = \frac{\mathbf{X}_j^O \times \mathbf{X}_k^O}{\mathbf{X}_i^O \cdot \mathbf{X}_j^O \times \mathbf{X}_k^O} = T^T \left[\frac{\mathbf{b}_{\beta j} \times \mathbf{b}_{\beta k}}{\mathbf{b}_{\beta i} \cdot \mathbf{b}_{\beta j} \times \mathbf{b}_{\beta k}} \right]. \qquad (3.19)$$

Knowles (1982) has indicated that this expression can be proved more rigorously by using tensor algebra.

Now it is clear that a face of an O-lattice unit cell, which is usually defined by two O-lattice vectors*, is

---

* A unit cell of O-lattice can be determined by O-lattice vectors transformed from any combination of three column vectors in (3.4) except for the combination among three <1 0 0>.

determined by an $\mathbf{OP}_i^*$ vector. Such a plane may contain relatively denser O-points than others. It is important to realize that a boundary lying along one of the faces can cut at most three sets of cell walls, while others will cut more.* We have assumed the lines of intersection of the O-cell walls with the boundary to be the dislocation lines. Therefore, the more O-cell walls a boundary may cut, the higher is the density of the dislocations in the boundary. As a result, the faces determined by $\mathbf{OP}_i^*$, transformed from the six close packed planes, $\mathbf{b}_{Bi}^*$ (i=1...6) in (3.12), are considered to be the most plausible candidates for the habit plane. The habit plane should taken to be the one that contains a minimum density of dislocations. It is assumed that the density of O-points gives an indication of the density of dislocations, as each pair of adjacent O-points in a habit plane is separated by a single dislocation line. Therefore, the habit plane is selected among the candidates to be the one that contains a minimum number of O-points per unit area or has the smallest plane spacing, corresponding to the largest magnitude of $\mathbf{OP}_i^*$. Since the energy of the interface cannot currently be predicted, this method of determining habit planes serves as a useful approximation.

---

* Any lines parallel to an O-lattice vector defined by equation (3.2) will intersect only one set of O-cell walls, while lines in other directions will cut more sets of O-cell walls. This can be seen from the plot of the O-lattice in Figure 3.2 (c). Similarly, a plane containing more than one O-lattice vectors will only cut the O-cell walls which are bisected by the vectors at the plane.

The faces of the O-lattice unit cell have been chosen by searching for the lowest energy boundaries (Bollmann and Nissen 1968). (For details see Section 2.5.4) The rationale given here for choosing a habit plane is not the same as that given by Bollmann and Nissen (1968), although a similar result could be obtained using either method. In Bollmann and Nissen's work, a particular unit cell was chosen and only three faces were investigated. Hall et al. (1986) have extended the choice of the unit cell of the O-lattice, but followed the criterion suggested by Bollmann and Nissen (1968).

3.4 A Comparison of Lines of Intersection of "Moiré Planes" with the Boundary and the "Mathematical" Dislocations

It has been shown in the last Section that "moiré planes" are identical with the faces of the O-lattice unit cell, among which one can be chosen as the habit plane. On the other hand, the faces of the O-lattice unit cell have been regarded as the simplified cell walls for a long time (for example, see Hall et al. 1986). Here, the real meaning of the lines of the intersection of the faces with a boundary is recognized: they are the locations of the least plane mismatch instead of the least point (atom) mismatch. It is the latter, so called a "mathematical" dislocation, whose Burgers vector can be clearly defined.

Generally speaking, the configurations of these two types of intersections are different. Given a boundary parallel to a face of a O-lattice unit cell, the lines of intersection of the cell walls with the boundary form a cell structure in two dimensions, as illustrated in Figure 3.2c. Usually each cell has three pairs of edges, and their geometry can been obtained by using equation (3.9-10). It has been indicated in Section 2.5.3 that the Burgers vector associated with the line of intersection of an O-cell wall with the boundary is simply the $\mathbf{b}_\beta$ defining the O-lattice vector bisected by the wall. Consequently, the Burgers vectors of the dislocations in the boundary are contained in the plane from which the plane in an O-lattice chosen as the boundary is transformed.

When one face of a unit cell is intersected by the boundary which is another face of the unit cell, the direction of the line of intersection is just the zone axis of these two faces:

$$\mathbf{u}_k = (\mathbf{OP}_i^*) \times (\mathbf{OP}_j^*), \qquad (3.20)$$

where $\mathbf{u}_k$ gives the direction of the zone axis, $\mathbf{OP}_i^*$ is defined in (3.19) and $\mathbf{OP}_j^*$, chosen as the boundary, is defined similarly by rotating the subscripts in (3.19). Because of the property of the reciprocal lattice, $\mathbf{X}^0_k$ is defined as:

$$\mathbf{X}^{O}_{k} = \frac{\mathbf{OP}_i^* \times \mathbf{OP}_j^*}{\mathbf{OP}_k^* \cdot (\mathbf{OP}_i^* \times \mathbf{OP}_j^*)} \quad . \qquad (3.21)$$

It is clear that $\mathbf{X}^{O}_{k}$ is parallel to $\mathbf{u}_k$. Thus, the lines of intersection of the face of the O-lattice unit cell with the boundary are simply parallel to the O-lattice vector. Following a similar analysis which led to the result in (3.10), the spacing of the lines is

$$mds_i = \frac{1}{|\mathbf{MD}_i|} = \frac{1}{|\mathbf{OP}_i^* \times \mathbf{bdy}^*|} \quad . \qquad (3.22)$$

where

$$\mathbf{bdy}^* = \mathbf{Op}_j^*/|\mathbf{OP}_j^*| \qquad (3.23)$$

If we take the six {110} planes in the BCC lattice into consideration, the configuration of the intersection of the "moiré planes" with the boundary will normally be a weave of three sets of lines, each of which is parallel to one of the three O-lattice vectors in the boundary plane. This is shown in Figure 3.2b as the three interweaving fringes; whereas the locations of the fringes are more clearly indicated in Figure 3.2c where they are compared with the positions of the O-lattice points and the O-cell walls. In fact, each line at the same time can be the line of intersection of the boundary with more than one set of "moiré planes". This is simply because an O-lattice vector, along the line of the intersection, could be

the zone axis of more than two sets of O-lattice planes transformed from the close-packed BCC planes. Thus, it is very ambiguous to assign a Burgers vector to these lines.

The same geometry describing these lines of intersection has been presented elsewhere (For example, see Knowles, 1982 and Hall et al. 1986). Nevertheless, only two of the three sets of lines of intersection were taken into consideration (as dislocation lines). Therefore, a parallelogram configuration of the lines was obtained.

3.5 Effective Invariant Line Condition

A strict invariant line strain is characterized by the existence of a line which is both unrotated and unextended during a transformation. Such an invariant line is defined mathematically by

$$\mathbf{A}\,\mathbf{x} = \mathbf{x}. \qquad (3.24)$$

where $\mathbf{A}$ is a transformation matrix and $\mathbf{x}$ is a vector which represents the direction of the invariant line.

An effective invariant line is defined by a direction which undergoes so small a change during a transformation that there is no physically significant difference in the

direction. This direction is determined by the vector **x** in the following equation:

$$\mathbf{Ax} = k\mathbf{x}, \tag{3.25}$$

where

$$k = 1 + \epsilon, \tag{3.26}$$

and ϵ can be chosen to be very small, depending on the particularly physical requirement. For example, take a precipitate, 100 μm long, with its longest axis along **x**. If its length is changed by 0.00001% (i.e. ϵ = 0.0000001). then the total change in length will be 0.01 nm, which is very small compared to the atomic spacing and can be neglected in the study of the interfacial structure.

There are three advantages for using an effective invariant line instead of a mathematical one. Firstly, an effective invariant line condition is more feasible than the mathematical invariant line condition. In the vicinity of a mathematical invariant line orientation, one can always find a direction along which ϵ is close but not equal to zero. Even if a phase transformation could be described exactly by an invariant line strain defined by (3.24), the calculation from the experimental data usually fails to satisfy the equality in (3.24) due to the limitation of the accuracy in measurements.

Secondly, for the true invariant line strain transformation, the matrix **T** in (3.2b) becomes singular; while, if k is very close but not equal to one, the calculation still can be carried out in the regular and simple way. Thirdly, because the effective invariant line is very close to the true invariant line, the properties of a mathematical invariant line are still applicable.

3.6 Properties of Invariant Line Strains

i. In any interface containing an invariant line, all dislocations should lie in one direction parallel to the invariant line. This can be easily proved by the dislocation theory of interfaces reviewed in Section 2.3, and has been demonstrated elsewhere (Dahmen, 1987). It should be emphasized that the parallel dislocations usually belong to more than one set; as this has not been widely recognized in the literature (For example, see Dahmen and Westmacott, 1981).

ii. An invariant line is the zone axis of all $\mathbf{OP}_i^*$ defined by (3.15). If we transpose the vectors in (3.15) and multiply them with the invariant line vector **x**, we get

$$(\mathbf{OP}_i^*)^T \cdot \mathbf{x} = (\mathbf{b}_{\beta i}^*)^T \cdot \mathbf{x} - (\mathbf{b}_{\alpha i}^*)^T \cdot \mathbf{x} \qquad (3.27)$$

Combining with equations (3.24 and 3.13), (3.27) becomes

$$(\mathbf{OP}_i^*)^T \cdot \mathbf{x} = (\mathbf{b}_{\beta i}^*)^T \cdot \mathbf{x} - (\mathbf{b}_{\beta i}^*)^T \mathbf{A}^{-1} \cdot \mathbf{A}\mathbf{x}$$
$$= (\mathbf{b}_{\beta i}^*)^T \cdot \mathbf{x} - (\mathbf{b}_{\beta i}^*)^T \cdot \mathbf{x}$$
$$= 0. \qquad (3.28)$$

(3.28) indicates that the invariant line is the zone axis of all "moiré planes". It can be shown that this property should also applicable to other planes similarly defined as $\mathbf{OP}_i^*$. The relation in (3.8) for defining the O-cell walls and the one in (3.16) associated with "moiré plane" are essentially the same, except for the difference in the vector variables. Therefore, this property is applicable to $\mathbf{OC}_i^*$, namely, an invariant line is also the zone axis of planes normal to $\mathbf{OC}_i^*$.

This property of the invariant line can be used in a TEM study for testing the existence of an invariant line. First, in the TEM studies, the moiré fringes due to the reflections from any two sets of planes related to each other by (3.13) should be parallel to the projection of the invariant line which is parallel to the principal set of dislocations in an interface containing the invariant line. Second, if one can bring the electron beam normal to the invariant line and also parallel to a low index zone axis, one should be able to see, from the selected area diffraction pattern, that the visible $\Delta\mathbf{g}$s are parallel to each other and perpendicular to the basic set of defect lines in the habit plane. This condition cannot always be realized, but one can

usually arrive a case close to it and find all Δgs nearly parallel.

iii. Corresponding to an invariant line in real space, there must exist an invariant line in reciprocal space, which defines a plane having an invariant normal. It will be shown that all displacements due to the invariant line strain are contained in such a plane. Given a transformation in real space (3.24), the corresponding transformation in reciprocal space is:

$$(\mathbf{A}^{-1})^{T}\mathbf{x}^{*} = \mathbf{x}^{*} \qquad (3.29)$$

where $\mathbf{x}^{*}$ is a reciprocal vector defining the invariant normal, because both $\mathbf{A}$ and $\mathbf{A}^{-1}$ have an eigenvalue equal to one. The displacement of a vector due to the transformation can be expressed as

$$\Delta\mathbf{x} = \mathbf{A}\mathbf{x} - \mathbf{x} \qquad (3.30)$$

where $\mathbf{x}$ is any vector. If we transpose both sides of (3.29) and multiply by $\Delta\mathbf{x}$, we find that

$$(\mathbf{x}^{*})^{T}\cdot\Delta\mathbf{x} = \mathbf{x}^{*T}(\mathbf{A}^{-1})\mathbf{A}\mathbf{x} - (\mathbf{x}^{*})^{T}\mathbf{x}$$

and hence

$$(\mathbf{x}^*)^T \cdot \Delta\mathbf{x} = 0. \qquad (3.31)$$

Therefore, displacements of all vectors lie necessarily in the plane with the invariant normal.

As mentioned in Section 2.8, Bollmann has noted that the deformation should be confined in a plane (b-subspace) if the rank of **T** in (3.2b) is two. From the relationship in (3.31), it is clear that this plane of b-subspace for an invariant line strain transformation is characterized by an invariant normal $\mathbf{x}^*$.

iv. The displacements of all vectors lying in a given interface containing the invariant line are in one direction. For an interface determined by **i**, the direction of the invariant line, and **n**, the direction normal to **i**, any direction **r** in the interface can be written as:

$$\mathbf{r} = a\mathbf{i} + b\mathbf{n}.$$

where a and b are any constants. The displacement in the **r** direction is:

$$\begin{aligned} \mathbf{Ar} - \mathbf{r} &= \mathbf{A}(a\mathbf{i} + b\mathbf{n}) - (a\mathbf{i} + b\mathbf{n}) \\ &= b(\mathbf{An} - \mathbf{n}), \end{aligned} \qquad (3.32)$$

because

$$\mathbf{Ai} - \mathbf{i} = 0.$$

Therefore the displacement in the **r** direction is proportional to that in the **n** direction. If **r** is taken as a unit vector, it is clear that the displacement is a maximum when b equals 1; namely, the deformation along the **n** direction is the largest in the interface.

This property and the previous one have been used in the phenomenological martensitic transformation theory (Bowles and Mackenzie 1954).

v. In reciprocal space there is a second property, similar to the one described above. Provided $\mathbf{r}^*$ is any reciprocal vector contained in a plane determined by the reciprocal vector $\mathbf{x}^*$, the invariant normal, and the reciprocal vector $\mathbf{u}^*$, normal to $\mathbf{x}^*$, it can be shown that the displacement of $\mathbf{r}^*$ due to the transformation is always parallel to the displacement of $\mathbf{u}^*$. We can write

$$\mathbf{r}^* = a\mathbf{u}^* + b\mathbf{x}^*$$

where a and b are any constants. Following the same analysis which led to (3.32) we can obtain:

$$
\begin{aligned}
&(\mathbf{r}^*)^T \mathbf{A}^{-1} - (\mathbf{r}^*)^T \\
&= a((\mathbf{u}^*)^T \mathbf{A}^{-1} - (\mathbf{u}^*)^T) \\
&= a(\mathbf{u}^*)^T (\mathbf{A}^{-1} - \mathbf{I}) \\
&= -a(\mathbf{u}^*)^T \mathbf{T} \qquad (3.33)
\end{aligned}
$$

because

$$(\mathbf{x}^*)^T \mathbf{A}^{-1} = (\mathbf{x}^*)^T.$$

Note that $(\mathbf{u}^*)^T\mathbf{T}$ is the reciprocal vector representing the "moiré planes" related to the mismatch of planes $\mathbf{u}^*$ with the corresponding planes in the other phase. Therefore, for any planes in the same zone axis as the invariant normal, $\mathbf{x}^*$, the "moiré planes" must be parallel to each other. Because the inverse magnitude of $a(\mathbf{u}^*)^T\mathbf{T}$ gives the spacing of the "moiré planes" related to $\mathbf{r}^*$, the smaller the value of a or the angle between $\mathbf{r}^*$ and $\mathbf{x}^*$, the larger the spacing of the "moiré planes" will become.

The above properties are very useful in the analysis of mismatch in the habit plane as will be discussed later.

3.7 Search for an Effective Invariant Line

The method developed here will be applied to a BCC/HCP system, though it can be applicable to many other systems too. The orientation relationship in Zr alloys is reported to be the Burgers orientation relationship (Burgers, 1934), or near it, and the phase transformation is characterized by an

invariant line strain (Perovic and Weatherly 1988). The TEM observations in the present work indicate that the orientation relationship in the Zr-2.5 wt% Nb precipitation system is not exactly the Burgers orientation relationship but is scattered around it within ~1.5°.

The orientation relationships in a region within 1.5° of the Burgers orientation relationship are searched to find those that can satisfy the effective invariant line condition. The procedure of calculation is:

1. Choose a value for ϵ in (3.26), say, ϵ=0.0000001, since the α precipitates are usually much shorter than 100μm.

2. Choose a particular orientation relationship from the variants of the Burgers orientation relationship (Burgers (1934):

$$(0\ 0\ 0\ 1)_\alpha \ /\!/\ (1\ 1\ 0)_\beta,$$
$$[1\ 1\ -2\ 0]_\alpha \ /\!/\ [1\ -1\ 1]_\beta,$$

and select an orthogonal coordinate system, as shown in Figure 3.3.

3. Determine the transformation matrix **A**: Following the procedure given by Bollmann (1974a), we first chose three non-coplanar vectors from ß, as the column vectors in matrix $\mathbf{B}_\beta$.

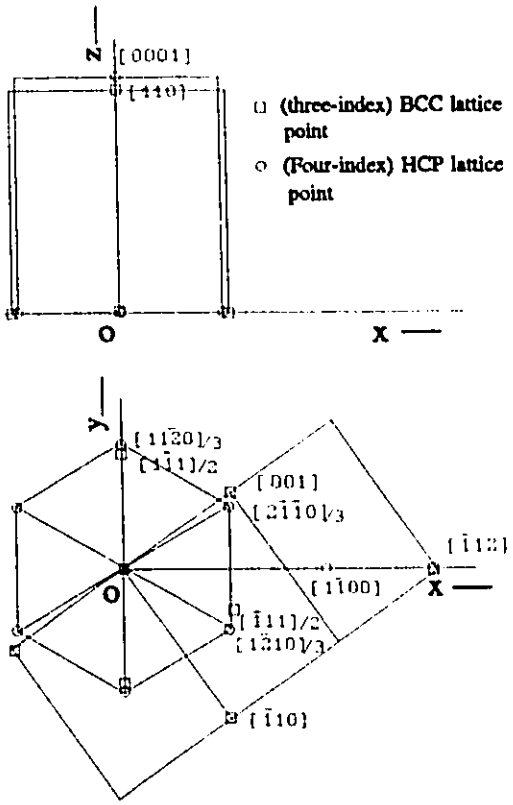

Fig. 3.3 The coordinates for O-lattice calculation.

Then the corresponding vectors in α phase are determined so that the nearest neighbours in both lattices are related. These are given in each column in $\mathbf{B}_\alpha$.

$$\mathbf{B}_\beta = \begin{bmatrix} 1 & .5 & 0 \\ 1 & -0.5 & 0 \\ 0 & .5 & 1 \end{bmatrix} \qquad (3.34)$$

$$\mathbf{B}_\alpha = \begin{bmatrix} 0 & 1 & 1 \\ 0 & 1 & 0 \\ 1 & 0 & 0 \end{bmatrix} \qquad (3.35)$$

Vectors in $\mathbf{B}_\alpha$ are expressed in the three-index hexagonal indexing system; they correspond to the column vectors in $\mathbf{B}_{\alpha m}$

in the four-index system:

$$\mathbf{B}_{\alpha m} = \frac{1}{3}\begin{bmatrix} 0 & 1 & 2 \\ 0 & 1 & -1 \\ 0 & -2 & -1 \\ 3 & 0 & 0 \end{bmatrix} \qquad (3.36)$$

Corresponding to $\mathbf{B}_\beta$ and $\mathbf{B}_\alpha$ in lattice coordinates, the matrices in orthogonal coordinates are $\mathbf{S}_\beta$ and $\mathbf{S}_\alpha$. They are defined by:

$$\mathbf{S}_\beta = a_\beta \begin{bmatrix} 0 & 0 & \sqrt{\frac{2}{3}} \\ 0 & \frac{\sqrt{3}}{2} & \sqrt{\frac{1}{3}} \\ \sqrt{2} & 0 & 0 \end{bmatrix} \qquad (3.37)$$

and

$$\mathbf{S}_\alpha = a_\alpha \begin{bmatrix} 0 & 0 & \frac{\sqrt{3}}{2} \\ 0 & 1 & \frac{1}{2} \\ rca & 0 & 0 \end{bmatrix} \qquad (3.38)$$

where a_β is the lattice parameter of the ß phase and

$$rca = c_\alpha / a_\alpha, \qquad (3.39)$$

where a_α and c_α are the lattice parameters of the hexagonal α phase.

The column vectors in (3.37) are related to those in (3.38) by the transformation $\mathbf{A}_b$, so that

$$\mathbf{S}_\alpha = \mathbf{A}_b \, \mathbf{S}_\beta. \qquad (3.40)$$

Therefore

$$\mathbf{A}_b = \mathbf{S}_\alpha \, (\mathbf{S}_\beta)^{-1} \qquad (3.41)$$

$$= 1/\mathrm{rbh} \begin{bmatrix} 0 & 0 & \frac{\sqrt{3}}{2} \\ 0 & 1 & \frac{1}{2} \\ \mathrm{rca} & 0 & 0 \end{bmatrix} \begin{bmatrix} 0 & 0 & \sqrt{\frac{2}{3}} \\ 0 & \frac{\sqrt{3}}{2} & \sqrt{\frac{1}{3}} \\ \sqrt{2} & 0 & 0 \end{bmatrix}^{-1}$$

where

$$\mathrm{rbh} = a_\beta / a_\alpha \qquad (3.42)$$

It can be seen from (3.41) that $\mathbf{A}_b$ is independent of the individual values of a_β, a_α and c_α, but depends on the ratios of a_β to a_α (rbh) and c_α to a_α (rca).* For the sample heat-treated at 650°C, the rca and rbh as measured in TEM are 1.588±0.003 and 1.091±0.002, respectively. When the effect of thermal expansion from room temperature to 650°C is taken into account (see Appendix 1), the values become: rca = 1.589, rbh = 1.094, as to be used in the calculation.

4. Rotate HCP α crystal until the effective invariant line condition is satisfied. The rotation in the three-dimensional space is divided into two steps. Firstly rotate α along z axis by $\mathbf{R}_1$, so that

---

*This is an advantage for a TEM study, because the determination ratios could be obtained free of errors due to the uncertainty in the camera length and the accelerating voltage.

$$\mathbf{x}_\alpha = \mathbf{R}_1\mathbf{A}_b\mathbf{x}_\beta, \qquad (3.43)$$

where $\mathbf{R}_1$ is a rotation matrix:

$$\mathbf{R}_1 = \begin{bmatrix} \cos\gamma & -\sin\gamma & 0 \\ \sin\gamma & \cos\gamma & 0 \\ 0 & 0 & 1 \end{bmatrix} \qquad (3.44)$$

and γ is an angle between -1.5° to 1.5°. The α crystal is then rotated along an axis in x-y plane by $\mathbf{R}_3$:

$$\mathbf{R}_3 = (\mathbf{R}_2)^{-1}\begin{bmatrix} \cos\phi & 0 & \sin\phi \\ 0 & 1 & 0 \\ -\sin\phi & 0 & \cos\phi \end{bmatrix}\mathbf{R}_2 \qquad (3.45)$$

where

$$\mathbf{R}_2 = \begin{bmatrix} \cos\theta & -\sin\theta & 0 \\ \sin\theta & \cos\theta & 0 \\ 0 & 0 & 1 \end{bmatrix} \qquad (3.46)$$

is the matrix for locating the rotation axis in the x-y plane. Due to the 2-fold symmetry in the $(1\ 1\ 0)_\beta/(0\ 0\ 0\ 1)_\alpha$ plane, only positive values less than 1.5° are chosen for angle ϕ, while the angle θ is varied between 0° and 180°. Consequently, the transformation matrix which takes into account the deviation from the exact Burgers orientation relationship is

$$\mathbf{A} = \mathbf{R}_3\mathbf{R}_1\mathbf{A}_b. \qquad (3.47)$$

5. Find suitable R_1 and R_3 in (3.47) so that **A** satisfies the effective invariant line condition: $\mathbf{Ax} = k\mathbf{x}$, where k should be equal to or slightly smaller than $1 + \epsilon$. The general method should be to solve for the eigenvalues of **A** and choose the one which can satisfy the condition for k. However, in practice one does not seek the eigenvalues of **A**. To simplify the calculation, we define

$$\mathbf{Tt} = \mathbf{I} - \mathbf{A}. \qquad (3.48)$$

It can be shown that if one of the eigenvalues of **A** is close to one, then there is one of the eigenvalues of **Tt** close to zero, and the determinant of **Tt**, $|\mathbf{Tt}|$, will also be close to zero. The results of this calculation indicate that for any values of θ and ϕ in the fixed range, $|\mathbf{Tt}|$ will change sign, as γ is varied from -1.5° to 1.5°. The zero point condition is sought numerically by setting a critical value for $|\mathbf{Tt}|$ corresponding to the value of ϵ. Angles ϕ and θ are divided into fine steps (for example $\Delta\phi$=0.05°,$\Delta\theta$=5°), while γ is sought by the optimum method,* which provides a means for fast searching. When $|\mathbf{Tt}|$ is smaller than the critical value, we regard the condition to be correspond to the zero point and

---

* In this method, we compare three $|\mathbf{Tt}|$ each time, corresponding to three γ values: a1, a2 = (a3-a1)*0.618 +a1, and a3, where a1 and a3 are the limits of range of search. The range of search is narrowed by substituting a2 for a1 or a3 depending where $|\mathbf{Tt}|$ changes the sign. The calculation is carried on until the critical value of $|\mathbf{Tt}|$ is reached; it usually takes about 20 cycles.

then the eigenvalues of **A** are checked to see if one of them is smaller than ϵ. We can always find a suitable critical value such that when $|\mathbf{Tt}|$ is smaller than it, the effective invariant line condition is satisfied. It is found that the smaller the ϵ is, the more precisely the γ is defined, namely, there are more significant digits in the value of γ, which can be defined too precisely to be physically meaningful in practice.

The results of the calculation show that for the measured lattice parameter ratios in the Zr-Nb alloy, the effective invariant line condition can be met in the whole range of θ (0°—180°). For any combination of θ and ϕ (0°—1.5°) and hence **R**3, we can always find a value of γ (in a range of $-1.1° < \gamma < 0.38°$) for $\mathbf{R}_1$ such that one of eigenvalues of **A** is closer to one than k, namely, requirement for an effective invariant line is met. However, at the exact Burgers orientation, the effective invariant line condition cannot be satisfied.

3.8 A Hypothesis for the Optimum Orientation Relationship

The results of the previous Section indicate that, in the vicinity of the Burgers orientation, there is an infinite number of orientation relationships available which satisfy the effective invariant line condition. From the TEM studies, it was noted that θ is not distributed over such a wide range as the calculation suggested, although the orientation relationship is not uniquely fixed. The question is now to determine which of the numerous possible choices of orientation relationship(s) is favoured by nature. It should be emphasized that the interphase boundary that we are dealing with is semicoherent in nature, for the misfit dislocations have been consistently observed in the boundaries. A second important observation is that only a single set of regularly spaced dislocations is observed consistently in the habit plane. In this Section we will attempt to choose appropriate orientations for the semicoherent precipitates, based on an analysis of the mismatch in the habit plane.

According to the method suggested in Section 3.3.2., the habit plane is predicted to be $(\mathbf{p}_i^*)$, which is transformed from $(1\ 0\ 1)_\beta$, because this vector always has the largest magnitude. An example of the result of an O-lattice calculation, when $\theta = -2°$, $\phi = 1.015°$, $\gamma = -0.290°$ is shown in Figure 3.4. The O-lattice points are projected in the habit

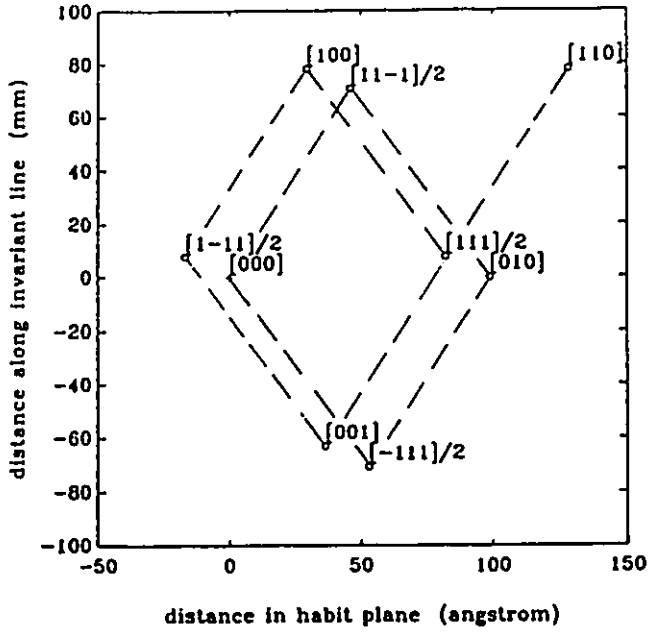

(a)

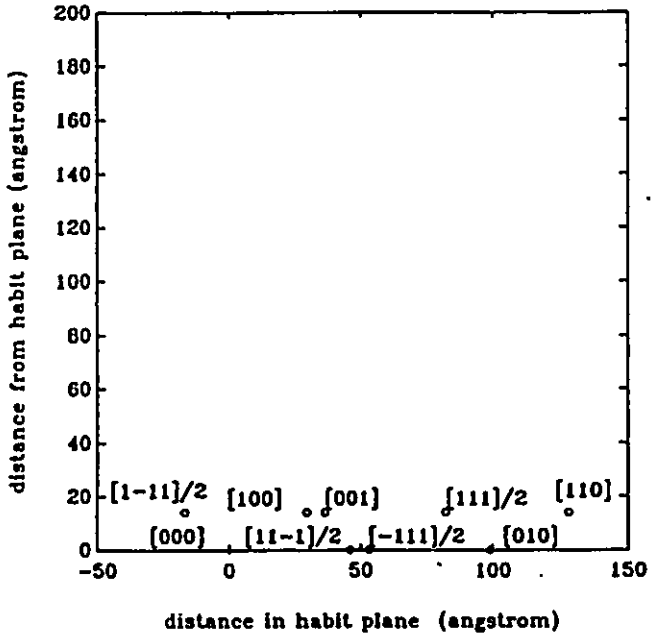

(b)

Figure 3.4 (a) the projection of O-lattice points in the habit plane; (b) the projection of O-lattice points along the invariant line. (The indices of the BCC lattice points corresponding to the O-lattice points are indicated.)

plane in Figure 3.4a, and projected along the invariant line direction in Figure 3.4b. Note the enormous difference in the scales along and normal to the invariant line. Actually, all O-lattice vectors are lying nearly parallel to the invariant line. The spacing of the lines of intersection of the O-cell walls with the habit plane is significant larger than the atomic spacing (for example, 90 vs 3.2 Å). Therefore, it is reasonable to assume that dislocations are formed corresponding to these lines. The dislocation structure in the habit plane, calculated using (3.9-10), consists of sets of effectively parallel lines*; this is consistent with the first property of the invariant line. However, the configuration of the dislocations, i.e. their spacing and direction (always parallel to the invariant line) for a particular orientation relationship are always different from those for the other orientation relationships. Also, the geometry of habit plane changes for the different orientation relationships.

Generally, the O-lattice calculation predicts that three sets of dislocations are needed to accommodate the misfit in the habit plane. It will be shown below that, in addition to the effective invariant line condition, the long

---

* There may be very small angles the between different sets of dislocations, but they are usually much smaller than 1°. For example, the angles are 1.6 x 10^{-5}°, 0.8 x 10^{-5}°, 0.8 x 10^{-5}° respectively between the dislocations with Burgers vectors [1 -1 -1] and [1 1 -1]; [1 -1 -1] and [0 1 0]; and [1 1 -1] and [0 1 0] in the habit plane corresponding to the O-lattice in figure (3.4).

range misfit strain in habit plane could be further reduced if only a single set of dislocations is required to accommodate the misfit in the plane. It is hypothesized that the total strain energy could be reduced if the strained regions are concentrated rather than spread out in an interface. Based on this hypothesis, the optimum orientation relationship can be analyzed.

According to the second property of an invariant line discussed earlier, the invariant line is the zone axis of all "moiré planes". The line of intersection of any "moiré planes" with the habit plane will be in the direction of the invariant line, as the habit plane itself is one of the "moiré planes". The intersection of a "moiré plane" with the habit plane defines a line along which the a plane of reference lattice matches poorly with the correlated plane in the other lattice. Normally, each set of "moiré planes" intersects the habit plane with a particular spacing, except for those related to the planes in the reference lattice in the same zone axis as $(1\ 0\ 1)_\beta$. The details of derivation for proof of this argument are provided in Appendix 2. A general case of an intersection of "moiré planes" with the habit plane is illustrated in Figure 3.5a. In Figure 3.5 the diagrams are oriented such that the invariant line is normal to the plane of paper, and the projection of habit plane is along the horizontal axis.

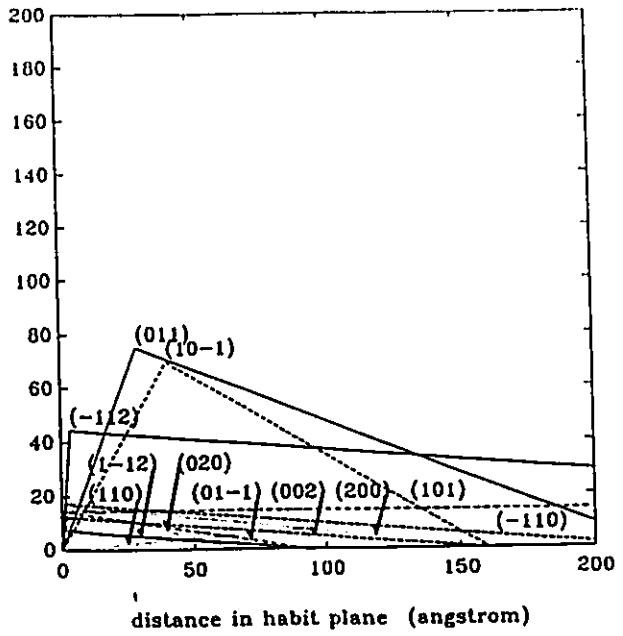

(a)

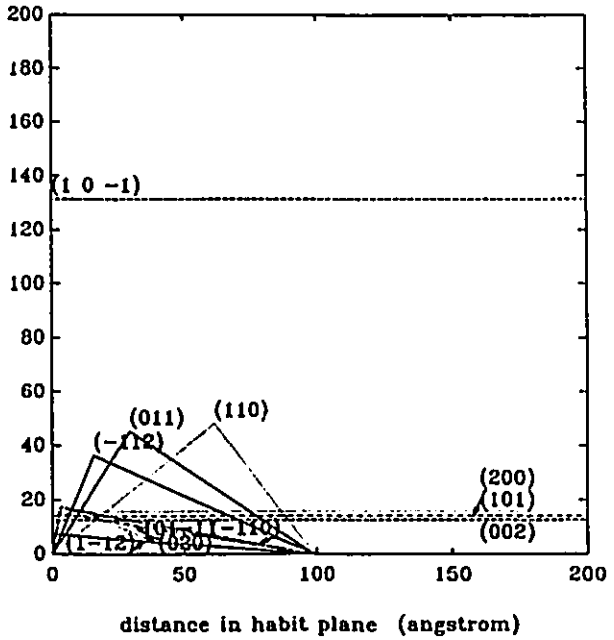

(b)

Figure 3.5 An illustration of "moiré planes" intersecting the habit plane; (a) a general case, (b) a special case for $\theta = -2°$, $\phi = 1.015°$, $\gamma = -0.2900.°$. The indexes of BCC planes related the "moiré planes" are indicated.

Each line radiating from the origin is defined by the vector $OP_i/|OP_i|^2$, (OP_i is defined by equation 3.15), and hence the direction and the magnitude of the vector give the normal and the spacing of a set of "moiré planes". Therefore, the line perpendicular to a radiating line represents the projection of a "moiré plane". Here, only one plane is drawn to represent a set of "moiré planes". The spacing of the lines of intersection of the set of "moiré plane" with the habit plane is defined by the distance from the origin to the point where the representative "moiré plane" intersects the habit plane. In Figure 3.5a, two intersection points could be seen, but there are other two points of intersection which are not shown because they are outside of the scale of the diagram. Supposing all "moiré planes" are plotted by repeating them at their spacing, one could expect the points of the intersection, i.e. the lines of the poorest plane matching, to be fairly spread out in the habit plane. For some special orientation relationships all "moiré planes" related to the low index planes of the reference lattice would intersect the habit plane either with the same spacing or with so large a spacing that the "moiré planes" do not actually intersect the habit plane*. This case is demonstrated in Figure 3.5b, where the points of intersection of many "moiré planes" with the habit plane are superimposed. Therefore the regions of poor

---

* As shown in Appendix 2, such "moiré planes" are shown to be parallel to the habit plane.

plane matching are concentrated in a small area in the habit plane and repeated periodically before the atomic relaxation. It is assumed that such a distribution of plane mismatch would diminish the local misfit strain in the habit plane.

It can be shown (for detail see Appendix 2) that the condition for the superposition of the lines of intersection of "moiré planes" with the habit plane corresponds to a single-set-dislocation configuration in the habit plane. The derivation in Appendix 2 suggests the Burgers vector associated with this set of dislocations to be $[0\ 1\ 0]_\beta$. In addition, the locations of the dislocations are shown to coincide with the positions of the superimposed intersection lines. Generally speaking, with these specially selected orientation relationships, there exists at least one $\mathbf{b}_\beta$, associated with the dislocations, lying in the plane determined by the invariant normal. Then, according to the third property of invariant lines, an O-vector can be solved from equation (3.2), which defines a one-dimensional O-lattice. On the basis of the analysis given in the Appendix 2, the habit plane will contain both this one-dimensional O-lattice and the invariant line. Therefore, the habit plane suggested by the calculation is characterized by highly localized and periodically distributed misfit strain. The misfit in each period could be described by a well defined Burgers vector. It is likely that after atomic relaxation the

misfit could be completely accommodated by a single set of dislocations in the habit plane, which might keep the same geometry of the periodical strain. The orientation relationship corresponding to this dislocation configuration is defined as the optimum orientation relationship. In other words, for the optimum orientation relationship the simplest dislocation configuration is obtained in the habit plane.

Among so many orientation relationships satisfying the effective invariant line condition, available in the vicinity of the Burgers orientation relationship, only a very small number belongs to the optimum orientation relationships. Figure 3.6 gives the angles θ, ϕ and $|\gamma|$ (γ has a negative value when $\theta > -26°$) in the rotation matrices **R1** (3.44), **R2** (3.46), and **R3** (3.45), corresponding to the optimum orientation relationships, and the total deviation angle ρ from the Burgers orientation relationship. ρ is calculated by the following formula:

$$\rho = \arccos(\cos\phi \times \cos\gamma).$$

Even though the possible candidates for a favoured orientation relationship are greatly reduced using this method, we still have many choices for the orientation relationship.

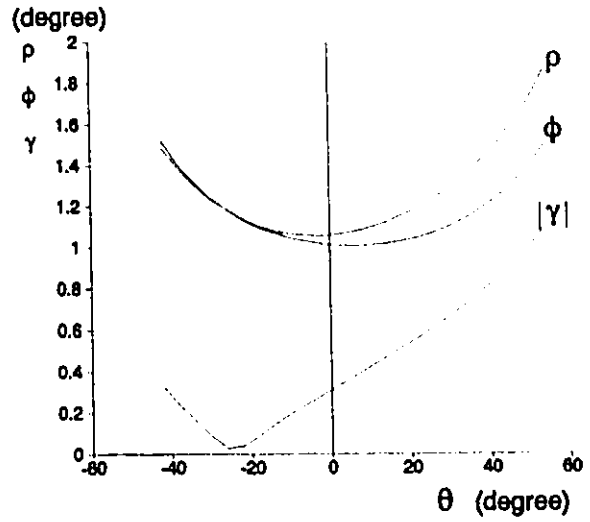

Figure 3.6 Rotation angles corresponding to the optimum orientation relationships.

In order to further limit the choices of orientation relationship, we can narrow the choices by considering the following two factors. Firstly, we can find the orientation relationship for which density of the dislocations in the habit plane is lowest. Secondly, we may look for the optimum orientation relationship with the smallest deviation angle ρ from the Burgers orientation relationship. The dislocation spacing (dsi) and the deviation angles (ρ) of the optimum orientation relationships from the Burgers orientation are plotted in Figure 3.7, where the orientation relationships corresponding to the maximum dsi. and the minimum ρ are indicated by arrows 1 and 2, respectively. The orientation

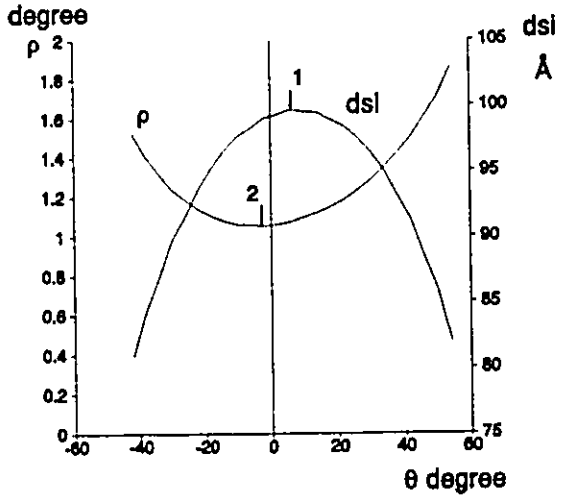

Figure 3.7 The rotations corresponding to the minimum deviation angle, ρ, and the maximum dislocation spacing, dsi..

relationship corresponding to the maximum dislocation spacing is the one when $\theta = 6°$, $\phi = 1.005°$, $\gamma = -0.381°$; while that to the minimum deviation angle from the Burgers orientation is the one when $\theta = -2°$, $\phi = 1.015°$, $\gamma = -0.290°$.

For the first case the density of misfit dislocations is reduced; while for the second case the best local atomic match is probably achieved. By plotting the atomic positions from both α and ß phases at the habit plane, it can be shown (see Appendix 3) that the habit plane is composed of stepped slices of $(1\ -1\ 0\ 0)_\alpha$ or $(-1\ 1\ 2)_\beta$ planes. Consequently, the correlated close-packed directions $[1\ 1\ -2\ 0]_\alpha$ and $[1\ -1\ 1]_\beta$; the c direction in HCP, $[0\ 0\ 0\ 1]_\alpha$, and its counterpart in the

BCC lattice, $[1\ 1\ 0]_\beta$, can all be found lying the habit plane at the atomic scale. While the deviation of these two pairs of directions from each other brings an invariant line between the two lattices, there may be additional short range distortions in the interface as an expense of greatly reducing the average misfit. The favoured orientation relationship is given by a balance of minimizing the dislocation density and the short range misfit strain.

Once the orientation relationship is selected, the geometry of the habit plane and the line direction, Burgers vectors, and spacing of the dislocations in the habit plane can be calculated for the given lattice parameters. The Burgers vector of the dislocations in the habit plane has been determined to be $[0\ 1\ 0]_\beta$, and spacings of dislocations are shown in Figure 3.7. Some results of the calculated habit planes and the invariant lines for different orientation relationships are plotted in the superimposed stereographic projections of the BCC and HCP crystals in Figure 3.8, referred to the BCC lattice. The orientation relationships chosen are for θ = -42°, -26°, -10°, -2°, 6°, 22°, 38°. The corresponding values for the angles ϕ and γ can be found in Figure 3.6. Due to small rotations from the Burgers orientation relationship, the geometry of the habit planes varies slightly, while the directions of the invariant lines change rapidly. When θ goes from -42° to 38° the habit plane

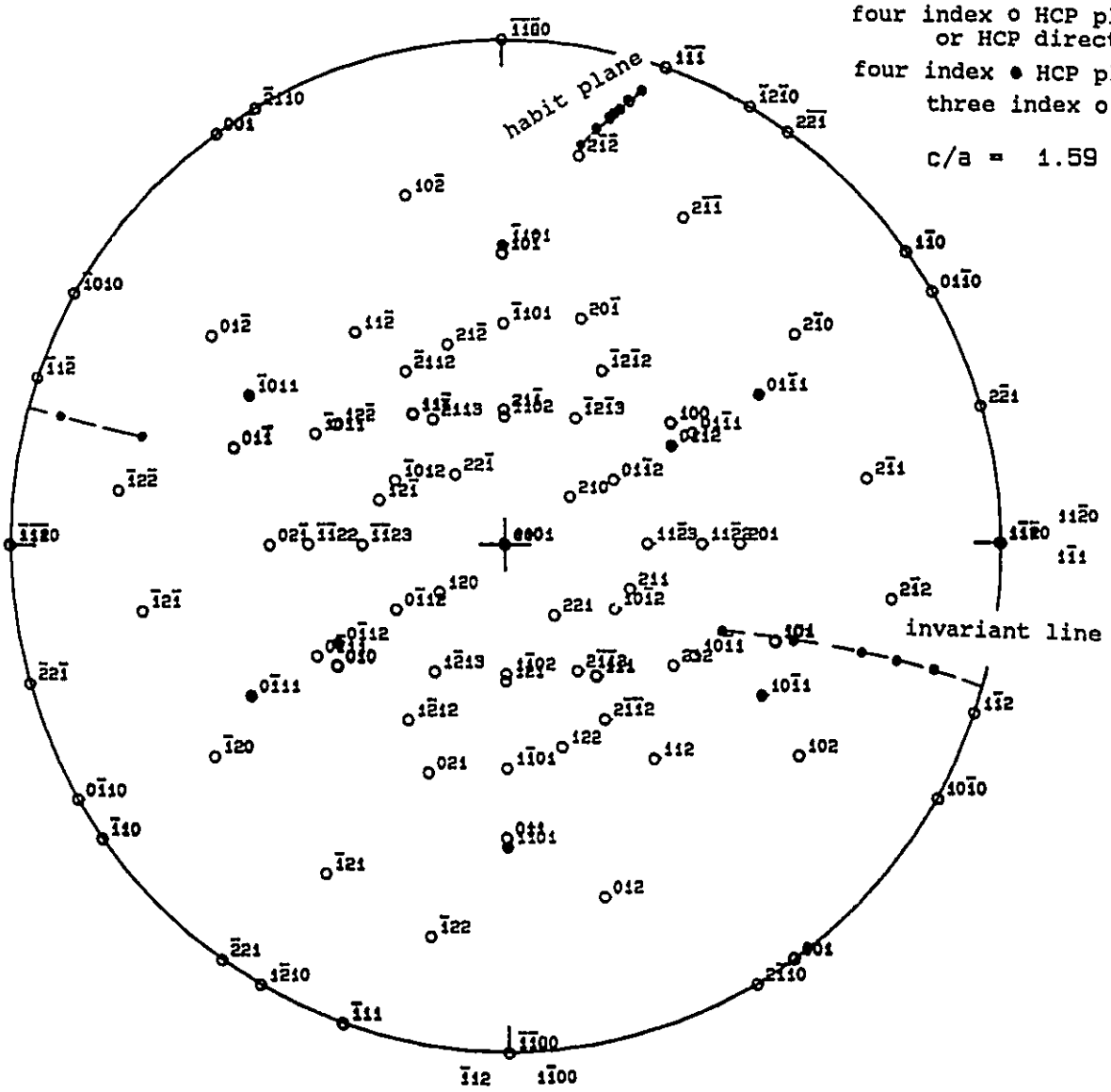

Figure 3.8 The habit planes and invariant lines for different orientation relationships plotted in the superimposed stereographic projections of BCC ([1 1 0]) and HCP ([0 0 0 1]), where the two lattices are oriented by the Burgers orientation relationship.

changes from near $(2\ -1\ -2)_\beta$ toward $(1\ -1\ -1)_\beta$, while the invariant line varies from near $[2\ 1\ 2]_\beta$ to near $[-1\ 2\ -2]_\beta$. Note that the geometry of the habit planes and the invariant lines as well as the orientation relationships corresponding to the two cases for selecting the orientation relationship (θ = -2°, 6°) are very close, so it is not easy to determine experimentally which of the two factors is more important. However, since they are so close, we may regard this small range of orientation relationships as the orientation relationship with which the interphase boundary will be in low interfacial energy states and hence favoured by nature.

An example of detailed results of calculation is given below. The orientation relationship is chosen to correspond to the rotations defined by equations (3.44-3.47) for θ = -2°, ϕ = 1.015°, γ = -0.290° corresponding to the one indicated by arrow 2 in Figure 3.7. Having obtained the transformation matrix from equation 3.47, one could calculate $\mathbf{OP}_4^*$ by inputting $\mathbf{b}_{\beta 4}^*$ defined in (3.12), into equations (3.13) and (3.15). Then the habit plane determined by the $\mathbf{OP}_4^*$ is

$$\mathbf{OP}_{\beta 4}^* = (3\ -2.1626\ -3.0521)_\beta$$

referred to the BCC lattice, or

$$\mathbf{OP}_{\alpha 4}^* = (-3\ 4.0543\ -1.0543\ 0.7172)_\alpha$$

referred to the HCP structure. The direction of the dislocation lines in the habit plane, i.e. the direction of the invariant line is

$$u_{\beta 6} = [2 \ -1.0247 \ 2.6919]_{\beta}$$

referred to the BCC lattice, or

$$u_{\alpha 6} = [4 \ 1.3709 \ -5.3709 \ 1.0839]_{\alpha}$$

referred to the HCP structure. This direction is obtained by finding the eigenvector of the transformation matrix, which corresponds to the eigenvalue almost equal to one. Since an optimum orientation relationship is used, the habit plane contains a single set of dislocations with $[0 \ 1 \ 0]_{\beta}$ as the Burgers vector. The spacing of the dislocations could be obtained by applying relation (3.10) for i = 6. The spacing is found to be 9.9 nm. The angle between the dislocation lines and the Burgers vector is 73.0°; thus the dislocations will be of mixed character. The angle between the Burgers vector and the habit plane normal is 63.2°. Therefore the dislocations may carry the strain outside of the habit plane. It should be kept in mind that the O-lattice calculation takes the three-dimensional lattice mismatch into account, while the mismatch in a planar interface is mainly of two dimensional character. Based on the assumptions given in Section 3.1, the geometric

result presented here is less likely to be effected by the relaxation of atoms near the boundary. However, it is not clear how the atoms near the boundary react upon the release of the constraint normal to the interface, which was assumed to exist in the initial calculation. This may influence the actual displacement field around the dislocations.

CHAPTER 4

EXPERIMENTAL STUDIES

4.1 Alloy Selection

In a recent study of a Zr-2.5 wt% Nb alloy, Perovic and Weatherly (1988) observed some interesting structures in the HCP/BCC (α/β) interphase boundaries. While the orientation relationship between the two phases and the Burgers vectors associated with the dislocations were determined in their work, the interpretation of the interfacial structures needs further elucidation. To obtain a clear understanding of the interfacial structures, an extensive study of the same alloy was carried out in the present work; the experimental results will be compared to the predictions of the model presented in Chapter 3.

A sample of as-received Zr-2.5 wt% Nb alloy* (the major impurity is 900-1300 ppm oxygen), about 2 x 1 x 1 cm^3 in

* The alloy was provided kindly by Dr. V. Perovic of Ontario Hydro Research.

size, was cut with a low-speed diamond saw into slices about 0.5 mm thick. The slices were then separately sealed, in evacuated quartz capsules for further heat treatment.

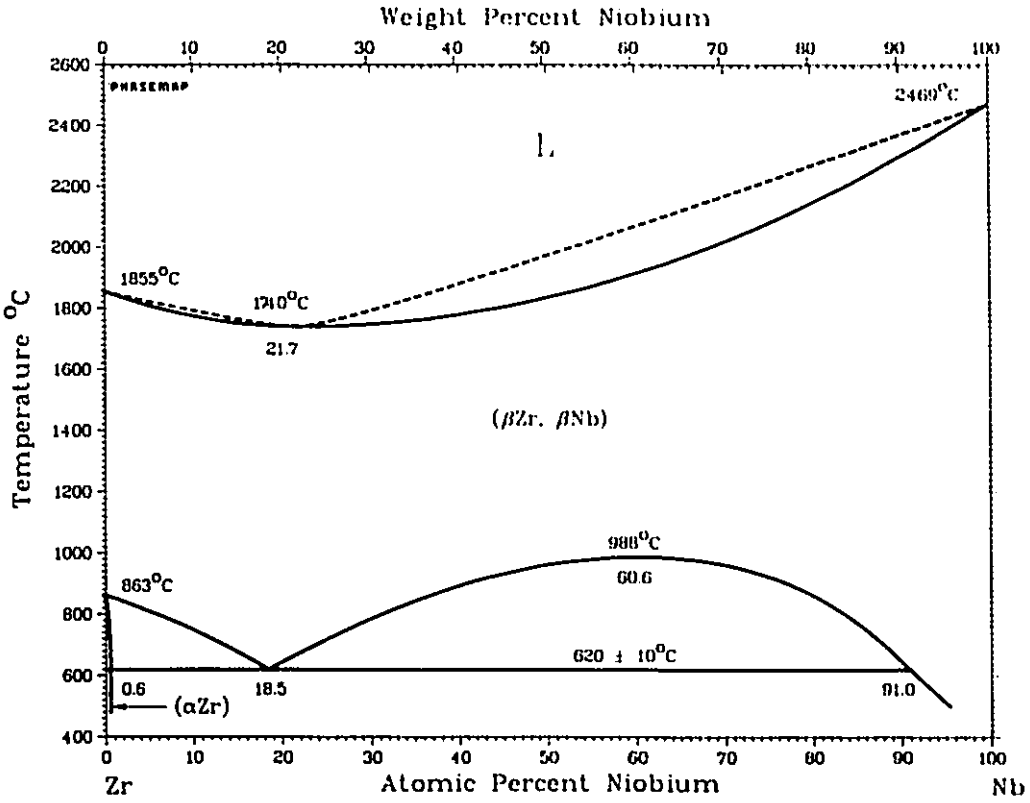

Figure 4.1 The Zr-Nb equilibrium diagram

4.2 Heat Treatment

As can be seen from the Zr-Nb equilibrium diagram (Figure 4.1, after Abriata and Bolcich, 1982), the pro-monotectoid α phase forms when the ß phase containing 2.5 wt% Nb is cooled below the ß/α+ß solvus line. According to Hehemann (1972), if the ß phase contains more than 6 wt% Nb martensite formation could be suppressed on quenching. As precipitation of α enriches the ß in Nb, after a sufficient fraction of α is precipitated, it is possible to retain at room temperature the α/ß interfaces formed at high temperature. In order to obtain a near-equilibrium α/ß interface for this study, the basic heat treatment steps should include a solution treatment in the ß phase field, in-situ cooling to give an isothermal transformation in the α + ß region, as suggested by Perovic and Weatherly (1988), followed by fast cooling.

All specimens were solution treated for one hour at temperature 1000° ± 10° C at the ß region, and then isothermal reacted in the α + ß field at various temperatures in the range of 650°C - 850°C. Some specimens were also treated isothermally by two-temperature steps. The martensitic transformation could be prevented by isothermal heat treatment below 770°C followed by a quench. However, this quench did not prevent the formation of the ω phase. The metastable ω phase

is a product of a diffusionless transformation of alloys (of critical Nb content) on quenching from the ß phase (Cometto, et al. 1965). When small ω phase particles are present, the Kikuchi lines from the ß phase regions are diffuse, and the contrast from the ß phase renders the investigation of the structures at the α/ß boundaries very difficult. When the volume fraction of ω is very large, the Kikuchi lines of ß could be almost totally replaced by those from the ω phase (for example, in the 770°C isothermal treated specimens). In order to obtain a clear TEM image of interfaces and to be able to identify the ß orientations during tilting the specimen by following the BCC Kikuchi map, the effect of ω should be diminished as much as possible. The TEM diffraction patterns in the present work have indicated that the lower the isothermal transformation temperature (i.e. the greater the enrichment of ß in Nb), the lesser the influence of the ω phase. This observation is consistent with Chang and Sass's (1976) work. In their study, the ω domains were observed to decrease in size as the Nb content increases. To minimize the effect of ω phase on the TEM interfacial study, the isothermal transformation temperature must be low. For this reason, the TEM study was concentrated on specimens isothermally transformed at 650°C, or transformed by two steps, the second of which was at 640°C. Any temperature change in a heat treatment was accomplished by transporting the specimens quickly from one furnace to an adjacent one. After the

isothermal transformation specimens were quenched by breaking the quartz capsule in iced water.

4.3 SEM and TEM Specimen Preparation

The specimens were initially chemically thinned using a solution of 45 vol.% HNO_3, 45 vol.% H_2O, and 10 vol.% HF to ~0.15mm thickness. These specimens were examined in a SEM (Philips 515). For TEM study, the chemically thinned specimens were punched into 3 mm diameter discs. The discs were lightly ground to 0.05-0.08 mm thickness with 600 grit emery paper to reduce the uneven thickness between α and ß phases left after chemical thinning. The final thinning of the TEM specimens was accomplished by electrochemical twin-jet polishing (with a E.A.F.). The electrolyte used was a mixture of (70%) perchloric acid 6 vol.%, butyl cellosolve 34 vol.%, and methanol 60 vol.%. The viscous butyl cellosolve was added to the conventional 10% perchloric acid solution in order to lessen the preferential polishing of the α phase. The optimum electropolishing conditions were achieved at a voltage of 7 ± 0.5 v (corresponding to a current of 40 ± 5 mA), at -40° ± 5°C.

4.4 TEM Analysis

A Philips CM12 TEM operating at 120 kV, equipped with a double tilt holder was used in this study. It is stressed that proper electron optical configuration were obtained each time.

The rotation between the image and the diffraction pattern was calibrated using MoO_3 crystal. Because of variations in the high tension supply and other factors that might occur to influence the path of the electron beam, the rotation was also checked whenever needed by using an overfocussed small spot size beam in the image mode*. Such an operation brings to the screen the electron intensity distribution above the Gaussian-image plane, which carries the electron diffraction information. This method was consistent with the one using MoO_3, though the accuracy of the former method (±2°) is not as good as the latter (±1°). However, the uncertainty of 180° involved in the result given by the latter method could be eliminated by the former method.

---

*The method was suggested by Dr. Y. Lin, Bell Northern Research, Ottawa.

4.4.1 Indexing Diffraction Patterns

The primary method used for indexing diffraction patterns was Kikuchi maps. Fully-indexed Kikuchi maps for HCP and BCC crystals were constructed according to the Kikuchi patterns available in the literature (for example, in Edington 1974). With the aid of these Kikuchi maps, Kikuchi lines observed in a convergent beam diffraction pattern could be indexed without specifying the particular indices from families of planes. The conventional method for indexing diffraction patterns was also used, especially for selected area diffraction patterns. The measured angles and the length ratios between diffracting vectors were compared with the standard patterns (Edington 1974). Since the data for HCP vary with c/a ratio, a table of the ratios and angles for c/a=1.59 has been computed. Sometimes, the results obtained from the Kikuchi line technique were also checked by this method.

Specific indices could be obtained by recognizing how the planes and directions from the α and ß phase are related with respect to the particular variant of orientation relationship between them (Figure 3.8). Due to the two fold symmetry of $[0\ 0\ 0\ 1]_{\alpha}/[1\ 1\ 0]_{\beta}$ axis (refer to Figure 3.8), there are two choices in indexing many planes and directions including the geometry of the interface. However, once the

reference for the interface is arbitrarily chosen*, other indices may be consistently assigned. Hence, it is possible to determine all indices uniquely with reference to the geometry of the interface.

An example of indexing a specific set of planes belonging to $\{1\ -1\ 0\ 1\}_\alpha$ is given below. There are six sets of planes in the $\{1\ -1\ 0\ 1\}_\alpha$ family. The first three indices can be fixed (except for their signs), from their relationships with the corresponding planes in the ß phase: $(1\ -1\ 0\ \pm1)_\alpha$ are nearly parallel to $\{1\ 1\ 0\}_\beta$, while $(1\ 0\ -1\ \pm1)_\alpha$ and $(0\ 1\ -1\ \pm1)_\alpha$ are loosely related to $\{1\ 1\ 0\}_\beta$ and $\{1\ 0\ 0\}_\beta$ respectively. Provided the invariant line is close to $[1\ 0\ 1]_\beta$ instead of $[0\ 1\ -1]_\beta$, a $(1\ -1\ 0\ \pm\ 1)_\alpha$ spot must be indexed as $(-1\ 1\ 0\ 1)_\alpha$ ($\sim\!/\!/ (1\ 0\ -1)_\beta$)) if a set of regular defect lines (invariant line) is seen to lie nearly in this plane; otherwise they should be indexed as $(1\ -1\ 0\ 1)_\alpha(\sim\!/\!/(0\ 1\ 1)_\beta)$.

4.4.2 Determining the Orientation Relationship

The zone axis of interest to the orientation relationship measurement is the $[0\ 0\ 0\ 1]_\alpha$ ($\sim\!/\!/[1\ 1\ 0]_\beta$), because the centre of $[0\ 0\ 0\ 1]_\alpha$ zone axis was easier to orient than the zone axes containing $(0\ 0\ 0\ 1)_\alpha$ ($\sim\!/\!/(1\ 1\ 0)_\beta$).

---

* They were chosen related to the positive sign of the angle ϕ, or the range of θ (0-180°) in Chapter 3, which were also arbitrarily determined.

Both convergent beam diffraction (CBD) patterns and selected area diffraction (SAD) patterns were used to determine the orientation relationship. In most cases a small beam spot size spot (200 nm) was used for CBD patterns. The CBD patterns were usually taken from both adjacent phases. Sometimes they were also taken from the boundary itself to determine if two sets of planes in the two phases were parallel. SAD patterns with the selected area aperture, 10 μm in diameter, (corresponding to a size of 0.24 μm in the specimen) were mainly used to determine the angles between two diffracting vectors. However, caution must be taken in such analysis, because this angle is usually so small that it could be of the same order of magnitude as the error that might occur due to the elongation of the diffraction spots.

4.4.3 Measuring the Geometry of the Interfaces

The habit plane between the α and ß phases is the preferentially oriented interface characterized by a set of parallel dislocations. The measurement of the habit plane was usually made on the flat portion of the broad face boundary, which is oriented edge-on (refer to Figure 5.19, 5.20). The edge-on habit plane was recorded at various orientations so that the measurements could be made convincing on the basis of many observations.

The direction of a regular set of defect lines has been measured using two methods. One method was applied when the lines could be oriented edge on. In this case the line direction was given by the beam direction recorded in the diffraction pattern. The other method was the trace analysis method (Edington, 1974). Various projections of the lines over a large range of orientations were recorded together with the diffraction patterns. The zone axis of all the planes, in which the projections of the lines were lying, gave the direction of the lines. The information obtained for the habit plane helps in determination of the direction of defect line, since the lines are contained in the habit plane.

4.4.4 Determining the Burgers Vectors

The most widely used method to determine Burgers vectors is the so called $\mathbf{g}\cdot\mathbf{b} = 0$ invisibility criterion. Here $\mathbf{g}$ is the diffracting vector, $\mathbf{b}$ the Burgers vector; unless otherwise specified this nomenclature will be used throughout this thesis. For complete invisibility of a general dislocation, the products $\mathbf{g}\cdot\mathbf{b}$, $\mathbf{g}\cdot\mathbf{b}_e$, and $\mathbf{g}\cdot\mathbf{b}\times\mathbf{u}$ must all be zero (Hirsch et al. 1977, Head, et al. 1973). Here $\mathbf{b}_e$ is the edge component of the Burgers vector, $\mathbf{u}$ is a unit vector in the direction of the dislocation line. This method was applied to the interfacial dislocation studies by many researchers (for examples, see review by Pond, 1984). Strictly speaking,

these criteria are only valid in elastically isotropic materials. According to the work of Fisher and Alfred (1968), HCP Zr is nearly elastically isotropic at room temperature (The data for BCC Zr is not available). It is reasonable to assume that this elastic property of pure Zr could be applied to the Zr-2.5 wt% Nb alloy, for the α phase contains very little Nb. Therefore, the $\mathbf{g}\cdot\mathbf{b} = 0$ invisibility criteria will be used in the present work. Because usually only faint residual contrast may occur when $\mathbf{g}\cdot\mathbf{b}=0$, and $\mathbf{g}\cdot\mathbf{b}_e$ and $\mathbf{g}\cdot\mathbf{b}\times\mathbf{u}$ are $\neq 0$, the '$\mathbf{g}\cdot\mathbf{b}=0$ effective invisibility' criterion has been used intensively by researchers. Here precaution will be taken in analyzing the defect images so as to recognize 'effective invisibility'.

The imaging condition was carefully controlled to obtain simple diffraction conditions. Diffraction reflections from both the α and ß phases were used for the contrast study. The optimum contrast of the defects was usually obtained in a dark field image, often when the two beam condition was satisfied in the ß phase. Usually, two working conditions were set up for the contrast study on interfacial structure. In both conditions, there was at least a two beam or systematic diffraction condition established in one of the phases. At some particular orientations, a pair of correlated planes in both phases could be at the Bragg condition simultaneously. The contrast effects in such a case would be close to that in

a single crystal. The result of a $\mathbf{g}\cdot\mathbf{b}$ analysis is then relatively reliable. However, this situation was not often obtained. The other condition was met more frequently. In this working condition, only one phase, either α or ß, was allowed to be in the two beam or systematic diffraction condition. The diffraction in the other phase was controlled as far as possible so that there was no strong reflection excited. Due to foil bending, normally the deviation from the two beam condition was not constant for one boundary. The image condition was adjusted near the two beam condition so that the structure in the boundary was best shown in dark field. At the same time the diffraction condition corresponding to the final adjustment was checked each time to ensure that the one of the above working conditions was maintained. Only low index $\mathbf{g}$ reflections were used in $\mathbf{g}\cdot\mathbf{b}$ analysis to avoid the confusion in determining the effective invisibility which may be caused by the weak image due to large index $\mathbf{g}$ reflections.

4.4.5 Obtaining Lattice Parameters

Two important factors limiting the accuracy of electron diffraction measurements of lattice spacing are: the difficulty in locating the centre of diffraction spots and the variations in the diffraction constant, λL, namely, in the high tension supply and the specimen position (Hirsch et al. 1977). An attempt has been made in this study to diminish the

errors due to these factors.

Sharp Kikuchi Lines of high index planes were taken, so that the centre of the diffraction spots could be better defined. The photographic plates were measured in a Vickers Projection Microscope; the uncertainty in the readings was small compared with the data obtained by using a magnifier (0.01 mm vs. 0.1 mm). In addition, the effect of beam tilt could be allowed for in the calculation, if the correct camera length, L, is given. Fortunately, L could be self-calibrated when a diffraction pattern contains two zone axes of known intersecting angle. With this information, high accuracy could be obtained in the ratios of the lattice parameters: c/a of the HCP lattice and the ratio a_β/a_α from the BCC and HCP lattices. This is important in the present work, because these ratios are the main input in geometrical calculations. The individual values of the lattice parameters, which require additional information on the accelerating voltage, are only used to determine the spacing of dislocations. The relative uncertainty in measuring the dislocation spacing was about 5%, while that in the accelerating voltage was about 2% in the TEM used. Therefore, the total errors associated with in the absolute value of the lattice parameters are acceptable for the purpose of this work. An example of obtaining c/a for the α phase is given in Appendix 1.

CHAPTER 5

EXPERIMENTAL RESULTS

5.1 Morphology of α Precipitates and General Features of the α/ß Boundaries

5.1.1 SEM Study

The structure in all specimens observed using SEM is dominated by intragranular needle-shaped α precipitates, known as the Widmanstätten structure. Generally a small number of allotriomorphs exists at ß grain boundaries. An example of an α precipitate structure is shown in the SEM micrographs (Figure 5.1), where the darker phase is α and the lighter one is ß. Due to the particular heat treatment temperature (650°C), the volume fraction of α precipitates was high, resulting in the microstructure consisting of α precipitates partly surrounded by the ß matrix. Figure 5.1a illustrates a microstructure developed for 20 minutes at 650°C. A relatively coarse structure was developed for 49 hours at 650°C * (Figure

* Many observations were made on specimens isothermally treated for 49 hours at 650°C; unless otherwise specified, the micrographs shown in this chapter are taken from this specimen.

5.1b; note the difference in magnification). After prolonged isothermal heat treatment the Widmanstätten structure is still retained; this suggests a strong anisotropy of interface energy.

However, since many interfaces in the specimen are α grain boundaries, the effect of the α grain coarsening could be confused with that of α precipitate ripening. To avoid any such confusion some specimens were treated by two steps: first at a rather high temperature (845°C) for two days, to let α precipitates grow while completely surrounded by ß; then at 650°C for 20 minutes, to retain ß phase to room temperature by producing more α precipitates. Figure 5.2 shows large α precipitates, grown at the higher temperature, together with smaller α crystals, precipitated at the lower temperature. The evidence that large α precipitates retain their needle shape viewed in two dimensions again implies the existence of low energy interphase boundaries. In Figure 5.2 the broad faces of both types of α are similarly oriented. This important fact suggests that the morphology of α freshly precipitated from ß may be also influenced by the anisotropic interfacial energy. The assumptions made in section 3.1 were partly due to such observations.

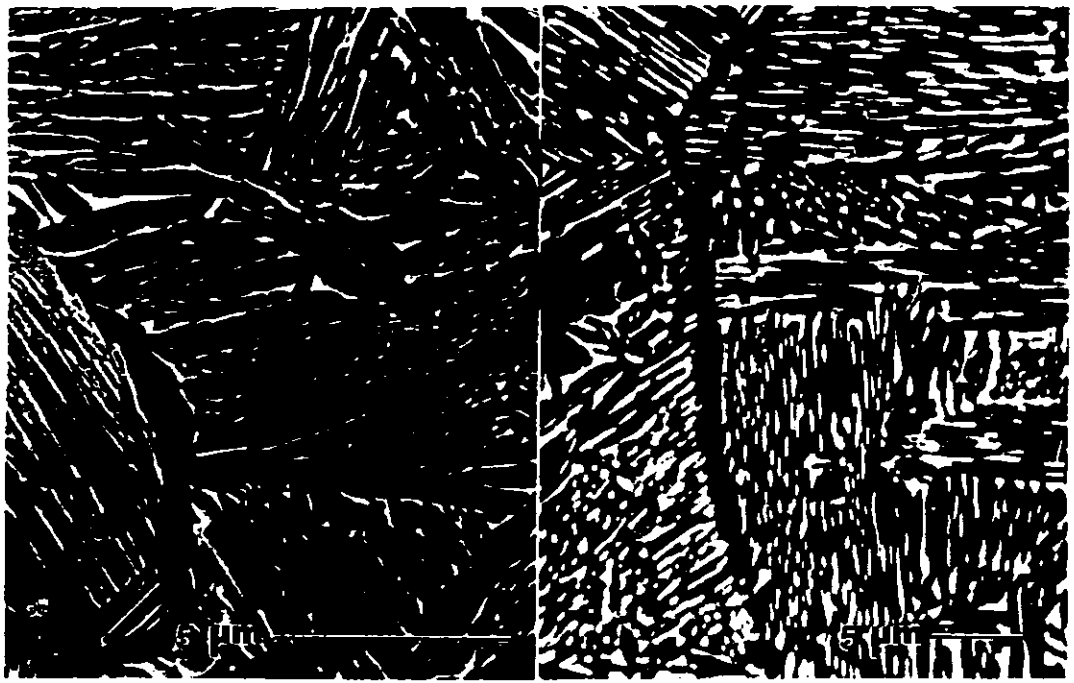

(a) (b)

Figure 5.1 SEM micrographs of α precipitates corresponding to different heat treatments: (a) 20 min at 650°C, (b) 49 hours at 650°C.

Figure 5.2 SEM micrograph of α precipitates from a two step precipitation treatment: 2 days at 845°C, followed by 20 min at 650°C.

5.1.2 TEM Study

In contrast to the two-dimensional information from SEM, TEM provides a technique to obtain three-dimensional information: interfaces could be viewed by being projected in various directions. A TEM microstructure of α precipitates is given in Figure 5.3, where the dark phase is ß and the light one is α. Almost all α precipitates analyzed within a given specimen were from a single ß grain, since the usable region in a TEM specimen was small compared to the size of ß grains. Because of the limitation of a thin foil, it was impossible to study the interface continuously around a whole α precipitate, which was much larger in size than the thickness of the foil. However, it was still possible to study interphase boundaries projected in various orientations within a specimen with the aid of double tilt device, due to the α precipitates being related to the ß grain by many variants of orientation relationship.

Based on the experimental observations, it could be postulated that all α precipitates have a similar morphology. The apparent difference in the shape of various α precipitates would then be due to sectioning effects. This implies that all of the interphase boundaries have developed according to a similar rule. With this postulation, we were able to deduce the general features of the morphology of an α precipitate

from the projections of many α particles taken from various crystallographic orientations.

It was observed that interfaces of a particular orientation tended to be much broader than others. An example is given in Figure 5.4, where the interface apparently preferred to lie at a certain orientation, indicating the existence of a habit plane between α and ß phases. However, a large area of perfect habit plane could not exist. The broad faces of α precipitates could be used for studying the habit plane, since they are composed of the habit plane predominantly. An example of the structure in a broad face boundary is given in Figure 5.5. The interfacial structure is dominated by a set of regularly-spaced parallel lines. Such a feature has been observed in broad face boundaries using various operating reflections, suggesting that the observed lines are the structural elements of the boundaries, i.e. they are interfacial dislocations*. Furthermore, this principal dislocation array was the only line feature that could be seen consistently from all broad face boundaries studied. Consequently, this set of dislocations could be considered as the characteristic feature of the habit plane. The spacing of the principal dislocations was measured as 9.5~10 nm, independent of the operating reflection. This spacing does not

---

*As already assumed early in section 3.1, interfacial dislocations could be associated with steps.

seem very sensitive to the heat treatment applied.

The appearance of the line features in an interface was very responsive to the change of the local orientation of the interface. When an interface slightly deviated from the ideal habit plane, irregular line features developed. In Figure 5.5, the irregular contrast variation intersecting the parallel dislocations and the interaction of line features in the centre part of the boundary are seen corresponding to the variation of the interface orientation.

When an interface is tilted strongly away from the habit plane, two typical features are found depending on the particular orientation of the interface. If the interface is rotated about the direction of the principal dislocations in the broad face boundary, the interface will still contain parallel lines along the rotation axis. Figure 5.6 shows a ß particle surrounded by α phase on three sides. Probably, the ß particle is bordered on each side with a different α precipitate, but these α precipitates have almost the same orientation relationship with the ß phase. The dislocations visible within α in Figure 5.6b indicate slight misorientation between α grains. The boundary surrounding the ß consists of two nearly parallel broad faces and one face at the edge of the ß (the edge face), inclined strongly to both of the broad faces. In Figure 5.6a, we see similar structures in the two

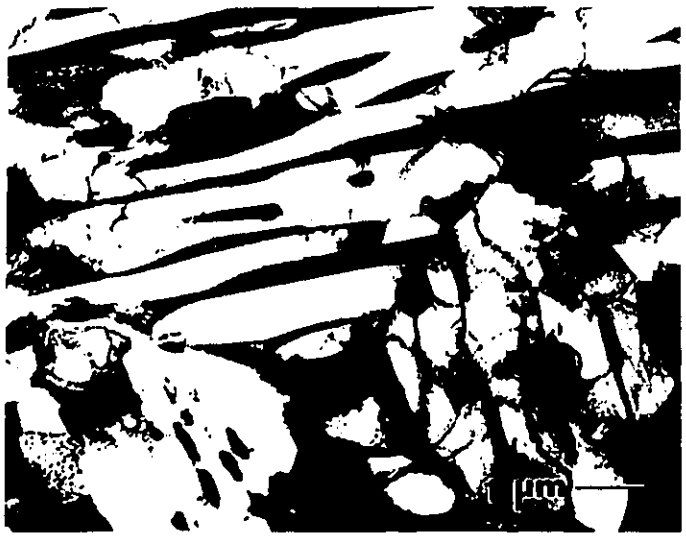

Figure 5.3 TEM micrograph of α precipitates.

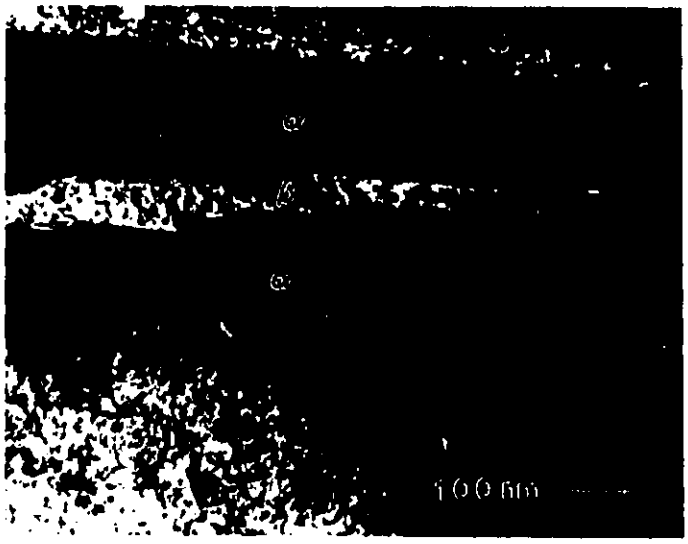

Figure 5.4 An interface showing the existence of the habit plane between the α and ß phases.

Figure 5.5 Dark field image of structure in a broad face boundary $g=(0\ 0\ 0\ 2)_{\beta}$. The specimen was treated 2 days at 740°C, followed by 1 hour at 640°C.

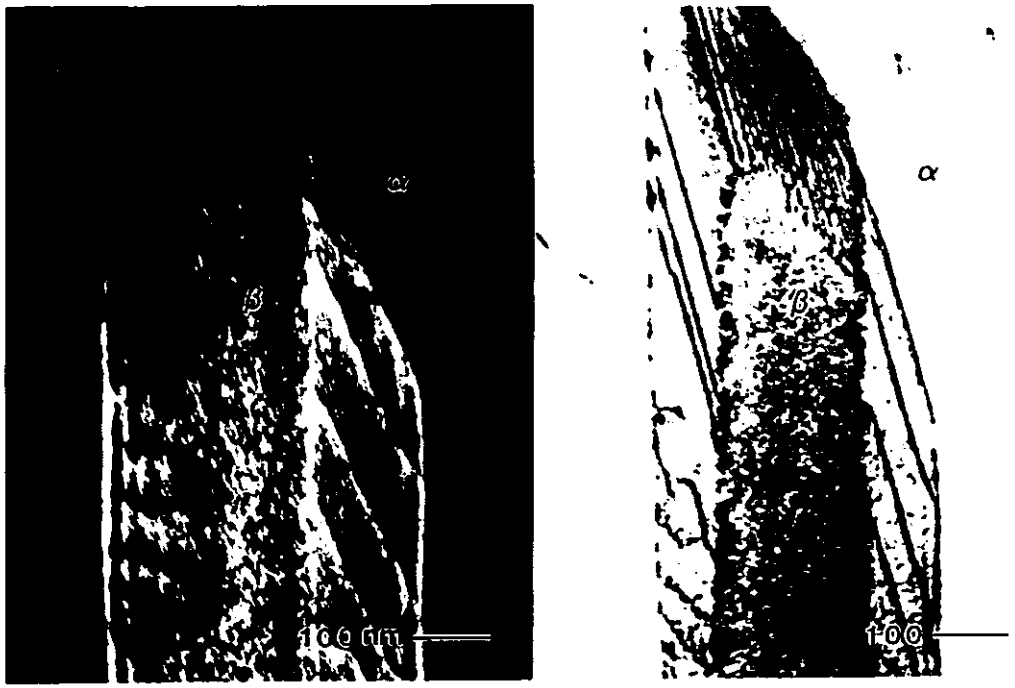

(a) (b)

Figure 5.6 The parallel line structures in both the broad and edge face boundaries; (a) $g = (0\ 1\ -1)_{\beta}$, (b) $g = (1\ 0\ -1)_{\beta}$. The specimen was treated 2 days at 740°C, followed by 1 hour at 640°C.

broad face boundaries, including the principal and the irregular dislocations. The contrast of the structure in the edge face boundary is different from that in the broad face boundaries. The structure in the edge face boundary was better imaged in Figure 5.6b. Though the principal dislocations in the broad face boundaries were invisible in this case, the visible irregular line features in the broad face boundaries serve as a helpful reference to show the directions of the parallel lines in both the broad and edge face boundaries are parallel. The parallelism relationship of lines in the two types of boundaries has been obtained at various orientations by using different operating reflections. This indicates that the parallelism holds in three dimensions and that those linear features in the edge face boundaries are also the structure elements of the boundaries. Although both the broad and edge face boundaries contain parallel lines, it was not difficult to distinguish these two types of faces. Besides the differences in the orientations of the boundary planes and the contrasts of the interfacial dislocations, the difference in projected width provided a fast way to distinguish them. The projected width in the direction perpendicular to the dislocations in the broad face boundary has been observed to be consistently much larger than that in the edge face boundary, especially in the specimens retaining relatively larger ß particles. However, since these α precipitates were only partly bounded by ß, it was difficult to estimate the

actual ratio of the lengths in the two directions.

The structure in the edge face boundary is more complicated than that in the broad face boundary. Besides the structure shown in Figure 5.6b, lines of very fine spacing (1.5 ~ 2 nm) were frequently observed in the edge face boundary when a $(0\ 1\ -1\ 0)_\alpha$, or $(1\ 0\ -1\ \pm1)_\alpha$ operating reflection is excited. A typical feature of the very-finely-spaced lines is shown on the right side of Figure 5.7. On one hand, these lines could be interpreted as moiré fringes, because the width and the spacing of these lines could be in agreement with the periodic contrast and the geometry developed in moiré fringes. On the other hand, some observations indicated that these lines seemed to be associated with the fine steps in the broad face boundary, as can be seen in the centre part of Figure 5.7. Another example of the finely spaced line features is given in Figure 5.8 where the edge face boundary is lying nearly parallel to the foil. The fringes curve at the edge of the boundary (arrowed), as if each fringe is associated with an interfacial step.

Generally, the edge face boundaries do not lie perpendicular to the habit plane. This edge face boundary seemed to have a preferential orientation. This is illustrated in Figure 5.9 when the electron beam was approximately along the parallel interfacial dislocations. The large steps, which

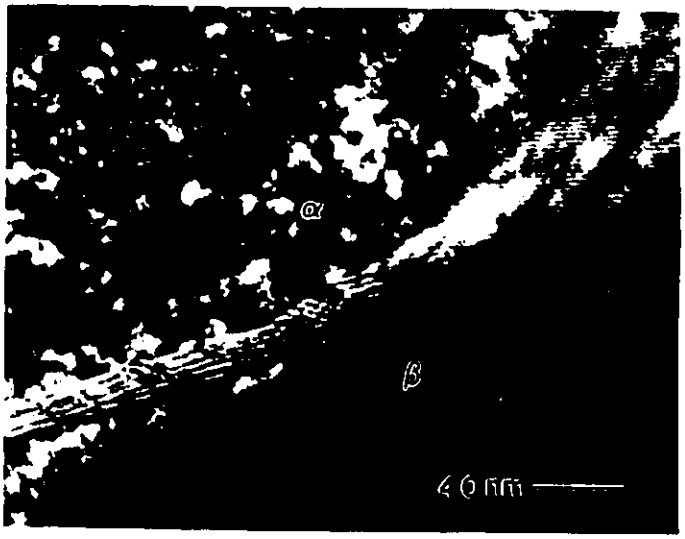

Figure 5.7 Fine steps in a broad face boundary and finely spaced lines in an edge face boundary, $\mathbf{g} = (0\ 1\ -1\ 0)_{\alpha}$. The specimen was treated 2 days at 770°C, followed by 1 hour at 640°C.

Figure 5.8 The curvature of fine lines in an edge face boundary $\mathbf{g} = (1\ -1\ 0)_{\beta}$; the specimen was treated 20 min at 650°C.

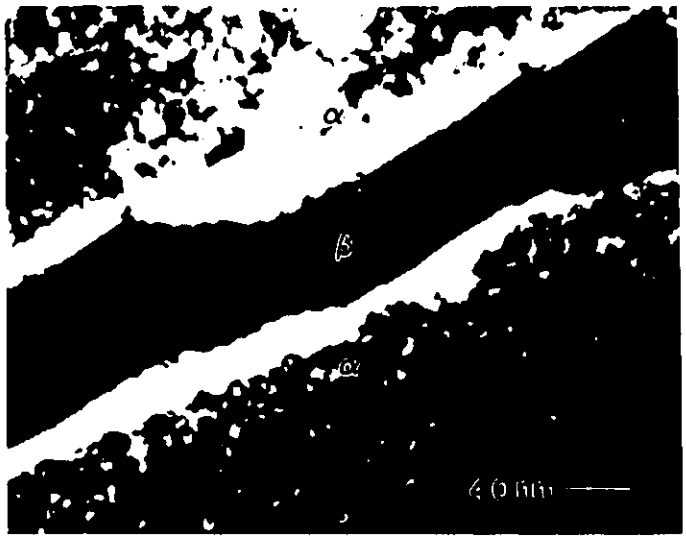

Figure 5.9 An interface viewed along the parallel interfacial dislocations (dark field, g = $(1\ -2\ 1\ 2)_{\alpha}$); the specimen was treated 20 min at 650°C.

could represent the edge face boundary, were found to lie nearly parallel to each other. However, facets of the broad face boundary still remain flat or nearly flat, with occasionally small perturbations, which could be explained as either fine steps or contrast caused by the strain field associated with the dislocations in the broad face boundary. The smallest step observed in the broad face boundary was ~1.5 nm high.

Normal to the parallel linear features in either the broad or the edge face boundaries, there exists another type of boundary with very complicated dislocation network. The upper part of the interface shown in Figure 5.10 is a broad face boundary; while the lower part is a boundary nearly normal to the characteristic dislocations in the habit plane. The network appears to consist of two sets of dislocations. If one observed closely the network near the parallel dislocations, one could see a honeycomb structure formed by three sets of dislocations. Such a honeycomb structure can be seen better in Figure 5.11. This type of boundary is normally curved. Actually, a network would be developed wherever the interface is deviated from the zone axis defined by the direction of the dislocations in the habit plane, as already seen in the centre part of Figure 5.5.

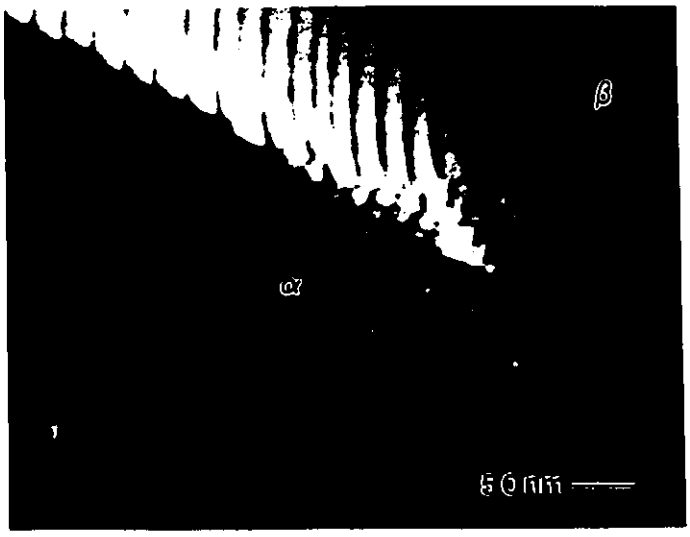

Figure 5.10 A network of dislocations at a boundary nearly perpendicular to the principal dislocations in the broad face boundary, g = $(-1\ 1\ 2)_\beta$; the specimen was treated 2 days at 770°C, followed by 1 hour at 640°C.

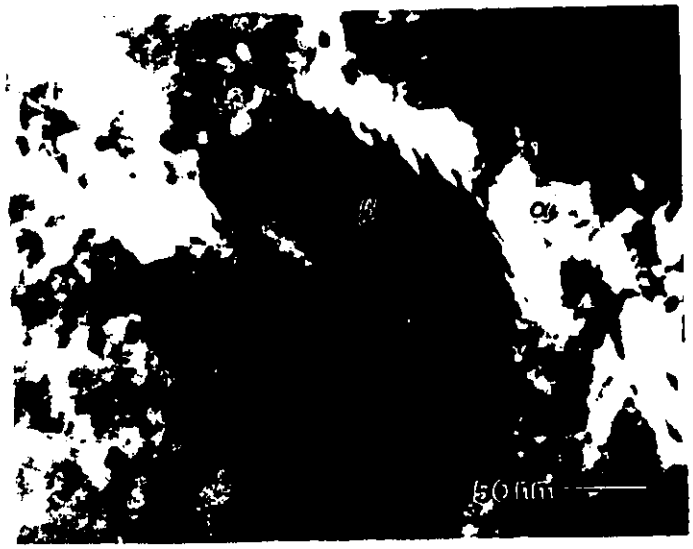

Figure 5.11 A honeycomb structure in a boundary nearly perpendicular to the principal dislocations in the broad face boundary (g = $(1\ -2\ 1\ 0)_\alpha$).

From the observations of different part of boundaries projected in various orientations, a sketch of an α precipitate could be drawn (Figure 5.12). Roughly speaking, an α precipitate can be described as a plate, or a lath, defined by three pairs of faces: the broad faces, which are nearly parallel to the habit plane; the edge faces, which represent the boundaries rotated from the habit plane about the direction of the principal dislocations in the broad face boundary; and the end faces, which are parts of the boundary covering the tips of the α plate. The dimensions of an α precipitate evaluated along the parallel dislocations in the broad face boundary appears much larger than that normal to them. The ratio of dimensions was difficult to obtain due to the impingement of α grains.

The general features of the interface and their contrast effects do not seem to vary corresponding to the particular heat treatment applied to the specimen. However the size of α precipitates, or the particles of remains of the ß phase may change due to different heat treatments.

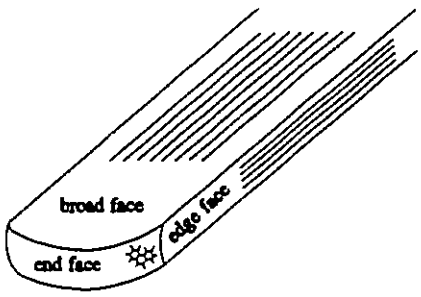

Figure 5.12 A sketch of an α precipitate.

Computer calculation further confirmed the observed morphology. A plate surrounded by parallel lines along its longest axis was plotted by using the measured geometry data of the plate (the data are given in the later sections). Given the normal, the thickness of the foil and the direction of the electron beam, the projection of the boundary of an α plate could be plotted. The comparisons were made on the angles between the trace of the boundaries and the line features, and the relative thicknesses of the broad and edge faces showed good agreement between the experimental observations and the computer simulations.

The interfacial dislocations were never seen to terminate within a boundary, unless they met dislocations from either the α or ß crystal. Figure 5.13 shows that the dislocations in the ß phase continued in the interphase boundary, as arrowed. In most cases, the dislocations formed closed loops. However, usually the apparent loops visible by using a particular operating reflection may consist of segments of different types of dislocations. An example of this is illustrated in Figure 5.14. The loops in Figure 5.14a and b are from the same boundary, but they have different appearances. In fact, they are the visible portion of the dislocation network. We have labelled some of the dislocation segments in Figure 5.14b based on the different contrast effects of the dislocations. Therefore, the loops in Figure

Figure 5.13 The connection of dislocations within the β phase with the dislocations in the α/β interface. The specimen was treated 2 days at 770°C, followed by 1 hour at 640°C.

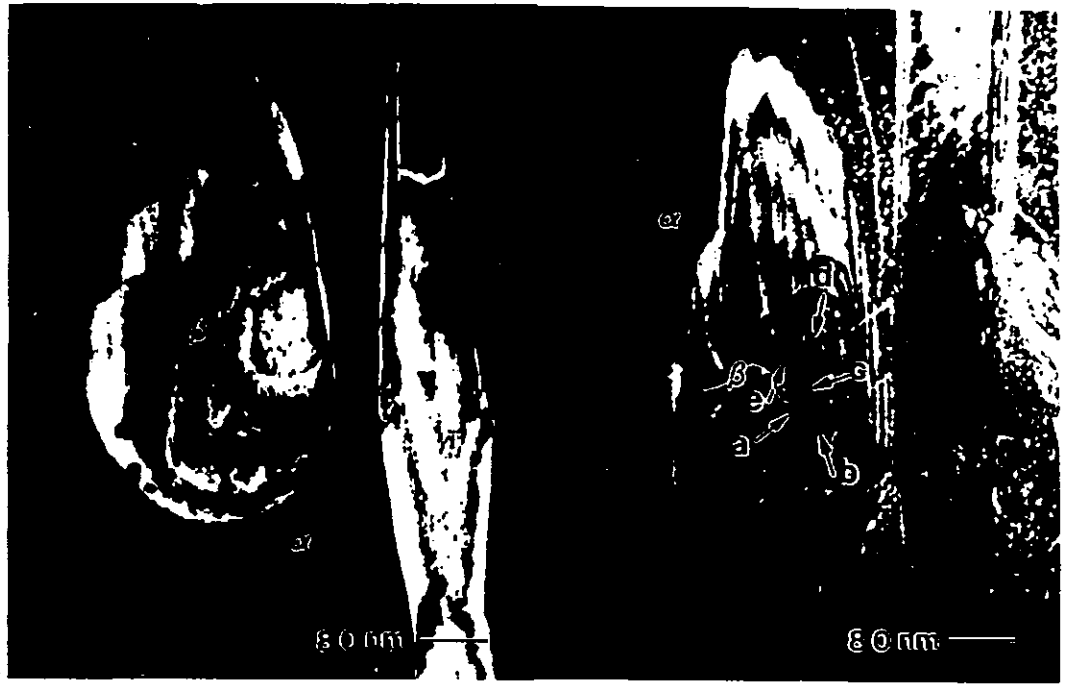

(a) (b)

Figure 5.14 Loops formed consisting of segments of different sets of dislocations; (a) $g = (1\ 0\ -1\ \pm1)_\alpha$, (b) $g = (1\ -1\ 0\ \pm1)_\alpha$.

5.14a consist of segments of a, b, d and probably other(s); the loops in Figure 5.14b consist of segments of b, c, d, e and other(s).

5.2 Crystallographic Studies

5.2.1 The Orientation Relationship Between α and ß

It was observed that all α plates have a similar orientation relationship with respect to the ß phase, regardless of the heat treatments. A close-packed plane and a close-packed direction in each phase were closely related, as could be described by the Burgers orientation relationship (Burgers, 1934). A particular variant of the Burgers orientation relationship used in this work is*

$$(0\ 0\ 0\ 1)_{\alpha} \parallel (1\ 1\ 0)_{\beta},$$
$$[1\ 1\ \bar{2}\ 0]_{\alpha} \parallel [1\ \bar{1}\ 1]_{\beta}.$$

However, when great care was taken in measurements, slight deviations from the Burgers orientation relationship were always detected.

These slight deviations have been obtained by various

---

* In this study, the specific indices assigned to the ß phase were variable according to α plate of interest, with respect with the particular variant.

means. One way is to study the orientation relationship at $[0\ 0\ 0\ 1]_\alpha$ zone axis. An example is given in Figure 5.15 (The index may carry 180° uncertainty) to show the deviation of $[0\ 0\ 0\ 1]_\alpha$ from $[1\ 1\ 0]_\beta$. In Figure 5.15a, the $[0\ 0\ 0\ 1]_\alpha$ axis in α plate was oriented to be exactly parallel to the electron beam. The diffraction pattern (Figure 5.15b), taken from the ß phase adjacent to the α, showed a slight deviation from the exact $[1\ 1\ 0]_\beta$ zone axis (When the foil tilting effect was taken into account, the deviation still existed). It was not possible to evaluate such a small deviation accurately. The rotation angles were found to be in the order of 0.5°, and the rotation axes were between $[1\ -1\ 0]_\beta$ and $[1\ -1\ 2]_\beta$ (The sign of the rotation axis was tentatively assigned). In selected area diffraction pattern taken from the boundary at $[0\ 0\ 0\ 1]_\alpha$($\sim$//$[1\ 1\ 0]_\beta$) zone axis the diffracting vector $g_{(-2\ 2\ 0\ 0)\alpha}$ was not exactly parallel to $g_{(1\ -1\ -2)\beta}$, as can be seen from Figure 5.15c. The angle between Δg (= $g_{(-2\ 2\ 0\ 0)\alpha} - g_{(1\ -1\ -2)\beta}$) and $g_{(-2\ 2\ 0\ 0)\alpha}$ is about 6°, and the angle between $g_{(-2\ 2\ 0\ 0)\alpha}$ and $g_{(1\ -1\ -2)\beta}$ is estimated to be about 0.2°. This implies that a slight rotation also exists between $(1\ 1\ -2\ 0)_\alpha$ and $(1\ -1\ 1)_\beta$, because they are perpendicular to $(-2\ 2\ 0\ 0)_\alpha$ and $(1\ -1\ -2)_\beta$ respectively. Therefore, the close-packed directions $[1\ 1\ -2\ 0]_\alpha$ and $[1\ -1\ 1]_\beta$ are not parallel since the plane normal and directions of these indices are in the same direction. It is interesting to note that many of the Δgs, including $g_{(1\ -1\ 0)\beta} - g_{(0\ 1\ -1\ 0)\alpha}$, $g_{(1\ -1\ -2)\beta} - g_{(-2\ 2\ 0\ 0)\alpha}$, $g_{(0\ 0\ -2)\beta} - g_{(-2\ 1\ 1\ 0)\alpha}$, and $g_{(-1\ 1\ -2)\beta}$ -

$g_{(-2\ 0\ 2\ 0)\alpha}$, align approximately in one direction, i.e. direction of $g_{(-3\ 4\ -1\ 0)\alpha}$. This diffraction pattern was taken from the boundary shown at centre of Figure 5.15d. In this orientation, the broad face boundary is almost at the edge-on orientation; while the edge face boundary usually has a large projected width. The dark region on the upper side of the labelled ß particle in Figure 5.15d is covered by the edge face boundary. Due to the diffraction condition in near zone axis, the defects in the edge face boundary are not clearly visible. Only at the very end of the boundary some parallel dislocations can be seen, which are enlarged and shown in the insert of Figure 5.15c. In Figure 5.15c, we see the Δgs are approximately perpendicular to the dislocations. This interesting observation will be discussed in the next Chapter.

The deviation of orientation relationship from the Burgers orientation was confirmed by studying the orientation relationship when the $[0\ 0\ 0\ 1]_\alpha(\sim//[1\ 1\ 0]_\beta)$ was lying normal to the electron beam, i.e. when $(0\ 0\ 0\ 1)_\alpha(\sim//(1\ 1\ 0)_\beta$ reflection was contained in diffraction patterns. At some orientations, it could be seen that the Kikuchi bands related to $(0\ 0\ 0\ 1)_\alpha$ and $(1\ 1\ 0)_\beta$ were clearly separated in convergent beam diffraction patterns taken from the interphase boundaries, as arrowed in Figure 5.16. Usually the angles separating the two bands were below 1°. This angle cannot represent the rotation angle between the two sets of planes

unless the rotation axis is known to be normal to the electron beam. However, the rotation axis in this case could not be determined precisely. One method of determining the rotation axis is to find the orientation where the two Kikuchi bands intersect with each other. The rotation axis was then defined by the beam direction. Because the angle between the two bands was very small and the bands were not sharp enough, the uncertainty in the measurement was large. Generally, the observed rotation axis was scattered between $[1\ -1\ 0]_\beta$ and $[1\ -1\ 2]_\beta$. An attempt was also made to determine the rotation angle between planes $(1\ 1\ 0)_\beta$ and $(0\ 0\ 0\ 1)_\alpha$ using selected area diffraction patterns when the two Kikuchi bands intersect with each other. An example is provided in the insert in Figure 5.16. A rotation between the diffracting vectors $g_{(0\ 0\ 0\ 1)\alpha}$ and $g_{(1\ 1\ 0)\beta}$ can be clearly seen. The angle between the Δg ($= g_{(0\ 0\ 0\ 1)\alpha} - g_{(1\ 1\ 0)\beta}$) and $g_{(1\ 1\ 0)\beta}$ is ~42°, and the rotation angle between $g_{(0\ 0\ 0\ 1)\alpha}$ and $g_{(1\ 1\ 0)\beta}$ is ~1.2°. Considering the uncertainty in the measurements the rotation angle would not exceed 1.5°. Such rotation has also been observed in diffraction patterns taken at $[1\ -1\ 1]_\beta$ (~//$[1\ 1\ -2\ 0]$) zone axis. An example is shown in Figure 5.17 (The index may carry 180° uncertainty), where the diffraction pattern was taken at an α/ß boundary in the insert. It was very difficult to detect the slight rotation between $[1\ 1\ -2\ 0]_\alpha$ and $[1\ -1\ 1]_\beta$ when they are nearly parallel to the beam, because the rotation angle was of the same order of magnitude as the uncertainty in

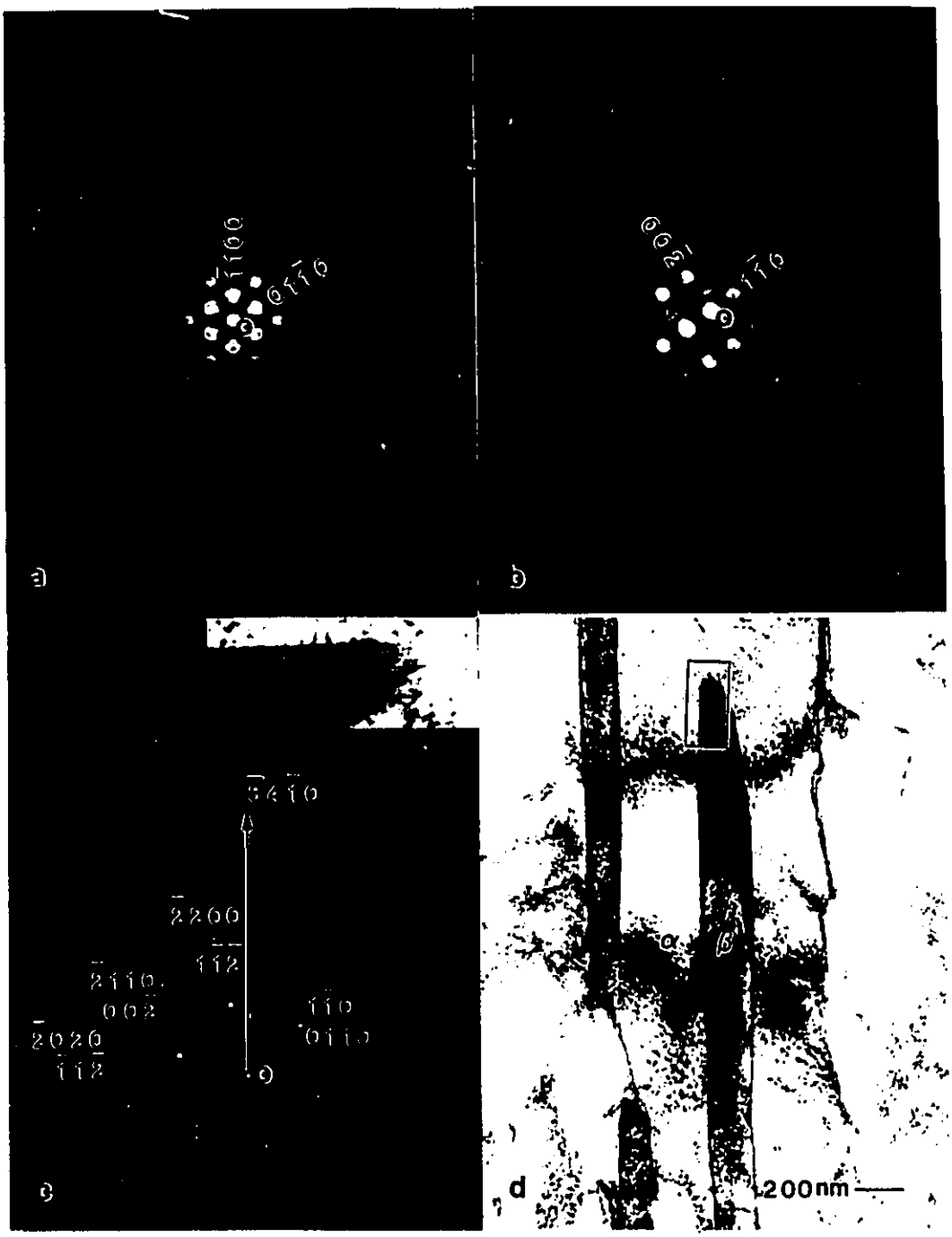

Figure 5.15 Diffraction patterns showing a deviation of the orientation relationship from the exact Burgers orientation relationship; (a) at the exact $[0\ 0\ 0\ 1]_{\alpha}$ zone axis, (b) a slight deviation from the exact $[1\ 1\ 0]_{\beta}$, (c) a selected area diffraction pattern and an enlarged part of the boundary in (d) (insert), (d) the α/β boundary (centre) from which the diffraction pattern in (c) was taken.

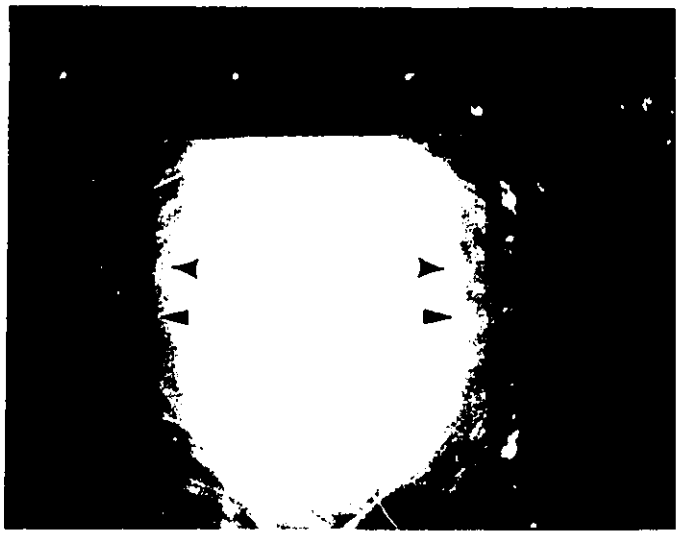

Figure 5.16 The separation of Kikuchi bands between $(0\ 0\ 0\ 2)_{\alpha}$ and $(1\ 1\ 0)_{\beta}$, and the deviation of $g_{(0\ 0\ 0\ 2)\alpha}$ from $g_{(1\ 1\ 0)\beta}$ (in the insert which was taken from the specimen treated 20 min at 650°C).

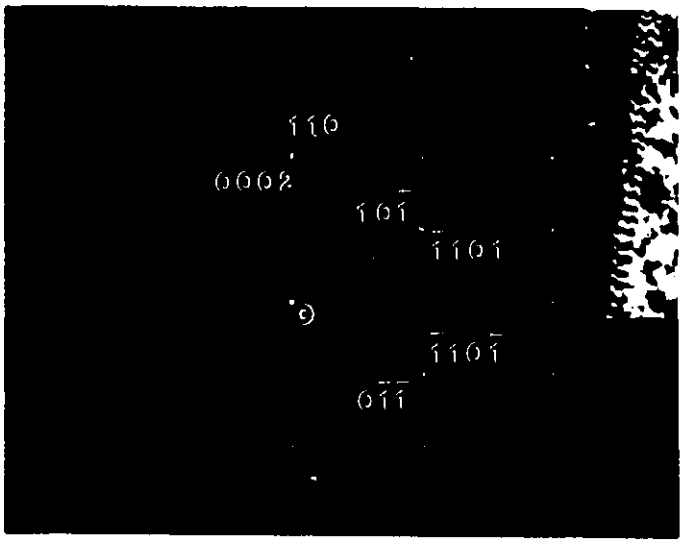

Figure 5.17 A Selected area diffraction pattern from an α/ß boundary (insert) at the $[1\ 1\ -2\ 0]_{\alpha}$ (~//$[1\ -1\ 1]_{\beta}$) zone axis; the specimen was treated at 20 min at 650°C.

defining the centre of the zone axes. In Figure 5.17, angles between $g_{(-1\ 1\ 0\ 1)\alpha}$ and $g_{(1\ 0\ -1)\beta}$, and between $g_{(1\ -1\ 0\ 1)\alpha}$ and $g_{(0\ 1\ 1)\beta}$ are clearly seen, though they are very small. This observation indicated the following parallelism of planes as required by Potter relationship (1973), i.e.,

$$(-1\ 1\ 0\ 1)_\alpha \ // \ (1\ 0\ -1)_\beta, \text{ or}$$

$$(1\ -1\ 0\ 1)_\alpha \ // \ (0\ 1\ 1)_\beta, \text{ and}$$

$$[1\ 1\ -2\ 0]_\alpha \ // \ [1\ -1\ 1]_\beta,$$

does not hold.

5.2.2 The Habit Plane of α Precipitates

The measured habit plane normals were scattered in a region indicated in Figure 5.18. The most striking result was that the habit plane was found consistently to be normal to Δg_4 $(=g_{(1\ 0\ 1)\beta} - g_{(1\ 0\ -1\ 1)\alpha})$. An example of this observation is given in Figure 5.19a. The right part of the boundary on the upper side of the ß particle in Figure 5.19a contains stepped flat segments of edge-on interface, suggesting again that the flat portion of interface is the preferential orientation of the interface, i.e. the habit plane. The diffraction pattern in the insert was taken from the boundary. It can be seen that the Δg_4 $(=g_{(1\ 0\ 1)\beta} - g_{(1\ 0\ -1\ 1)\alpha})$ is exactly perpendicular to the habit plane. Moiré fringes due to the double diffraction of $g_{(1\ 0\ 1)\beta}$ and $g_{(1\ 0\ -1\ 1)\alpha}$ are seen in the left part of the boundary in

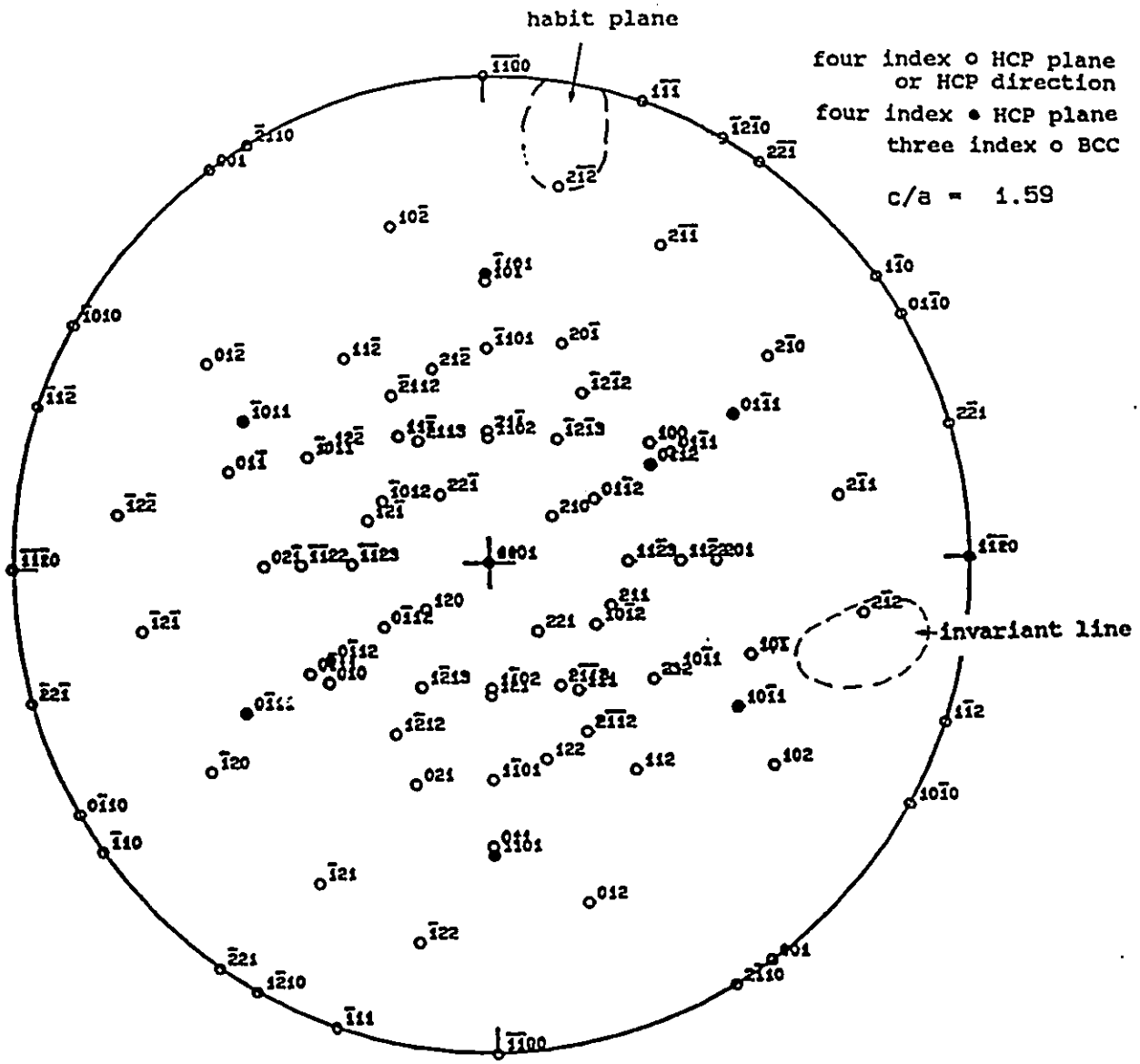

Figure 5.18 The measured habit planes and the directions of the parallel interfacial dislocations plotted in the superimposed stereographic projections of BCC ([1 1 0]) and HCP ([0 0 0 1]), where the two lattices are oriented by the Burgers orientation relationship.

Figure 5.19a. These fringes are perpendicular to the Δg_4, as predicted by the contrast theory (Hirsch, 1977). The trace of the habit plane is exactly parallel to the moiré fringes, which further confirms that Δg_4 is normal to the habit plane. This evidence was taken by single exposure in one plate. As a result, it does not carry the uncertainty in determining the rotation between the image and the diffraction pattern, and hence it is very convincing.

Strictly speaking, the index of Δg_4 is not rational because there was no diffracting vector parallel to Δg_4 in the orientation where it was obtained. Figure 5.19b shows the convergent beam diffraction pattern taken from the boundary at the same orientation as the selected area diffraction pattern inserted in Figure 5.19a. The $\pm g_{(1\ 0\ 1)\beta}$ and the $\pm g_{(1\ 0\ -1\ 1)\alpha}$ were excited simultaneously near the $[1\ 3\ -1]_\beta$ ($\sim // [-1\ -1\ 2\ 3]_\alpha$) zone axis. Along the beam direction the $(1\ 0\ 1)_\beta$ planes and the $(1\ 0\ -1\ 1)_\alpha$ planes intersect with each other. Due to the elongation of diffraction spots, some of spots from $[1\ 3\ -1]_\beta$ ($\sim // [-1\ -1\ 2\ 3]_\alpha$) zone axis other than $g_{(1\ 0\ 1)\beta}$ and the $g_{(1\ 0\ -1\ 1)\alpha}$ are visible in Figure 5.19b. It can be seen that three diffraction spots: $(2\ 0\ 2)_\beta$, $(2\ 0\ -2\ 2)_\alpha$, and $(6\ -5\ -1\ 1)_\alpha$ are aligned in one direction as indicated by a line. This direction is determined by $g_{(6\ -5\ -1\ 1)\alpha} - g_{(2\ 0\ -2\ 2)} = g_{(4\ -5\ 1\ -1)\alpha}$. Therefore, at this orientation, Δg_4, ($// 2\Delta g_4 = g_{(2\ 0\ 2)\beta} - g_{(2\ 0\ -2\ 2)\alpha}$), is approximately parallel to $(4\ -5\ 1\ -1)_\alpha$. However, a

small rotation around $[-1\ 0\ -1]_\beta$ should be considered for the true Δg_4 direction. The rotation angle is ~1.1°, (using a right-hand rule for the sense of rotation) taking the Bragg angle of $(1\ -1\ 0\ 0)_\alpha$ as the reference. After taking the rotation into consideration, Δg_4 could be indexed approximately to be $(3.0\ -3.8\ 0.8\ -0.6)_\alpha$ referred to the HCP structure, and $(-3.0\ 2.2\ 3.4)_\beta$ referred to the BCC lattice*.

Another important observation was that Δg_7 ($=g_{(2\ 0\ 0)\beta} - g_{(0\ 1\ -1\ 2)\alpha}$) was also normal to the habit plane. The diffraction pattern in Figure 5.20b was taken from the α/β phase boundary in Figure 5.20a, when both $g_{(2\ 0\ 0)\beta}$ and $g_{(0\ 1\ -1\ 2)\alpha}$ were excited simultaneously. In the left part of the Figure 5.20a the broad face on either the upper or the lower side of the ß is imaged as a straight line. They could represent the edge-on habit planes. Moiré fringes formed due to the double diffraction of $g_{(2\ 0\ 0)\beta}$ and $g_{(0\ 1\ -1\ 2)\alpha}$ are seen in the right part of Figure 5.20a, where the interface is deviated from the habit plane. These moiré fringes, enlarged in the insert in Figure 5.20b, are again parallel to the trace of habit plane, and perpendicular to the Δg_7. The beam direction was near the zone axis $[2\ 1\ -3\ -2]_\alpha$. The habit plane normal, determined by Δg_7,

---

* The translation of reference lattice from HCP to BCC was carried out by assuming that the orientation relationship is defined by the one given by the No. 2 orientation relationship in Figure 3.7, i.e. for $\theta = -2°$. The same orientation relationship will be used in the translations hereafter.

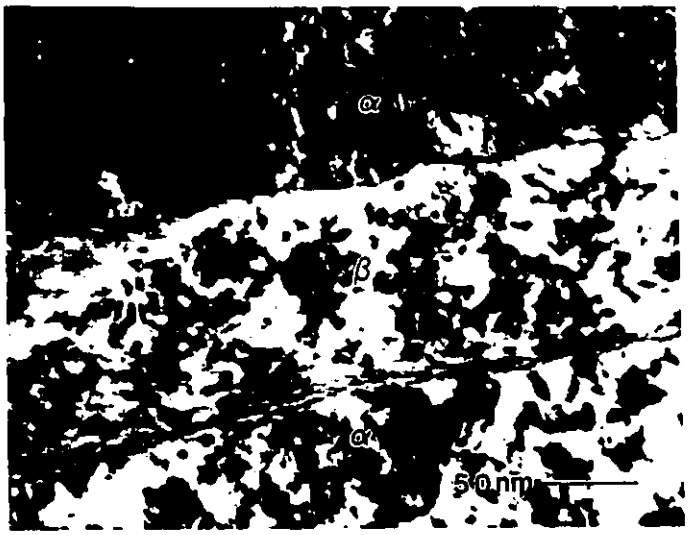

(a)

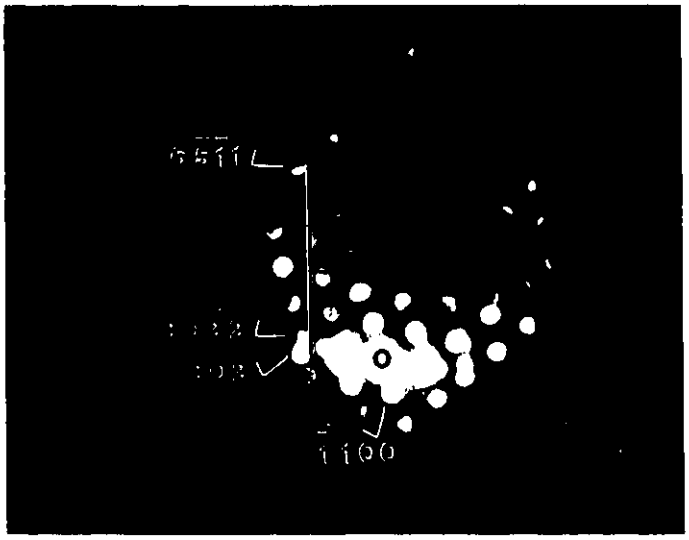

(b)

Figure 5.19 The determination of the habit plane using Δg_4; (a) the edge-on habit plane normal to Δg (insert), (b) a convergent beam diffraction pattern from the boundary in (a).

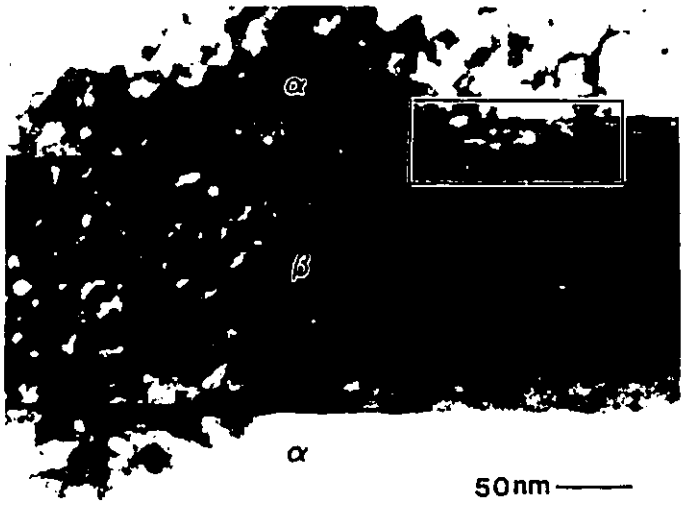

(a)

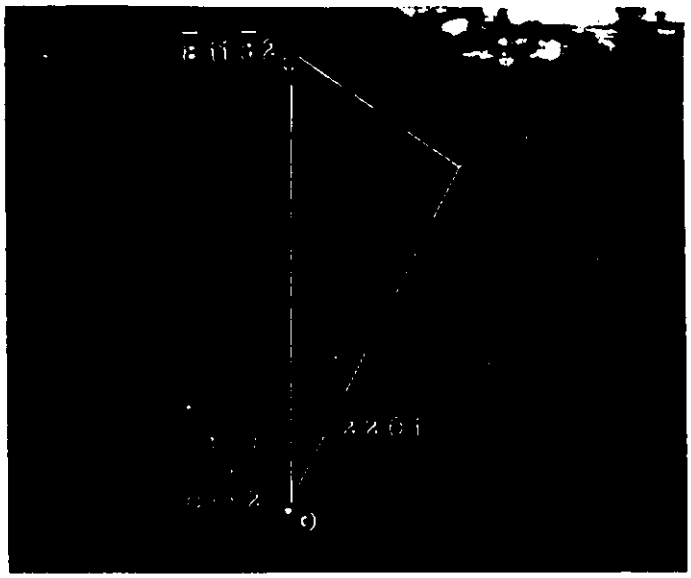

(b)

Figure 5.20 The determination of the habit plane using Δg_7; (a) a near edge-on habit plane on the left side, and the moiré fringes in the boundary deviated from the habit plane on the right side , (b) the diffraction pattern taken from the boundary and the enlarged moiré fringes (insert).

was closely parallel to $(-8\ 11\ -3\ 2)_\alpha$, or $(-3.0\ 4.1\ -1.1\ 0.8)_\alpha$, corresponding to $(3.0\ -2.2\ -3.0)_\beta$ with respect to the ß phase.

5.2.3 The Direction of the Parallel Dislocations in Either the Broad or the Edge Face Boundaries

The direction of the parallel dislocations was determined by the methods mentioned in section 4.3.3. An example of the determination of the dislocation direction in either the broad or the edge face boundaries is given below. In Figure 5.21a, both the broad face on the left side and edge face on the upper side of the labelled ß particle were oriented edge-on, as they are sharply imaged as lines. As a result, the electron beam was aligned parallel to the zone axis of the face boundaries, which is the direction of the parallel dislocations in both faces. The boundaries on other two sides of the ß particle were not very sharp due to foil bending or other random factors. On the lower side of the ß particle very short dislocation segments could be seen nearly edge-on, indicating the direction of electron beam was very close to the direction of the dislocation lines. This further confirms the parallelism of the electron beam and the dislocations on the edge-on sides. The dislocation direction, given by the direction of the electron beam, was determined by the diffraction pattern in Figure 5.21b. The beam direction was nearly along the zone axis $[10\ 4\ -14\ 3]_\alpha$, corresponding

approximately to $[2.0\ -1.0\ 2.5]_{\beta}$. Compared with the uncertainty in rotating the interface to the edge-on orientation, which could be 2° at least, the small deviation (<1°) of the beam direction from the exact zone axis was neglected*.

The dislocation direction was very sensitive to the actual orientation relationship between α and ß phases. A slight rotation of ß due to the existence of small angle boundary would result in a significant change in the dislocation direction. An example of such a case is given in Figure 5.22, where the dislocations in the habit plane are rotated about 15° due to the slight change in the ß orientation. Therefore, besides the uncertainty in the measurements, it is expected that the direction of the parallel interfacial dislocations is truly scattered. The measured dislocation directions have been shown to fall in the region indicated in Figure 5.18.

---

* The normal of the habit plane can also be measured here, as approximately $(3\ -4\ 1\ 0)_{\alpha}$ contained in $[10\ 4\ -14\ 3]_{\alpha}$ zone axis.

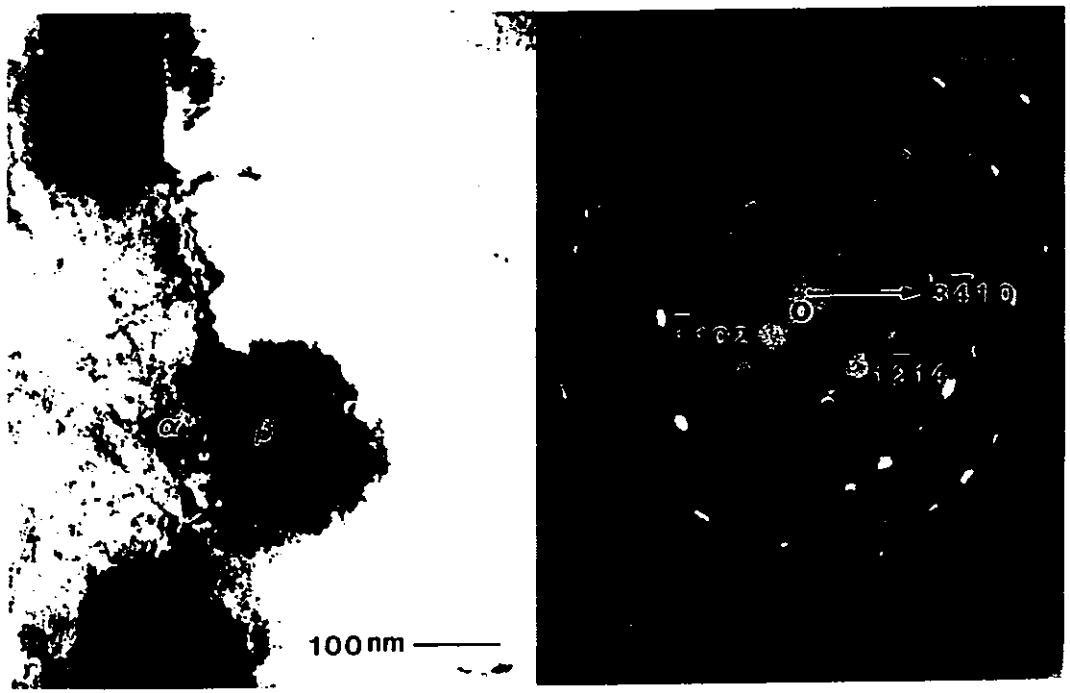

Figure 5.21 The determination of the direction of the parallel interfacial defects; (a) an edge-on interface, (b) the diffraction pattern for determining the beam direction.

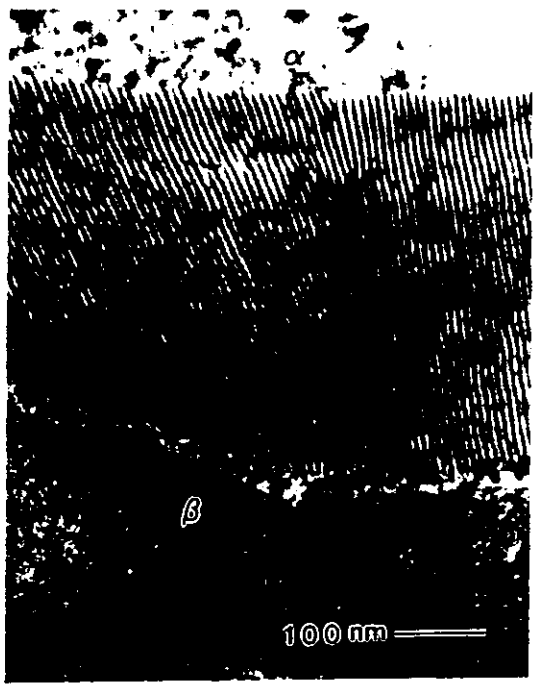

Figure 5.22 The change of direction of dislocations due to a slight change in the crystal orientation; the specimen was treated 2 days at 770°C, followed by 1 hour at 640°C.

5.3 Contrast Study and Burgers Vector Analysis of the Defects in the Broad Interfaces

It has been observed that the contrast of the dislocation structure varied according to the operating reflections for generating the TEM images. Generally, the contrast was stronger using the operating reflections from ß than using those from α. Most times, reflections from $\{1\ 1\ 0\}_{\beta}$ and $\{2\ 0\ 0\}_{\beta}$ planes were used. Sometimes, {1 1 2} planes were used since the dislocation contrast by using them could be fairly strong.

5.3.1 The Principal Dislocations in the Broad Face Boundaries

The contrast analysis was concentrated on the broad face boundaries, where the structure of the habit plane could be most readily studied. By using a particular operating reflection, reproducible contrast was obtained from the principal dislocations which are the characteristic feature of the habit plane. These dislocations could be studied at different orientations and imaged with many low index operating refections, since their characteristic contrast may be used to identify them. Some examples of the contrast study of this set of dislocations are given below.

The contrast of the fine structure in a broad face boundary was studied using six operating reflections (g) to form dark field images, as indicated in each micrograph in Figure 5.23. The array of principal dislocations are seen as the regularly spaced linear feature using one of the following operating reflections $(0\ 2\ 0)_\alpha$ $(\sim(0\ -1\ 1\ 2)_\alpha)$, $(1\ -2\ 1\ 0)_\alpha$, and $(1\ -1\ 0)_\beta$ $(\sim(0\ 1\ -1\ 0)_\alpha)$ (Figure 5.23a,b,c). Several positions with contrast effect different from that of the principal dislocations could be noticed. These irregularly spaced features are better shown using the operating reflection $(0\ 1\ -1)_\beta$ $(\sim(-1\ 0\ 1\ 1)_\alpha$ (Figure 5.23d). The contrast of the principal dislocations in Figure 5.23d is weaker compared with those in Figure 5.23a,b,c. The principal dislocations are totally invisible using the $(1\ 0\ -1)_\beta$ $(\sim /\!/(-1\ 1\ 0\ 1)_\alpha)$ and nearly invisible using the $(2\ 0\ 0)_\beta$ $(\sim(0\ 1\ -1\ 2)_\alpha)$ operating reflections, as shown respectively in Figure 5.23e and f. The irregular defects exhibit sharp contrast when the $(1\ 0\ -1)_\beta$ operating diffraction is used, while they are broad in the image formed using the $(2\ 0\ 0)_\beta$ operating diffraction.

Invisibility conditions for the principal dislocations have been obtained repeatedly using the $(1\ 0\ -1)_\beta$ and $(2\ 0\ 0)_\beta$ operating reflections. This is demonstrated by another example given in Figure 5.24. The principal dislocations are visible using the $(1\ -1\ 0)_\beta$ and $(0\ 1\ -1)_\beta$ operating reflections (Figure 5.24a and b), and are again invisible when using the $(1\ 0\ -1)_\beta$

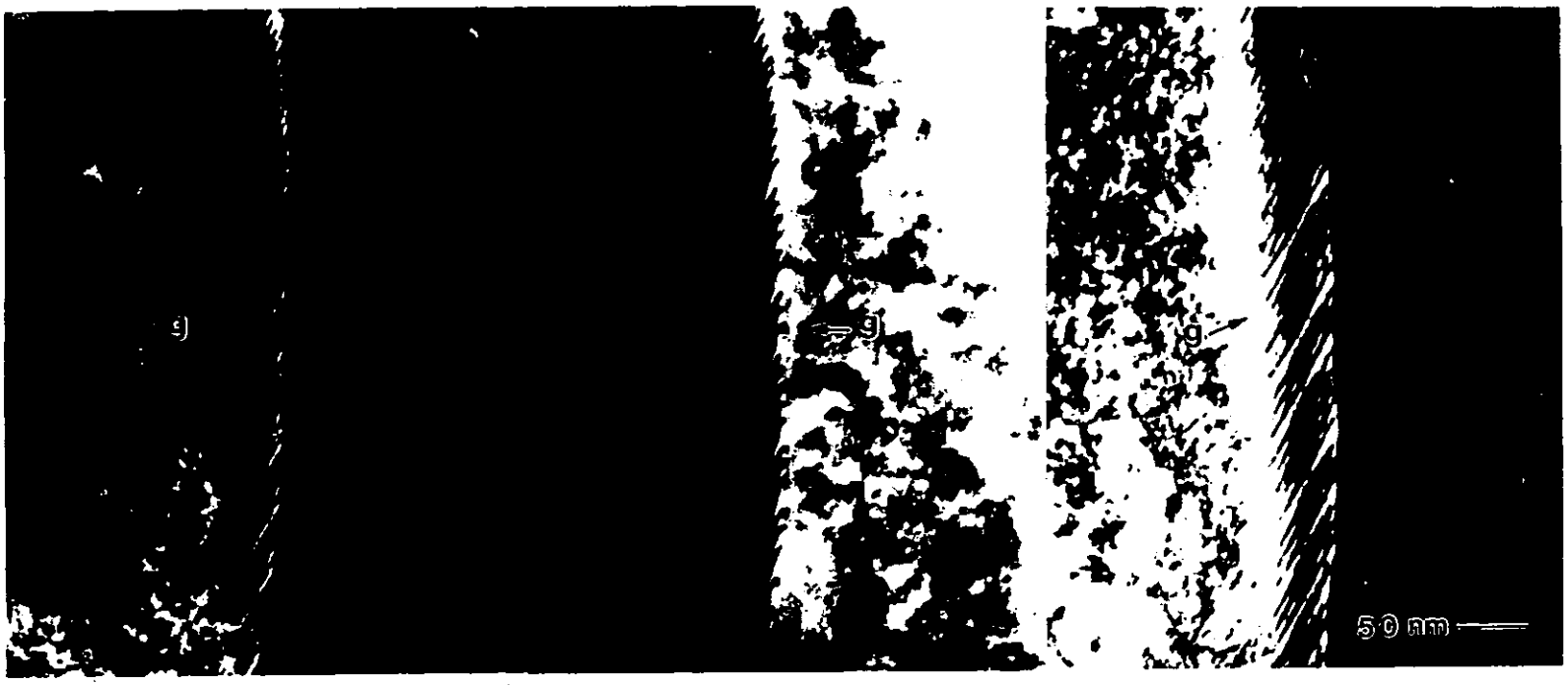

Figure 5.23 Dark field images of dislocations in a broad face boundary using six different operating reflections: (a) $g = (0\ 2\ 0)_{\beta}$, (b) $g = (1\ -2\ 1\ 0)_{\alpha}$, (c) $g = (1\ -1\ 0)_{\beta}$, (d) $g = (0\ 1\ -1)_{\beta}$, (e) $g = (1\ 0\ -1)_{\beta}$, (f) $g = (2\ 0\ 0)_{\beta}$.


50 nm
(f)
(e)
(d)

Figure 5.24 Dark field images generated by (a) $\mathbf{g} = (1\ -1\ 0)_\beta$, (b) $\mathbf{g} = (0\ 1\ -1)_\beta$, (c) $\mathbf{g} = (1\ 0\ -1)_\beta$, (d) $\mathbf{g} = (2\ 0\ 0)_\beta$ used to obtain invisibility conditions for the principal dislocations.

and $(2\ 0\ 0)_{\beta}$ operating reflections (Figure 5.24c and d).

When the specimen was oriented near the $[1\ -1\ 1]_{\beta}$ ($\sim$//$[1\ 1\ -2\ 0]_{\alpha}$) zone axis, the $(1\ 1\ 0)_{\beta}$ and $(0\ 1\ 1)_{\beta}$ operating reflections could be used. The typical image of interfacial structure using the $(1\ 1\ 0)_{\beta}$ ($\sim$//$(0\ 0\ 0\ 1)_{\alpha}$) operating reflection is shown in Figure 5.25a, where sharp dislocation lines are regularly arranged around the ß particle. In this boundary two types of linear defects are revealed by using the $(1\ -1\ 0\ 0)_{\alpha}$ operating reflection (Figure 5.25b). Those dislocations with weaker contrast in Figure 5.25b are the principal dislocations in the broad face boundary. As usual, they are invisible using the $(1\ 0\ -1)_{\beta}$ ($\sim$//$(-1\ 1\ 0\ 1)_{\alpha}$) operating reflection (Figure 5.25c). However a sharp image of this set of dislocations has been obtained when the $(0\ 1\ 1)_{\beta}$ ($\sim$//$(1\ -1\ 0\ 1)_{\alpha}$ operating reflection is used (Figure 5.25d).

If the Burgers vectors of dislocations are of pure **a** or pure **c** type as referred to HCP structure, the contrast of the dislocations must be the same or similar using the pair of operating **g** vectors $(1\ -1\ 0\ \pm1)_{\alpha}$. However, the distinctly different contrasts of the principal dislocations have been obtained by using this pair of $(1\ -1\ 0\ \pm1)_{\alpha}$ operating reflections. This suggests that the Burgers vector associated with the principal dislocations should not be either pure **a** or pure **c** type of dislocations.

Assuming that the Burgers vector of the principal dislocations is a lattice vector of the BCC lattice, it could be either $<1\ 1\ 1>_{\alpha}$ or $<1\ 0\ 0>_{\beta}$ type. The complete invisibility of the principal dislocations suggests that the possible Burgers vectors should be among $[1\ -1\ 1]_{\beta}$, $[1\ 1\ 1]_{\beta}$, and $[0\ 1\ 0]_{\beta}$. Since the dislocations are clearly visible using the operating reflections $(1\ 1\ 0)_{\beta}$ (Figures 5.5, 5.22 5.25a) and $(0\ 1\ 1)_{\beta}$ (Figure 5.25d), the Burgers vector can not be $[1\ -1\ 1]_{\beta}$. They are also visible using the operating reflections $(0\ 1\ -1)_{\beta}$ (Figure 5.6a, 5.23d, 5.24b) and $(1\ -1\ 0)_{\beta}$ (Figures 5.23c and 5.24a). Hence the Burgers vector can not be $[1\ 1\ 1]_{\beta}$, either. The dislocations are strongly visible using the $(0\ 2\ 0)_{\beta}$ operating reflection (Figure 5.23a), indicating the contrast from {2 0 0} operating reflections is strong enough for the contrast analysis. The fact that dislocations are hardly visible using the $(2\ 0\ 0)_{\beta}$ operating reflection (Figures 5.23e and 5.24d) suggests then that the Burgers vector should be $[0\ 1\ 0]_{\beta}$ ($\sim[0\ -1\ 1\ 1]_{\alpha}/2$).

5.3.2 The Irregular Line Features in the Broad Face Boundaries

Usually irregular dislocations in the broad interface are strongly visible by using the $(1\ 0\ -1)_{\beta}$ operating reflection, (Figure 5.6b, 5.23e, 5.24c and 5.25c). However, these irregular dislocations appear to present at local boundaries which are deviated from the habit plane by a

particular sense of rotation. As arrowed in Figure 5.25a, there is a small curvature of the interface on the right side of the boundary. Those irregular dislocations having broad images in Figure 5.25b, or those clearly visible in Figure 5.25c, do not seem related to the curvature. Instead, the dislocations associated with the part of curved boundary tend to exhibit the same contrast as the principal dislocations in the broad face boundaries. In Figure 5.26, two small ß particles were taken in the neighbourhood of the ß particle in Figure 5.25. On the right side of the labelled ß particle, the upper part of the boundary deviates gradually from the habit plane in the lower part. The sense of the curvature from the habit plane is opposite to that in Figure 5.25. When the $(1\ 0\ -1)_{\beta}$ operating reflection was used (Figure 5.26a), the dislocations in the habit plane are again invisible. As the boundary deviates from the habit plane many dislocations become visible. In contrast to Figure 5.26a, the dislocations are visible in the habit plane and are invisible in the upper part of the boundary, if the $(0\ 1\ 1)_{\beta}$ operating reflection is used (Figure 5.26b). By carefully comparing the individual spacing of the irregular dislocations in Figure 5.25b, c, with Figure 5.25d, one could determine that the irregular dislocations in the broad face boundary are also invisible when using the $(0\ 1\ 1)_{\beta}$ operating reflection.

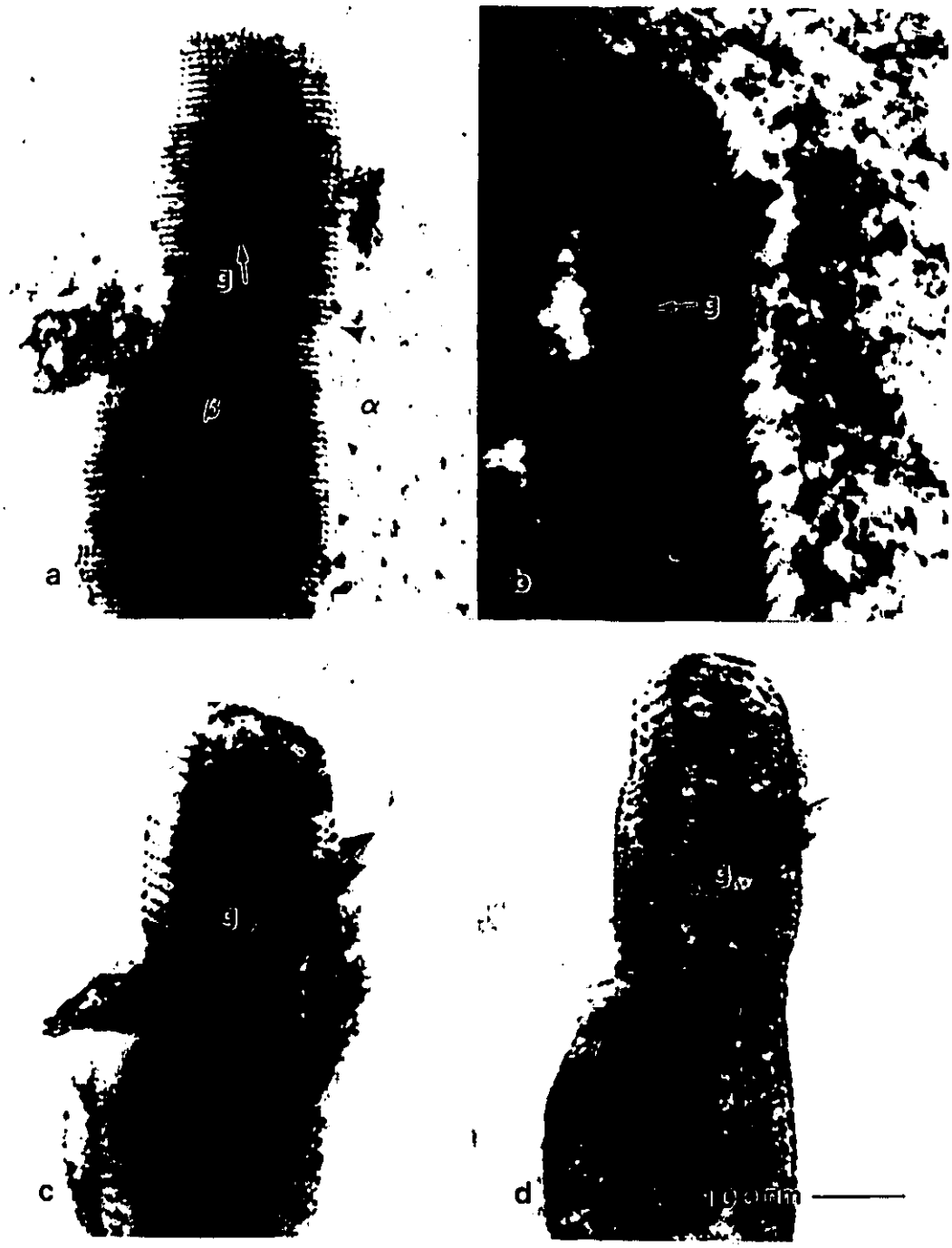

Figure 5.25 A contrast study of dislocations in a broad face boundary recorded near the $[1\ -1\ 1]_{\beta}$ zone axis; (a) bright field, g = $(1\ \ 1\ 0)_{\beta}$, (b) dark field, g = $(1\ -1\ 0\ 0)_{\alpha}$, (c) bright field, g = $(1\ 0\ -1)_{\beta}$, (d) bright field g = $(0\ 1\ 1)_{\beta}$.

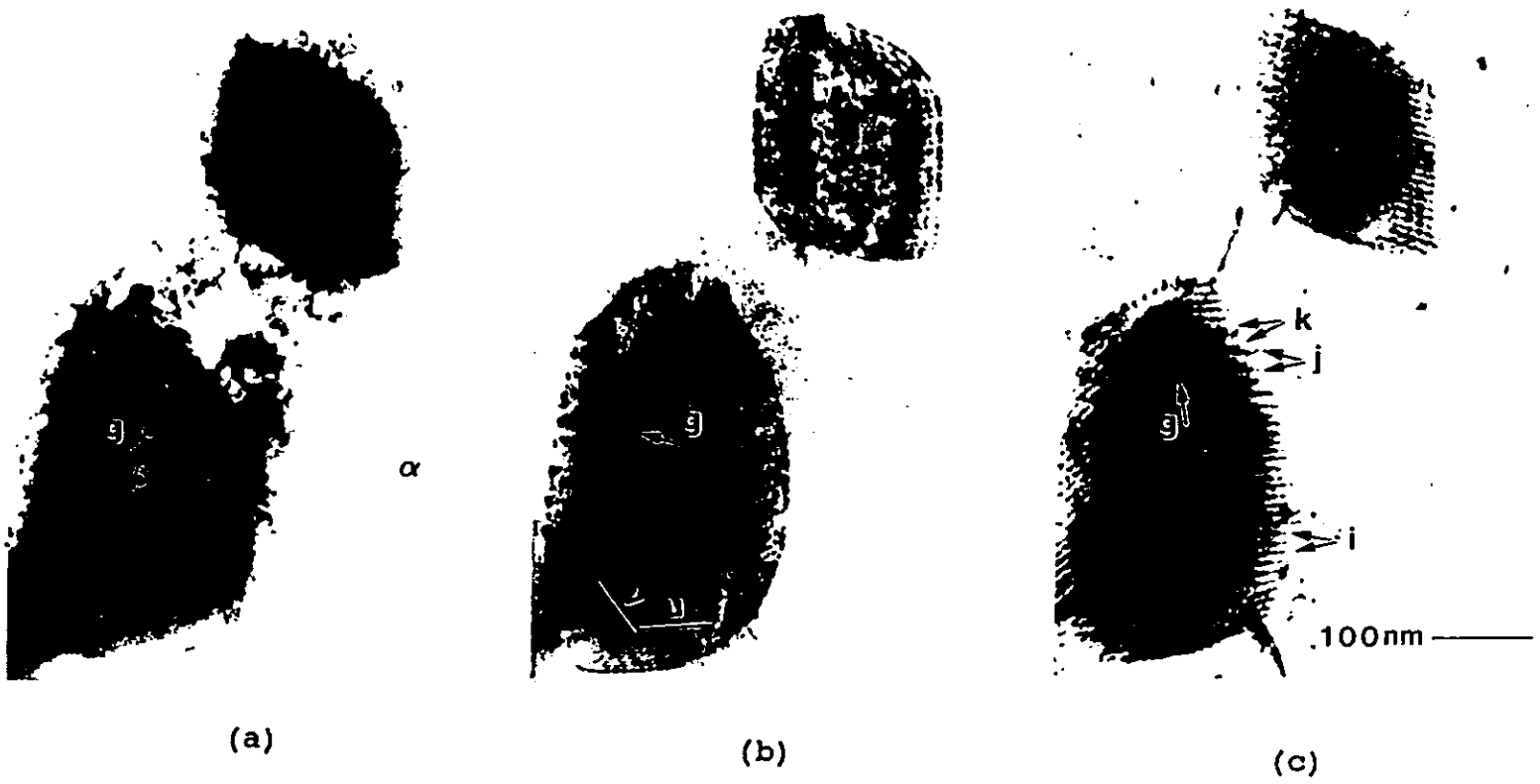

Figure 5.26 A contrast study of dislocations in an interface deviated generally from the habit plane (bright field); (a) $g = (1\ 0\ -1)_{\beta}$, (b) $g = (0\ 1\ 1)_{\beta}$, (c) $g = (1\ 1\ 0)_{\beta}$.

The boundary of this ß particle in Figure 5.26 (labelled) is a good example to show the complexity of the irregular interfacial dislocations. Although they are all invisible using the $(0\ 1\ 1)_{ß}$ operating reflection, the dislocations in the boundary on the upper-right side of the ß particle do not seem simply to belong to one set. In Figure 5.26a, the contrast of the visible dislocations in this part of boundary is not even. This difference in contrast of the dislocations is distinct in Figure 5.26c when $(1\ 1\ 0)_{ß}$ operating diffraction was used though by using the same **g** in Figure 5.25a a similar contrast was obtained for both the principal dislocations and the irregular dislocations. This observation indicates there likely exist at least three types of parallel dislocations on the right side of the ß particle, arrowed by i— the principal dislocations, visible in Figure 5.26b and c, invisible in Figure 5.26 a; j— the irregular dislocations, visible in Figure 5.26a and c, invisible in Figure 5.26b; k— irregular dislocations visible in Figure 5.26a, barely visible in Figure 5.26c, invisible in Figure 5.26b. For the most part, to distinguish one type of irregular dislocations from another has been very difficult.

Another observation often obtained from the irregular dislocations was that when the irregular dislocations intersect with the principal dislocations, they were often invisible using the $(1\ 1\ 0)_{ß}$ operating reflection (Figure

5.5), and strongly visible using the $(1\ 0\ -1)_B$ and $(0\ 1\ -1)_B$ (Figure 5.6) (More examples about this will be given in the following Section).

5.3.3 The Relationship of the Irregular Dislocations in the Broad Face Boundary and the Dislocations in Other Interfaces

Usually the irregular dislocations in a broad face boundary are associated with the dislocations in the boundaries other than the broad face boundary. Less work has been done on the dislocations in the interfaces other than the broad face boundary. Here, only some preliminary results will be presented.

The irregular dislocations strongly visible using the $(1\ 0\ -1)_B$ operating reflection in the broad face boundary, are frequently observed to be associated with the regularly-spaced dislocations in the edge face boundary. An example is given in Figure 5.27a, where each irregular dislocation in the broad face boundary connects to a regularly spaced dislocation line, which forms a parallel set in the edge face boundary*. It is interesting to note that the principal dislocations in the

---

* Here the broad face is narrower than the edge face due to the sectioning reason. In this case the faces were identified by their orientation and the typical interfacial structures.

broad face boundary connect to the curved dislocations in the edge face boundary in the image formed by using the $(1\ 0\ 1)_{\beta}$ operating reflection (Figure 5.27b). Another interesting observation concerns the presence of kinks along the irregular dislocations, as can be seen in Figure 5.27a, suggesting that there is an energetic tendency for the irregular dislocations to lie parallel to the principal dislocations. These kinks are often observed along the irregular dislocations.

One more example of the dislocations in the edge face boundary is given in Figure 5.28 when the interface lies nearly parallel to the foil. Figure 5.28a ($\mathbf{g} = (0\ 1\ 1)_{\beta}$) shows the coarsely spaced dislocations in the edge face boundary; each of them appears to connect to a dislocation from the broad face boundary, which was now nearly edge-on oriented at the vertical edges of the ß particle. In Figure 5.28b, almost all features in this interface, including the very closely spaced linear feature mentioned earlier, are visible when they were imaged by using the $(1\ 0\ 1)_{\beta}$ operation reflection. While these finely spaced lines are still visible, the coarsely spaced parallel dislocations can hardly be seen if the $(1\ -1\ 0)_{\beta}$ operating reflection is used (Figure 5.28c). This is the typical image of the edge face boundary using this operating reflection, as already shown in Figure 5.7 and 5.8. However, the edge face boundaries should be studied with caution. Sometimes, the edge face boundary was observed to consist of

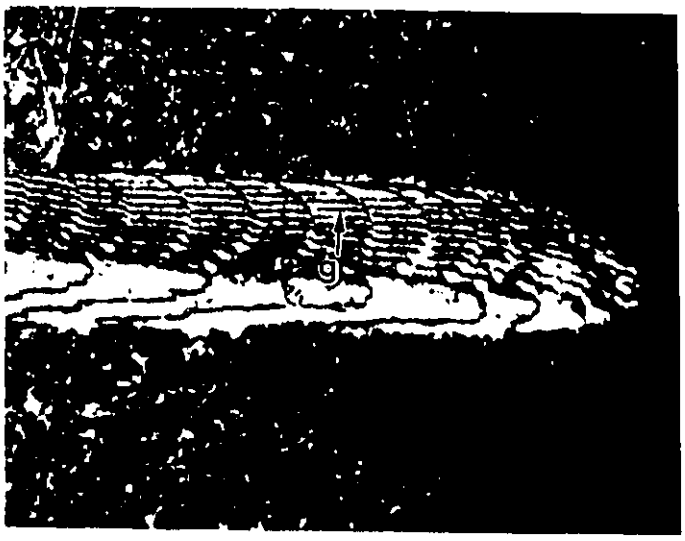

(a)

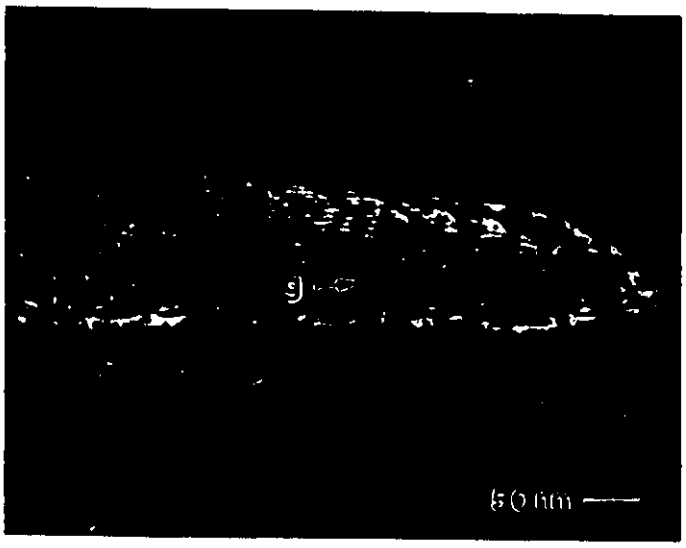

(b)

Figure 5.27 The correspondence of dislocations in a broad face boundary and an edge face boundary (dark field); (a) $g = (1\ 0\ -1)_{\beta}$, (b) $g = (1\ 0\ 1)_{\beta}$.

(a) (b) (c)

Figure 5.28 Dislocations in an edge face boundary; (a) $\mathbf{g} = (0\ 1\ 1)_{\beta}$, (b) $\mathbf{g} = (1\ 0\ 1)_{\beta}$, (c) $\mathbf{g} = (1\ \bar{1}\ 0)_{\beta}$. The specimen was treated 2 days at 770°C, followed by 1 hour at 640°C.

more than one facet plane. For example, there are two faces at the lower edge of the labelled ß particle in Figure 5.26b. The traces of the two faces are labelled 'u' and 'v', respectively. The structure in the facet with trace 'u' is visible using the $(0\ 1\ 1)_{\beta}$ operating reflection; while the structure in the one with trace 'v' is invisible.

When the spacing of irregular dislocations intersecting the parallel dislocations becomes smaller, the interface orientation changes toward that of end face (refer to Figure 5.12). A structure of this type of interface is illustrated by a dark field image of $g = [0\ 2\ 0]_{\beta}$ in Figure 5.29a. Roughly speaking, on the upper side of the boundary there is a network of dislocations consisting of cells having three pairs of sides, as illustrated in Figure 29e. The lower part of the interface is an edge face boundary predominant by the parallel dislocations (coarse spacing). The finely spaced lines in

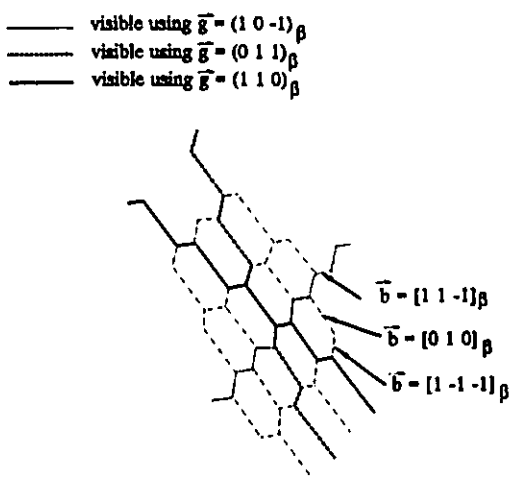

Figure 5.29e Schematic diagram of the network of dislocations and the possible Burgers vectors associated to them.

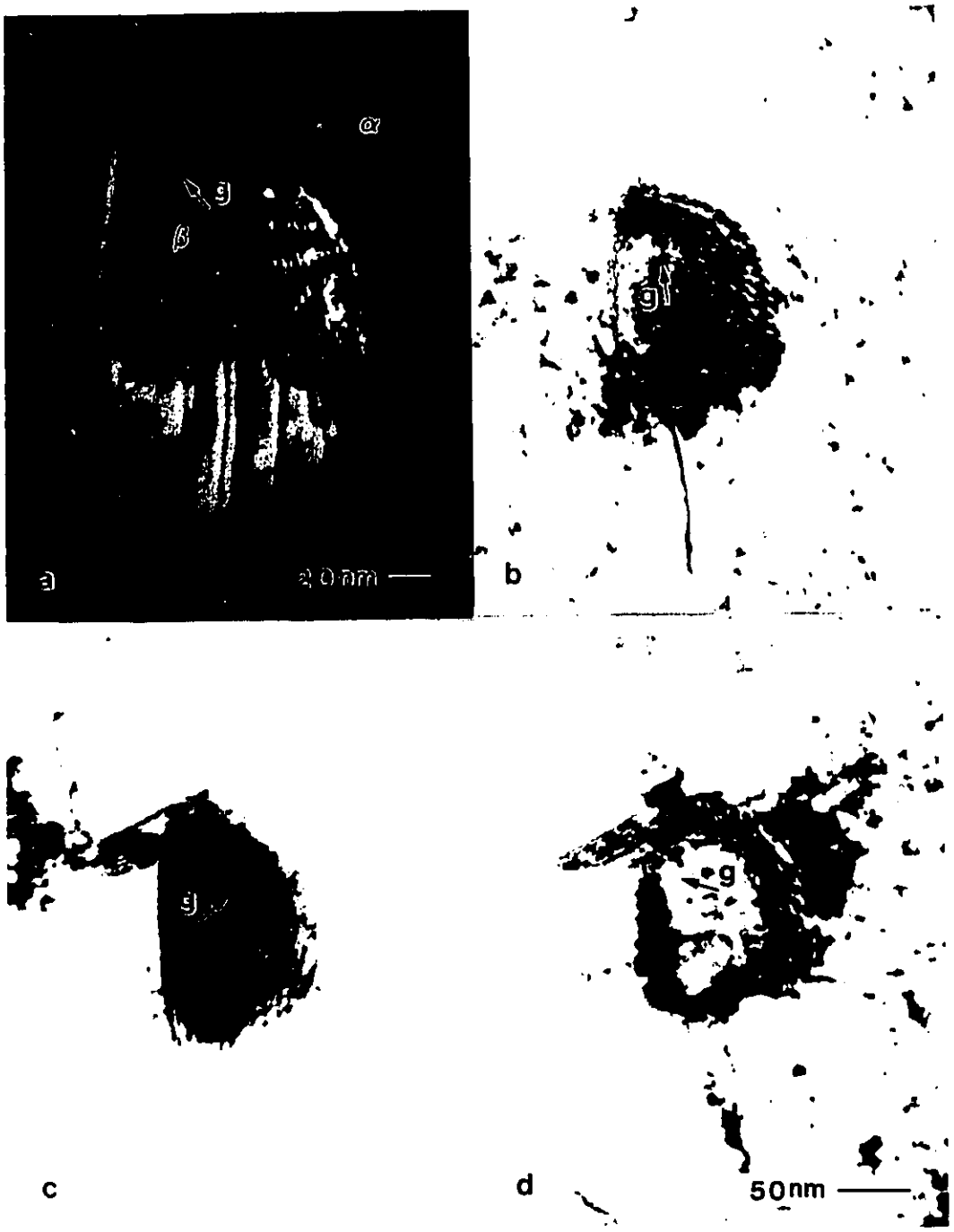

Figure 5.29 A network of interfacial defects in an end face boundary; (a) $g = (0\ 2\ 0)_\beta$, (b) $g = (1\ 1\ 0)_\beta$, (c) $g = (1\ 0\ -1)_\beta$, (d) $g = (0\ 1\ 1)_\beta$.

Figure 5.28b and c could also be observed in both the edge face and the end face boundaries in Figure 5.29a. The network in the end face is likely to be described only in three dimensions, because the interface is not flat. Three different images of this interface obtained using the $(1\ 1\ 0)_{\beta}$, $(1\ 0\ -1)_{\beta}$, $(0\ 1\ 1)_{\beta}$ are presented in Figure 5.29b, c, d, respectively. The finely spaced lines visible in Figure 5.29a are invisible in Figure 5.29b, c, d. In each of the three micrographs only two sets of dislocations are visible in the end face boundary, as demonstrated in Figure 5.29e. Provided the Burgers vectors are from the lattice vectors of BCC lattice, possible Burgers vectors could be deduced from the contrast analysis, as given in Figure 5.29e. Although local consistency can be satisfied in this case, further work is needed for generalization of the observations.

The observation made in the boundary in Figure 5.29 indicated that curved dislocations often consist of segments of dislocations of various types. Caution should be always taken to study the structure in which the parallel dislocations are intersected by another set of dislocations, because an interface with such a structure might contain more set(s) of dislocations than that it does apparently. Another example of this case is presented in Figure 5.30. In Figure 5.30a the dark curved dislocation lines change direction smoothly within the boundary; the other set of dislocations

(shorter) has relatively weaker contrast. Figure 5.30b shows a typical image of the dislocations by using the $(1\ 1\ 0)_{\beta}$(~//$(0\ 0\ 0\ 2)_{\alpha}$) operating reflection. In the left-lower corner, the boundary is close to a habit plane, the defects across the parallel dislocations are almost invisible. However, the dislocations visible in the left-lower corner of Figure 5.30b actually consist of the long segments of the principal dislocations and short segments of dislocation located at the intersection points of straight and curved dislocations visible in Figure 5.30a. The length of the shorter segments of dislocations increases in the centre of the Figure 5.30b, which causes a zigzag feature clearly visible. Consequently, this interface contains three sets of dislocations: one set invisible, the other two sets visible by using the $(1\ 1\ 0)_{\beta}$ operating reflection.

Though many irregular defects in the broad face boundaries could be the intrinsic interfacial dislocations associated with a local deviation of the boundary from the exact habit plane, some of them could be the extrinsic dislocations inherited from the ß crystal. The contrast of the extrinsic interfacial dislocations was usually different from that of the dislocations inside the crystal. For example, the irregular interfacial dislocations are shown to be associated with the dislocations inside the ß crystal in Figure 5.31. In Figure 5.31a both the lattice dislocations within the ß phase

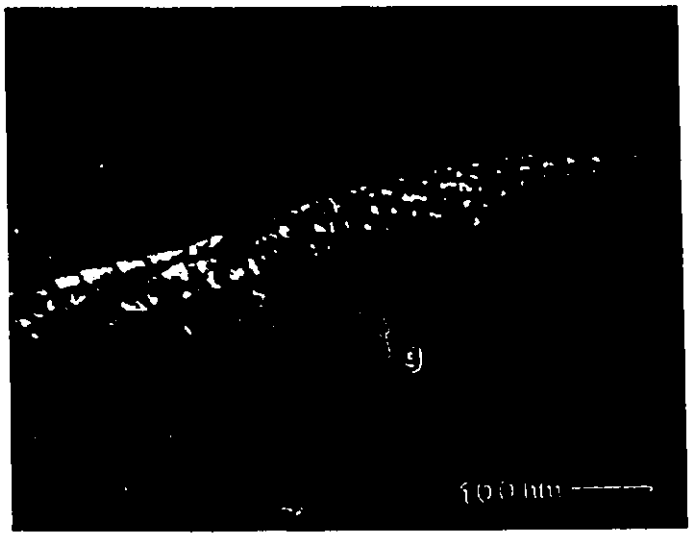

(a)

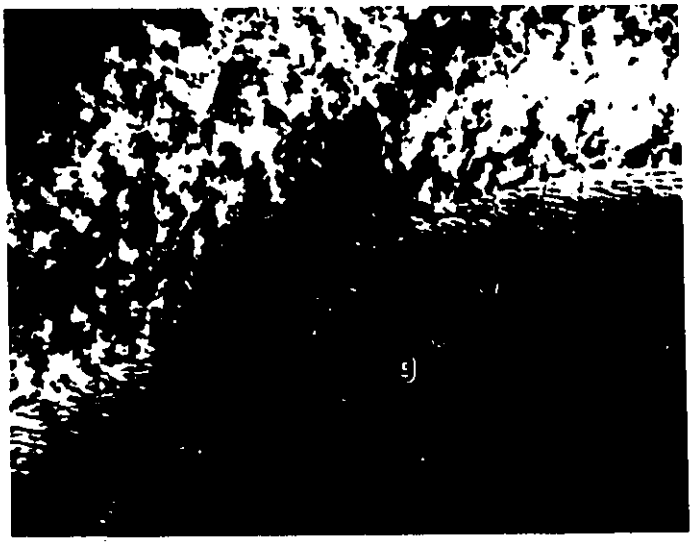

(b)

Figure 5.30 The zigzag feature of the apparently curved defects (dark field); (a) g = $(0\ 1\ -1)_{\beta}$, (b) g = $(1\ 1\ 0)_{\beta}$.

(a)

(b)

Figure 5.31 Image of extrinsic interfacial dislocations; (a) g = $(1\ 0\ -1)_{\beta}$, (b) g = $(0\ 1\ -1)_{\beta}$.

and the irregular interfacial dislocations are visible. While the dislocations inside the ß phase are invisible in Figure 5.31b, where the irregular interfacial dislocations are still clearly visible. This suggests that some reactions might have happened between the strain field of the interphase boundary and the lattice dislocations, but the details are not yet clear. Since the curvature was also associated with the extrinsic interfacial dislocations, as can be seen in Figure 5.31, it is very difficult to distinguish the extrinsic and the intrinsic irregular interfacial dislocations.

CHAPTER 6

DISCUSSION

It has been noted in Chapter 5 that parallel dislocations are observed consistently at all broad face boundaries studied. A few irregular defects have been seen as well due to random effects. This evidence implies that these dislocations likely lie along a strain free direction, or along an invariant line. In this Chapter we will discuss the experimental observations together with the results predicted by the effective invariant line model presented in Chapter 3.

6.1 The Orientation Relationship Between α and ß Phases

As noted in Section 5.2.1, a slight deviation of the orientation relationship from the Burgers one was always detected by various ways of measuring an orientation relationship. The calculation in Chapter 3 indicates that an effective invariant line can be obtained for numerous orientation relationships close to the Burgers relationship, but cannot be obtained when the α and ß are related by the exact Burgers orientation relationship. In spite of this,

though there is a small scattering, the observed orientation relationship appeared to correspond to more closely defined angular ranges than those suggested by the calculations. This implies that additional conditions might effect the orientation relationship. A requirement for highly localized mismatch in the habit plane could be one of the conditions. Actually, in any interfacial dislocation model it is implied that the formation of interfacial dislocations is driven by the reduction of energy due to the concentration of mismatch in the interface. By choosing the optimum orientation relationship proposed in Section 3.8 on the basis of localization of the mismatches in a habit plane, we may have much narrowed choices of orientation relationships. For the specimens treated at 650°C, the predicted range for rotation angle γ around $[1\ 1\ 0]_\beta$ is between -1.1° ~ 0.3°, and that for the angle ϕ around an axis in $(1\ 1\ 0)_\beta$ is between 1° to 1.5°, as shown in Figure 3.6. Furthermore, the two factors demonstrated in Figure 3.7 make the orientation relationships close to the Burgers one. They are for θ = 6°, ϕ = 1.005°, γ = -0.381° corresponding to the maximum dislocation spacing, and for θ = -2°, ϕ = 1.015°, γ = -0.290° corresponding to the minimum deviation angle from the Burgers orientation.

It was not possible to measure both γ and ϕ using the selected area diffraction patterns at the same time. Considering the existence of true scattering of orientation

relationship, we could not obtain a specific orientation relationship for a specimen. Here we only make some general comparisons. The measured angle γ was usually smaller than ϕ, which agrees with the prediction given in Figure 3.7. The angle γ was observed to be small (for example $\gamma \approx -0.2°$), which was within the range of the predicted optimum orientation relationships. The sign of γ could be determined because the direction for $[0\ 0\ 0\ 1]_\alpha$ could be fixed according to the observed orientation relationship*. The γ angle was found always to have negative values, implying $\theta > -26°$. However, the measured angle ϕ was $<1.2°$; relatively smaller compared with the range for the optimum orientation relationships, though the large value of ϕ is within the predicted range. The rotation axis at the $(1\ 1\ 0)_\beta$ plane, was measured with larger relative uncertainty. This was found to correspond to $\theta = -20 \sim 35°$ ($[1\ -1\ 2]_\beta \sim [1\ -1\ 0]_\beta$), which is within the range of the predictions ($-40 \sim 60°$) for the optimum orientation relationships and also consistent with the conjecture from the γ measurement. Considering the larger relative uncertainty carried by the angle measurements, the agreement between the prediction and the experimental observations is reasonable. Therefore the observed deviations of the orientation relationship from the Burgers one were

---

*An $[0\ 0\ 0\ 1]_\alpha$ zone axis is defined when the orientation relationship was similar to the one given in Figure 3.3. If a $(1\ -1\ 0\ 0)_\alpha (\sim // (-1\ 1\ 2)_\beta)$ spot was found by a 60° rotation clockwise instead of count-clockwise from the $(0\ 1\ -1\ 0)_\alpha$ $(\sim (1\ -1\ 0)_\beta)$, then we defined the zone axis as $[0\ 0\ 0\ -1]_\alpha$.

quite probably associated with the formation of an effective invariant line. Some uncertainty also exists in the measured lattice parameters. However, a small deviation from the exact Burger orientation was always needed to satisfy the effective invariant line condition when a certain amount of variation was given to the lattice parameters.

Dahmen and Westmacott (1981) have noticed that, in the Cu-Cr system, the invariant lines along which coherent precipitates tend to lie are much more widely scattered than those found after the precipitates lose coherency. They believed that only those precipitates which had appropriate orientations would survive and grow. The criterion for growth of these precipitates was that the shear component should lie along a Burgers vector, since process of gaining interfacial dislocations was regarded to be relevant to a shear deformation of the parent phase. Perovic and Weatherly (1988) have also considered the parallel interfacial dislocations observed in α/ß boundaries in a Zr- 2.5 wt% Nb to be associated with a slip on the $\{1\ -1\ 0\ 1\}_{\alpha}(//\{1\ 0\ -1\}_{\beta})$ plane. The present model derives from a purely geometrical point of view, without dealing with either the formation of the interfacial dislocations or the mechanism of interface migration. The present model tends to support the view that the range of orientation relationships for semicoherent precipitates would be narrower than that for coherent

precipitates. Being aware of the controversy existing in the literature on precipitates with the Widmanstäten structure being transformed either martensitically or by the jumping of individual atoms across disordered transformation fronts (Aaronson and Reynolds, 1988), we comment based on our observations. Let us consider two cases: supposing a transformation is a martensitic one, the dislocations in the parent phase should be largely inherited in the daughter phase; in contrast, if the transformation proceeds by atoms jumping individually across disordered transformation fronts, there is no reason for the dislocations from the parent phase to leave traces without being destroyed at the disordered transformation fronts. Now, our observation is that the dislocations from ß phase are neither inherited in α, nor destroyed completely in the interfaces. They leave traces in the boundaries in the process of reaction with the strain field of the boundaries (Figure 5.13, 5.31). This implies the existence of certain degree of coordinated movement of atoms during the phase transformations.

6.2 The General Features of α/ß Boundaries and the Morphology of α Precipitates

According to the first property of invariant lines (Section 3.6), if a boundary contains an invariant line, the interfacial dislocations should lie along it. The fact that

parallel lines observed at both the broad and the edge faces lie in one direction agrees with this property, supposing the lines are in fact along the invariant line. Comparing the measured line direction (Figure 5.18) with that from the calculations (Figure 5.12), we have noted that the measured data tend to agree with the prediction for small θ ($\approx$ -10 ~ 5°). This result again suggests that the possible orientation relationships are close to the Burgers one, because the deviation angles ρ are small corresponding to $\theta \approx$ -10 ~ 5° (refer to Figure 3.6). The line direction given by the particular example is $[2.0\ -1.0\ 2.5]_\beta$, in reasonable accord with the prediction $[2\ -1.0247\ 2.6919]_\beta$ for θ=-2°. This is strong evidence that the parallel dislocations lie along an invariant line.

Now we will interpret the general interfacial structure according to the invariant line model. Approximately, the broad face and the edge face of a α precipitate lie in the zone axis of the invariant line, while the end face is normal to the invariant line. According to the second property of invariant lines, all O-cell walls, or the planes of the poorest mismatching, should be in the zone axis of the invariant line. Any boundary contained in the zone axis of the invariant line, will intersect the walls at parallel lines along the invariant line; otherwise the lines of intersection form a network. This is in agreement with the

schematic diagram in Figure 5.12 drawn on the basis of the observation. When the interface is interpreted in the frame of invariant line, there exists only a one-dimensional O-lattice even in the case of the optimum orientation relationship. Therefore, there are no periodic cell walls in two dimensions available from the model. Hence, the relaxation of the atoms in a boundary, intersected by many walls representing the poorest mismatches of different planes or directions, could be very complicated, especially when the boundary is nearly perpendicular to the invariant line. Consequently, the habit plane, which contains both the invariant line and the one-dimensional O-lattice is better understood (to be discussed in a later section). Though an example of Burgers vectors analysis has been given to the network structure at an end face (Figure 5.29), more work needs to be done before we can fully understand the structure of the closed boundary between α and ß.

The morphology of plate shaped α precipitates could be understood in terms of an existence of the invariant line. For the specimens treated for a long time (2 days), the interfaces are likely to be closer to equilibrium. The morphology of α precipitates may be determined largely by minimizing the total interfacial energy. The part of a boundary having especially low energy will, therefore, have the largest area, compared to other parts. This will causes α precipitates to have the plate

shape, with the habit plane parallel to the broadest face. The other face containing the invariant line is likely to have lower energy than the one normal to the invariant line, which will cover the smallest area of the interface. Consequently, the longest axis is parallel to the invariant line. In other words, providing the data of the interfacial energies were known, one would be able to deduce the shape of a plate for the α precipitate according to the Wulff construction.

For specimens treated within short times (15 ~ 20 min), the Widmanstätten structure formed could be understood with both dynamic and kinetic considerations. During the transformation of ß to α, the increase of the interfacial energy and the local strain energy per mole is expected to be smaller in the direction along the invariant line than in any other directions. Therefore, the pure driving force for α to grow, (or the probability of atoms jumping from ß to α) may be the highest in the direction of the invariant line compared to that in other directions. As a result, α might grow much faster along the direction of the invariant line. Aaronson (1962) noted that the rate of migration of a semicoherent interphase boundary should be far less than that of a disordered boundary. The interfacial structure observed in the end face boundaries suggests that the boundary about the tip of a precipitate plate (at least for α/ß boundaries in Zr-Nb alloy) should not be completely disordered. However, the

degree of average mismatch could higher in the end face than that in any interfaces containing the invariant line. Following Aaronson's idea (1962), the mobility of interfaces of different structure might vary depending on the degree of atomic match achieved at the interfaces. As a result, the end face, the interface of the worst atomic matching, could be the most mobile interface. Hence the relative rates of migration of end face boundary could be the highest. In addition, once the tip of a plate is formed, the concentration gradient near the tip (end face) of a precipitate is expected to be steeper than those regions adjacent to other parts of interface. This may cause a precipitate to grow more rapidly along the invariant line. Consequently, all of the above arguments are in favour of producing a Widmastätten precipitate structure, with the longest axis of each precipitate lying along an invariant line.

It has been indicated in Section 5.1.2 that the edge face tends to have a preferential (facet) orientation. Moreover, the edge face consisting of two differently oriented facets were occasionally observed. Each facet is characterized by a particular structure, though both structures may be parallel linear features. Examples can be found in Figure 5.26b. As the observed boundaries appear to surround ß instead of α particles, an enclosed interface could be related to several α precipitates. Since the edge face seems to present

preferential orientations, it is probable that other cusps of interfacial energy exist besides the one corresponding to the habit plane. However, the reason for preferential interfaces other than the habit plane is not clear at present.

6.3 The Orientation of the Habit Plane and Δgs

Based on the O-lattice theory (Bollmann, 1970), we have determined the plane of the lowest lattice mismatch. This plane was found to be the one with the smallest plane spacing among the O-lattice planes related to the low index planes in the reference lattice. By definition, the habit plane is determined to be such a plane. The calculation in Chapter 3 indicated that the habit plane is determined by Δg_4 ($= g_{(1\ 0\ 1)\beta} - g_{(1\ 0\ -1\ 1)\alpha}$). It has been shown in Section 5.2.2 that the observed habit plane was indeed normal to Δg_4, recorded directly in the diffraction pattern (Figure 5.19). In addition, the measured direction of Δg_4 is in reasonable agreement with one predicted by the model (For example $(3\ -2.2\ -3.4)_\beta$ vs. $(3\ -2.1626\ -3.0521)_\beta$).

According to the fifth property of invariant lines and proposal given in Chapter 3 the following Δg's should be also parallel to Δg_4, i.e. normal to the habit plane. They are: Δg_3 ($= g_{(1\ 0\ -1)\beta} - g_{(-1\ 1\ 0\ 1)\alpha}$), Δg_7 ($= g_{(2\ 0\ 0)\beta} - g_{(0\ 1\ -1\ 2)\alpha}$), and Δg_9 ($= g_{(0\ 0\ 2)\beta} - g_{(2\ -1\ -1\ 0)\alpha}$). To determine Δg correctly, it should be

measured where the two gs intersect each other. $g_{(1\,0\,-1)_\beta}$ and $g_{(-1\,1\,0\,1)_\alpha}$ are nearly parallel, and so are the $g_{(0\,0\,2)_\beta}$ and $g_{(0\,1\,-1\,2)_\alpha}$. It is difficult to define precisely the orientation at which these nearly parallel related planes truly cross each other. Therefore, only Δg_7 has been measured, and the result was given in Figure 5.20. Again the habit plane was shown to be perpendicular to Δg_7, and the plane normal, $(3.0\ -2.2\ -3.0)_\beta$, agrees very well with the predicted habit plane, $(3\ -2.1626\ -3.0521)_\beta$, with respect to the particular orientation relationship, i.e. for $\theta = -2°$. The fact that the habit plane is determined by both Δg_4 and Δg_7 exhibits the property of invariant lines, and supports the hypothesis of optimum orientation relationship.

There are other ways of predicting habit planes. One is to find the least deformed plane, i.e. the plane with the minimum net content of Burgers vector (Knowles and Smith, 1982). Another is to obtain an unrotated plane determined by the two eigenvectors corresponding to the eigenvalues which are closer to 1.0 (Ryder and Pitsch, 1966, Luo and Weatherly 1988).

In this work, the habit plane defined by the first method is determined as follows*. Recalling equation (3.5),

---

*Here, the idea suggested by Knowles and Smith (1982) is followed, but a different method is used.

we assume $\mathbf{b}_\beta$ to be any vector variable of unit length; the locus of points $\mathbf{b}_\beta$ will define a sphere. The transformation in (3.5) will then change the sphere into an ellipsoid. An $\mathbf{x}^0$ defines a distance in a direction, across which the deformation is unity. Therefore, the plane of the least deformation is the plane of the largest section area, which is determined by the two longer axes of the ellipsoid. The direction and the length of these axes are given by the eigenvectors and eigenvalues of the matrix **VT** defined by:

$$\mathbf{VT} = (\mathbf{T}^{-1} * (\mathbf{T}^{-1})^T)^{1/2} \qquad (6.1)$$

The calculated result for the same orientation relationship given as the example in Section (3.8), i.e. for $\theta = -2°$, is listed in Table 1 (referred to BCC):

Table 1. Data for the least deformed plane

eigenvalues	eigenvectors
2.848×10^8	[2.0 -1.0247 2.6919]
5.1958	[2.0 -1.7675 -2.1588]
31.1327	[2.0 2.7837 -0.4262]

The least deformed plane, which is defined by the first and the third eigenvectors, is $(3.0\ -2.6512\ -3.2382)_{\beta}$. For the same orientation relationship the eigenvalues and eigenvectors of the transformation matrix, **A**, are given in Table 2 (referred to BCC):

Table 2. Data for the unrotated plane

eigenvalues	eigenvectors
$1 - 9.2 \times 10^{-8}$	[2.0 -1.0247 2.6919]
1.0055	[2.0 -0.9140 2.4788]
1.0463	[2.0 -2.4754 2.4795]

The unrotated plane determined by the first two eigenvectors is $(0.0334\ 2\ 0.7862)_{\beta}$.

The first eigenvectors in Table 1 and 2 are the same; both indicate an effective invariant line, which is also the same as provided previously in Section 3.8. The first eigenvalue in Table 1 gives a distance, over which the deformation along the effective invariant line is a unit. Take an atomic spacing (for example ~3.2 Å) as a unit (roughly equivalent to one dislocation). The distance, or the dislocation spacing for this case is many orders of magnitude higher than the atomic spacing. This indicates effective

invariance, in the scale of our concern, lying along the direction defined by the first eigenvector. The first eigenvalue in Table 2 reveals the effective invariance from another respect. This value is so close to one, that a line, within the length of precipitates, along the first eigenvector is effectively invariant after the transformation.

Let us compare the prediction from the present calculation with the above result. It is found that the habit planes predicted by the present model and the above two models contain a common direction, i.e. the effective invariant line. For the case of $\theta = -2$, the angle between the habit plane determined by Δg_4 and the least deformed plane is 4.4°, while the angle between the plane determined by Δg_4 and the unrotated plane is 48.5°. Since the observed habit plane agrees with the present prediction, it is unlikely that the habit plane in this alloy is the unrotated plane, which is strongly tilted away from the present prediction. However, the least deformed plane is fairly close to the present prediction. Had we only obtained the data of the habit plane normal, it would have been difficult to decide which factors influence more the formation of the habit plane due to the experimental uncertainty. It has been noted that Δg_4 is consistently observed normal to the habit plane, whose trace is parallel to the moiré fringes perpendicular to Δg_4. In this case, if the habit plane were the least deformed plane, the

angle (for example 4.4°) between the moiré fringes and the trace of the habit plane should be detectable. The comparison tells us that though the plane of minimum mismatch given by Δg_4 is close to the least deformed plane, the observations tend to agree with the former. This evidence further supports the idea that the low energy state of a semicoherent boundary is influenced by the discreet nature of the crystals.

It is very interesting to note that the habit plane observed in this investigation is fairly close to (within 10° of) the habit plane for martensite, in pure Zr and some Zr-Nb alloys which also has the Burgers orientation with respect to the ß phase (Gaunt and Christian, 1959, Banerjee, Krishnan, 1971). From trace analysis of the surface relief, Gaunt and Christian (1959) found the habit plane of martensite in pure zirconium to be near $\{3\ 3\ 4\}_\beta$. The habit plane of martensite was found to be near $(4\ 3\ -3)_\beta$ for the particular orientation relationship under study, and, corresponding to this orientation relationship, the habit plane observed in the present investigation (refer to section 5.2.2 $(-3.0\ 2.2\ 3.4)_\beta$) will be $(4\ 2.6\ -3.6)_\beta$. The $\{3\ 3\ 4\}_\beta$ habit plane of martensite was also observed using TEM in a number of Zr-Nb alloys (Banerjee and Krishnan, 1971). Both the lath boundary of the massive martensite and the average interface of the twinned martensite were reported to be of the $\{3\ 3\ 4\}_\beta$ type. For the orientation relationship used, Banerjee, Krishnan (1971) noted

that individual twin interfaces were found to lie along $(4\ -4\ 3)_\beta$ (the longer portion) and $(-4\ 3\ 3)_\beta$ (the shorter portion) planes, with the average habit plane of $(-4\ 3\ -3)_\beta$. Corresponding to this orientation relationship, the habit plane observed in the present study (for example $(-3.0\ 2.2\ 3.4)_\beta$) will be $(4\ -3.5\ 2.6)_\beta$. Therefore, the α precipitates tend to have the habit plane similar to that of martensite. Such a habit plane, as could be predicted by the purely geometrical model proposed in Chapter 3, may also be interpreted in terms of the phenomenological theory of the martensitic transformations. If this is not a coincidence, a possible explanation could be either that the interface minimum mismatch is favoured by martensite or that there are some aspects common to both the α precipitation and martensitic transformations.

We have seen that the message carried by Δgs is very useful for studying the habit plane. The geometry of mismatches of planes of crystals, or the geometry of planes of the O-lattice recorded directly in diffraction patterns provides a possible way to measure the O-lattice planes directly. However, Δgs other than those related to $(1\ 0\ 1)_\beta$, $(2\ 0\ 0)_\beta$, and $(1\ 1\ 0)_\beta$ planes have attracted less attention. Here only two more points will be made about our Δg study. First, it was interesting to note that almost all Δgs appear parallel to each other in the selected area diffraction

pattern in Figure 5.15c. They are approximately normal to the defects in the boundary, while in Figure 5.17 Δgs are in different directions. It has been indicated by the second property of invariant line that all Δgs are in the plane with the invariant line as its normal. Assuming the invariant line is $[-2\ -1.0247\ 2.2919]_\beta$, as predicted for $\theta = -2°$, the angle between the invariant line and $[1\ 1\ 0]_\beta$ and $[1\ -1\ 1]_\beta$ are about 79° and 20°, respectively. When the beam is along $[1\ 1\ 0]_\beta$, the plane normal to the invariant line is oriented steeply with respect to the screen. Then the projections of any directions in the plane should lie nearly parallel and normal to the invariant line, in the direction of the parallel interfacial dislocations. That is what we have seen in Figure 5.15c. If the beam is in the $[1\ -1\ 1]_\beta$ direction, the invariant line is close to the beam direction (that is why the projections of the dislocations are very short at this orientation). The plane determined by the invariant line is inclined to the screen at a small angle. Therefore the projections of Δgs in the plane lie in different direction. Although Δgs observed at both zone axes are only an approximation, the tendency that the observations agree with the invariant line property provides further support for the effective invariant line model.

Another point we wish to mention here is that the correspondences between directions in real space do not necessarily hold in reciprocal space. Caution should be taken in analysis dealing with correlated reciprocal lattice vectors. For example, in real space $[1\ -1\ 1]/2_\beta$ is related to $[1\ 1\ -2\ 0]/3_\alpha$ as defined in Figure 3.3. Based on the same orientation relationship, one could obtain the relationship in reciprocal space: $(2\ -2\ 2)_\beta$ is correlated with $(2\ 1\ -3\ 0)_\alpha$, and $(2\ 2\ -4\ 0)_\alpha$ is correlated with $(3\ -3\ 2)_\beta$ in reciprocal space. If we extend the diffraction spots in Figure 5.15c, we would find that only the Δg between the above correlated planes can be nearly parallel to other Δgs. In spite of the fact that $(2\ -2\ 2)_\beta$ is nearly parallel to $(1\ 1\ -2\ 0)_\alpha$, they are not the correlated planes defined by the transformation. This phenomenon is not simply due to the index system of HCP. As we know, any direction in $(0\ 0\ 0\ 1)_\alpha$ plane is parallel to a plane normal of the same index (in four indices system). It has been shown in Chapter 3 that the cell walls in the O-lattice could be expressed as a transformation of the faces of the Wigner-Seitz cell. One of the face of the Wigner-Seitz cell is determined by $[1\ -1\ 1]/2_\beta$. Although the $[1\ -1\ 1]/2_\beta$ and $[1\ 1\ -2\ 0]/3_\alpha$ are closely related (as shown in Figure 3.3), the locations of cell walls in O-lattice corresponding to the displacements of $[1\ -1\ 1]/2_\beta$ and $[1\ 1\ -2\ 0]/3_\alpha$ are different. The example shown above clearly indicates that the cell walls of O-lattice will be differently defined if the reference

lattice is changed as already noted by Bollmann (1970), though in practice the difference caused by the two definitions might possibly be physically insignificant.

6.4 The Interfacial Structures

6.4.1 The Broad Face Boundaries

It has been indicated in Chapter 3 that, when the α and ß have an optimum orientation relationship, the mismatches in the habit plane could be completely accommodated by a single set of dislocations with the Burgers vector $[0\ 1\ 0]_{\beta}$. We have noted that only one set of principal dislocations has been observed consistently at the broad face boundaries. This array of dislocations was then considered as the characteristic feature of the habit plane because the broad face boundary is composed largely of the habit plane. The contrast study suggested the Burgers vector of this set of dislocations to be $[0\ 1\ 0]_{\beta}$, which is in accord with the prediction. In addition, the spacing of the dislocations is 9.5~10 nm. Comparing this to the calculated results in Figure 3.7, we could see that the measurement agrees very well with the calculations for $\theta \approx -20 \sim 30°$. This is consistent with the measurements of orientation relationship and the conjecture made from the invariant line measurements.

An O-lattice calculation takes the mismatches in three-dimensions into account. During the formation of the interface, the constraint normal to a boundary is likely to be removed. However, it was shown in the above comparison that both the observed contrast and the spacing of the principal dislocations still support the prediction from the three-dimensional calculation. The Burgers vector, $[0\ 1\ 0]_\beta$, referring to BCC is not one of the smallest lattice translation vectors <1 1 1>. Since the <0 1 0> type of dislocations have been observed frequently in BCC metals (Amelinckx, 1979), it is possible that interfacial dislocations have a Burgers vector of $[0\ 1\ 0]_\beta$. The counterpart of $[0\ 1\ 0]_\beta$ in the HCP crystal is $[0\ -1\ 1\ 1]_\alpha/2$, which is not a basic lattice translation vector. However, due to the structure of HCP lattice, there is an atom located at either $[0\ -2\ 2\ 3]_\alpha/6$ or $[0\ -4\ 4\ 3]_\alpha/6$ point, which is very close to $[0\ -1\ 1\ 1\ ]_\alpha/2$ (with difference of $[0\ -1\ 1\ 0]_\alpha/6$). For this reason, there would not be a problem regarding the atomic correspondence, since a local shift of $[0\ -1\ 1\ 0]/6_\alpha$ is likely to occur in a boundary. An $[0\ -1\ 1\ 1]_\alpha/2$ dislocation would be defined as a partial dislocation with respect to the HCP crystal, because it must be associated with stacking fault if it is within the crystal. In HCP/BCC interface, we may assume the lattice in HCP to be conserved along the boundary. The displacement of $[0\ 1\ 0]_\beta$ would not change the periodicity of

BCC structure. Hence, the periodicity of interfacial structure could be conserved.

It is difficult to interpret the details of the contrast behaviour of the dislocations, without knowledge of the relaxation of atoms near the boundary. It was interesting to note a correspondence between the contrast of the principal dislocations in the broad face boundaries and the component of the mismatches of the planes used for operating reflection in the habit plane. It has been observed that the contrast of the principal dislocations is usually stronger using $(1\ 1\ 0)_\beta$ and $(0\ 1\ 1)_\beta$ than using $(1\ 1\ 0)_\beta$ and $(0\ 1\ -1)_\beta$ (For example, see Figure 5.24a and b, 5.25a and d), though the values of the $\mathbf{g}\cdot\mathbf{b}$ are the same for all four gs: $(1\ 1\ 0)_\beta$, $(1\ -1\ 0)_\beta$, $(0\ 1\ 1)_\beta$, and $(0\ 1\ -1)_\beta$. Figure 3.5b illustrates the "moiré planes" related to some low index planes intersecting the habit plane for $\theta = -2°$. We see the angles relating to the $(1\ 1\ 0)_\beta$, $(0\ 1\ 1)_\beta$ planes are considerably larger than those relating to $(-1\ 1\ 0)_\beta$, $(0\ 1\ -1)_\beta$ planes. As noted in Chapter 3, a set of "moiré planes" represents the poorest matching regions of two sets of planes. The intersection lines in a boundary would represent the regions where the correlated planes deformed most strongly. With the optimum orientation relationship, all "moiré planes" related to low index BCC planes either intersect the habit plane at the same lines as the $[0\ 1\ 0]_\beta$ dislocations or do not intersect it at all. Presumably, a

relaxation could exist normal to the habit plane, the degree of the local deformation of a pair of correlated planes in the habit plane would be influenced by the inclination of the "moiré planes" to the interface. For this reason, the contrast of the dislocations might be related to the inclination of the "moiré planes" (associated with the planes responsible for the operating reflection) to the habit plane. In Figure 3.5b we also see that the "moiré planes" relating to the $(1\ 0\ -1)_\beta$ and $(1\ 0\ 1)_\beta$ are parallel to the habit plane. Ideally, the principal dislocations should be invisible using either the $(1\ 0\ -1)_\beta$ or $(1\ 0\ 1)_\beta$ operating reflections. Besides, for these two gs the condition of $\mathbf{g}\cdot\mathbf{b} = 0$ is also achieved. Hence the dislocations should be invisible or nearly invisible according to the $\mathbf{g}\cdot\mathbf{b} = 0$ criterion. However, this is true only when $(1\ 0\ -1)_\beta$ operating reflection is used (Figure 5.6b, 5.23e, 5.24c, 5.25c, 5.26a, 5.27a, 5.31a). In Figure 5.27b the principal dislocations are visible using the $(1\ 0\ 1)_\beta$ operating reflection. This contrast was reproducible, though generally it was not strong. In spite of this, the contrast using all other $\{1\ 1\ 0\}_\beta$ is in reasonable agreement with the predicted $[0\ 1\ 0]_\beta$ Burgers vector. The reason for the disagreement is not clear. It is possibly due to the details of the relaxation of the atoms near the boundary.

The irregular features at the broad face boundary are not well understood. Though many observations made on the

irregular defects are reproducible, the contrast analysis of the irregular defects is far from complete. This is partly due to the following difficulties. Firstly, the irregular defects in the habit plane are recognized generally by their configuration, i.e. the irregular spacing and the random direction. Usually when they change direction the Burgers vectors do not remain the same along the lines. The non-parallel defects were seen to consist of segments of different types of defects, though the zigzag feature in Figure 5.30 could not be always detected. It is not easy to identify correctly either the segments of different types of dislocations from smoothly curved defect lines, or the irregularly spaced parallel defects from the principal dislocations when the contrast of former is similar to or weaker than the latter. Secondly, there could exist more than one type of the parallel irregular defects, as in the example given in Figure 5.26. By studying carefully and comparing Figure 5.24a and b, one can also see two types of contrasts associated with the irregular lines in the interface in Figure 5.24a: One type is darker, and the other is lighter than the principal dislocations. It could be misleading to identify the same type of irregular defects at different boundary simply by their irregular feature though we have tried to generalize the irregular defects in this way. In addition, some irregular defects are extrinsic dislocations (Figure 5.13 and 5.31). Little is known about the reactions between a boundary with

the dislocations from the ß phase. Because the boundaries in TEM specimens are usually a small section of enclosed interface it is impossible to know if the irregular dislocations of interest are connected to the dislocations within the ß phase somewhere separated from the present specimen. Thirdly, the contrast study of the irregular defects could be influenced by the steps usually associated with them. An example is in Figure 5.24a, where the trace of the boundary is perturbed slightly corresponding to the irregular defects as arrowed, showing steps are possibly associated with the arrowed defects. Finally, the irregular defects sometimes have very wide images, as can be seen in Figure 5.23 d and f, 5.25b. The images of these defects would have the width close to the dislocation spacing, especially when they are parallel to the array of principal dislocations. It is possible that this contrast forms due to the effect other than a strain field, though more details remain to be determined. This effect would certainly influence a Burgers vector analysis based on their strain contrast.

6.4.2 The Edge Face boundaries

Generally two types of lines are observed at an edge face boundary. One type of lines is the coarsely spaced dislocations, whose spacing is close to that of the principal dislocations at the broad face boundary (Figure 5.27). Another

type has very fine spacing; the contrast of these lines is very similar to that of moiré fringes (Figure 5.28). Let us first assume that the Burgers vectors associated with those coarse defects are the basic lattice vectors of BCC, and the fine spaced lines are simply due to moiré effect. Then it will be difficult to interpret why the broad face boundary is so much more favoured by nature now that the densities of the dislocations in both broad and edge face boundaries are similar. An alternative explanation is that those finely spaced lines are the structure elements of the interface. The Burgers vector associated with them could be $[1\ -1\ 1]_\beta$, because they are invisible by using three $\mathbf{g}$s in the $[1\ -1\ 1]_\beta$ zone axis (Figure 5.29). Each finely spaced line could also represent the unit layer of the habit plane. The minimum spacing of these lines (~1.5 nm) agrees with the smallest spacing of the "moiré planes" to which the habit plane is parallel. The misfit patterns in the interface will be conserved if the interfacial steps have the height equal to an integral number of spacings. In such a way, an interface could always lie along the O-lattice planes of the best lattice matching. The smallest step observed was indeed about 1.5 nm, in agreement with the above idea. However, in spite of these interesting conjectures, the structure study of the edge face boundary has yet to be completed.

6.5 A Comparison Between This Work and the Studies in Other HCP/BCC Boundaries

The studies of interfacial structures of HCP/BCC (α/ß) boundaries have been carried out mainly in Zr-Nb and Ti-Cr alloys. In spite of the difference in the lattice parameters, the orientation relationships in both systems are close, i.e. near the Burgers orientation relationship (Perovic and Weatherly, 1988, and Furuhara, 1989). In addition, invariant lines are claimed to exist in both systems, although the models for producing the invariant lines are different. In spite of differences in details and in the points of view about the observations, the experimental result in this work is in agreement with their observations in the above two aspects.

It is expected that due to the heat treatment differences the interfacial structure should change, although, based on the present observations, the interfacial structures are essentially similar in specimens of various heat treatments. In a Zr-2.5 wt% Nb alloy treated by furnace cooling from ß or α + ß field, Perovic and Weatherly observed α/ß boundaries containing arrays of dislocations. In the flat facet plane the structure is dominated by a single straight array of dislocations. In addition to this array of principal dislocations, one or more other arrays of dislocations were

observed. The density and the configuration of the additional dislocations vary in a systematic way as the orientation of the boundary changes locally. The general interfacial structure observed in this study tends to agree with the experimental result of Perovic and Weatherly (1988). Some more specific comparisons are made in Table 3, where the Burgers vectors and the dislocation (disl.) spacings are given with respect to the principal dislocations at the broad face boundaries. To make a better comparison, we have transformed some geometry data from their work into those with respect to the particular orientation relationship variant used in this work.

Table 3. A comparison between the present work and the work by Perovic and Weatherly

Refer to BCC	Habit plane	Invariant line	Burgers vector	Spacing of disl.
Present	(3 -2.2 3)	[2 -1.0 2.5]	[0 1 0]	10 nm
Perovic Weatherly	flat facet plane ~{1 1 1}	[2 -1 2]	[1 3 1]/2	6 nm
difference	8°	6°	25°	4 nm

From Table 3, it can be seen that both the orientations of the habit planes and the invariant lines in the present work are in approximately agreement with their

results. The Burgers vector analyzed by Perovic and Weatherly was based on the dislocation contrast analysis by using mainly operating reflections from the α phase ($\mathbf{b} = [1\ -2\ 1\ 3]/3_\alpha (\sim // [1\ 3\ 1]/2_\beta)$. Actually, the contrast observed in this work could be also interpreted reasonably well if the Burgers vector was assumed to be $[1\ 3\ 1]/_\beta$. The main disagreement is the dislocation spacing. It has been pointed that, according to the calculation in Chapter 3, the misfit in the habit plane could be completely accommodated by a single set of $[0\ 1\ 0]_\beta$ of ~10 nm in spacing. On the other hand, if the Burgers vector is $[1\ 3\ 1]/2_\beta$, there would be an additional set of dislocations needed to take up the extra mismatch in the habit plane. Though this additional set of dislocations has not been observed, we have tried to calculate the spacing of the set of $[1\ 3\ 1]/2_\beta$ dislocations for the same orientation relationship often taken as an example ($\theta = -2°$). The result showed that the spacing of the $[1\ 3\ 1]/2_\beta$ dislocations is 5.9 nm, which is consistent with Perovic and Weatherly's measurement. Presumably, a displacement of $\langle 1\ 3\ 1\rangle/2_\beta$ type could be a lattice dislocation Burgers vector, since some of $\langle 1\ 3\ 1\rangle/2_\beta$ are correlated to directions $\langle 1\ -2\ 1\ 3\rangle/3_\beta$ in α phase. Now, a question will be raised about the Burgers vector not being the $[1\ 3\ -1]/2_\beta (\sim // [-1\ -1\ 2\ 3]/3_\alpha)$, lying not only approximately in the habit plane, but also being nearly normal to the invariant line. In such a case the dislocations may carry the misfit in the habit plane effectively. The contrast analysis does not

appear to support this case. However, due to the rather large uncertainty inherent in the Burgers vectors analysis, the result could be spread over a wide range of directions. In the present study, the dislocations in the habit planes were observed to show a very strong contrast when the $(0\ 0\ 0\ 2)_\alpha$ operating reflection was used. The same results were reported in both Zr-Nb and Ti-Cr alloys (Perovic and Weatherly, 1988, and Furuhara, 1989), while different Burgers vectors were deduced: $[0\ 1\ 0]_\beta$— present work; $[1\ 3\ 1]/2_\beta$(~//$[1\ -2\ 1\ 3]/3_\alpha$)—Perovic and Weatherly's work; $[1\ 1\ 0]/2_\beta$(//$[0\ 0\ 0\ 1]/2$)—Furuhara's work in a Ti-Cr alloy.

We have also attempted to apply the present model to the boundaries between 'normal α' precipitates and ß in a Ti-6.62 at% Cr alloy by using the data provided by Furuhara (1989). Among the many optimum orientation relationships predicted, the one related to the largest dislocation spacing is chosen (θ = 10°, ϕ = 0.805°, γ = -0.4781.°). The interfacial structure corresponding to this orientation relationship is given in Table 4 along with Furuhara's calculation for comparison. The results are given for the particular variant of orientation relationship applied in Furuhara's work. It has been shown by Furuhara (1989) that the observed habit plane and invariant line were scattered around those of his prediction. Therefore, the present predictions are also consistent with his observations, since the

differences between the predictions of the habit plane and the invariant line are small.

Table 4. A comparison of the predictions of the present model and Furuhara's model

Refer to BCC	Habit plane	Invariant line	Burgers vector	Spacing of disl.
Present	(-13 9.6 12)	[5 2.7 3.2]	[0 1 0]	11.8 nm
Furuhara	(-13 11 11)	[5 3 3]	[0 -1 1]/2	11.15 nm
difference	5°	3°	45°	0.65 nm

Initially, Furuhara's model predicted that the dislocation had $[0\ -1\ 1]_\beta$ ($/\!/[0\ 0\ 0\ 1]_\alpha$ Burgers vector with spacing of 22.3 nm. The observed dislocation spacing was 12 nm in his work. Thus the actual Burger vector was deduced to be $[0\ -1\ 1]_\beta/2$. The dislocation spacing predicted by the present model is consistent with Furuhara's measurement. The Burgers vector analysis based on the contrast study is subject to large uncertainty, and may need further testing. Nevertheless, apart from the Burgers vector, the present prediction and Furuhara's observations are in very good agreement. Consequently, the structure at the broad HCP/BCC interface in the Ti-Cr alloy could be also interpreted in the light of the minimum lattice mismatch principle based on the O-lattice theory.

O-lattice analyses have been conducted by Menon and Aaronson (1981) in the same Ti-Cr alloy used by Furuhara. As indicated by Furuhara (1989) the agreement between the O-lattice calculation and the observations was not particularly good. The O-lattice calculations in the present work and the one in Menon and Aaronson's (MA) work are different mainly in two aspects: firstly, MA used the simplified O-lattice cells. We have introduced a method for calculating the O-lattice cells without simplification. The difference in these two types of cells has been discussed in detail in Chapter 3. Secondly, MA made the O-lattice in an exact Burgers orientation relationship. We have allowed for a small tolerance in the orientation relationship, which could be due to either the uncertainty in measurements or the presence of true scattering, so that an effective invariant line could be obtained. As a result, in MA's theoretical prediction the angles between dislocation lines (O-lattice vectors) could be as small as 0.6°. When the angle between O-lattice is so small, an effective invariant line is likely to be obtained by slightly varying either the orientation relationship or the lattice parameters within the range of uncertainty or scattering. Furuhara (1989) realized the possibility of the existence of an invariant line. He further developed structural ledge model and combined the invariant line idea in his study of the Ti-Cr alloy (for details see Chapter 2). It is shown in Appendix 3, that the habit plane predicted in the

present study is also stepped on an atomic scale. This is not surprising; steps should exist wherever a boundary is irrational or of high index due to the discrete nature of crystals. Based on the present study the habit plane appears to be composed of $(1\ -1\ 0\ 0)_\alpha$ $(\sim//(-1\ 1\ 2)_\beta)$ facets, similar to Furuhara's result (1989). Furuhara has shown terraces of $(1\ -1\ 0\ 0)(\sim//(-1\ 1\ 2)_\beta)$ of about four atomic spacings in width in beautiful high resolution TEM micrographs. However these terraces may be actually about two atomic spacings in width, due to the existence of another layer of $(1\ -1\ 0\ 0)_\alpha$ atomic plane (see Appendix 3 for details). This second layer plane could not be shown in the high resolution image of the boundary, simply because the lattice image is not a projection of atoms.

6.6 Concluding Remarks and Further Work

In this chapter, the experimental observations have been compared with the results of the geometrical calculations. The parallel dislocations observed in either the broad face or the edge face were found to lie along the invariant line (or the effective invariant line) in agreement with the report by Perovic and Weatherly. The measured orientation relationships tended to correspond to a particularly defined angular range. The directions of the parallel dislocations, which should be the function of the

orientation relationship, appeared to scatter in a narrower region than that required by effective invariant line condition. These observations show support for the hypothesis of optimum orientation relationships. In addition, the experimental evidence that the habit plane is determined by both Δg_4 and Δg_7, and that only one set of $[0\ 1\ 0]_\beta$ dislocations was observed in the habit plane provide further support for the hypothesis of optimum orientation relationship. The observed structure (the direction, spacing, and the Burgers vector of the interfacial dislocations) in the habit plane could be well understood using the model developed in Chapter 3.

Further work will focus on the following aspects:

a) For the better understanding of the development of interface structure, a comprehensive investigation must be made of the interfaces other than the habit plane. The ideal microstructure for further investigation would consist of small α precipitates completely surrounded by the ß phase. To obtain such a microstructure an alloy with higher Nb content is desired.

b) Contrast of many interfacial dislocations, especially the irregular dislocations in the broad face boundary still remains unclear. It is suspected that the rather wide images

corresponding to the irregular dislocations may be related to a phase shift due to the strain field associated with the dislocations not corresponding to translation vectors of the HCP lattice. To better interpret the contrast of the interfacial dislocations and increase the certainty in determination of Burgers vectors, an in-depth study on contrast analysis will be needed.

c) In order to obtain the information of the atomic relaxation near the α/β boundary and provide fine details of the interfaces which might elucidate the mechanism of the phase transformation, the characterization of interfacial structure at atomic scale by high resolution electron microscopy would be important. An improved knowledge of interfacial structure would also help in controlling the properties of interest in practical applications of Zr-Nb alloy.

d) The method of construction of the cell structure in an O-lattice is expected to be helpful for improving the general applications of the O-lattice model. Therefore, this method should be applicable to other types of interfaces. To test the generality of the ideas of the effective invariant line and the optimum orientation relationship the model developed in Chapter 3 should be extended to other precipitation systems, such as BCC/FCC.

CHAPTER 7

CONCLUSIONS

1. The O-lattice has been studied in reciprocal space. This offers a simple method to obtain two important pieces of information: the geometry of the cell structure of the O-lattice and the habit plane defined as the plane of least lattice mismatch.

2. The invariant line model has been further developed in two aspects: firstly, the idea of an effective invariant line was introduced so that the O-lattice calculation could be carried out in three dimensions. Secondly, the properties of invariant lines were summarized, and on this basis the mismatch in a habit plane was analyzed.

3. It is proposed that, among the orientation relationships satisfying the effective invariant line condition, those corresponding to the simplest dislocation configuration (single-set-dislocation structure, equivalent to the existence of a one-dimensional O-lattice) would be the optimum orientation relationship. In addition, large

dislocation spacing and small rotation between the close-packed planes and between the close-packed directions could be the factors which further narrow the choices of orientation relationships.

4. The geometrical analysis based on minimum mismatch in the habit plane was applied to a Zr-2.5 wt% Nb alloy. The habit plane was predicted to be determined by Δg_4 ($=g_{(1\ 0\ 1)_\beta} - g_{(1\ 0\ -1\ 1)_\alpha}$) for a general orientation relationship near the Burgers relationship. More Δgs will be parallel to Δg_4 when there is a optimum orientation relationship between the α and β phases. In such a case, the Burgers vector of the single set of dislocations in the habit plane is $[0\ 1\ 0]_\beta$.

5. The experimental observations tend to support the predictions of the geometrical analysis. The general interfacial structure in α/β boundaries is in accord with the properties of invariant lines. The habit plane was characterized by one set of dislocations. The geometry of the habit plane and the direction, spacing, and the Burgers vector of the dislocations in the habit plane are all in agreement with the results of the model.

6. The interfacial structures in boundaries other than the habit plane are less well understood. Normally, the apparent dislocation loops imaged by a particular operating

reflection would consist of segments of dislocations of different Burgers vectors.

REFERENCES

Aaronson, H.I., (1962) "The Proeutectoid Ferrite and the Proeutectoid Cementite Reactions" Decomposition of Austenite by Diffusional Processes Zackay, V.F. and Aaronson, H.I. eds., Philadelphia, Pennsylvania.

Aaronson, H.I., Clark, W.A.T. , and Smith, D.A. (1983) "O-lattice Analysis of fcc-bcc Interfaces", Scripta Metall., **17**, 785.

Aaronson, H.I. and Reynolds, W.T.Jr, (1988) "Reply to a Discussion by J.W. Christian and D.V. Edmonds of Papers by Aaronson and Coworkers on the Proeutectoid Ferrite and Bainite Reactions", Scripta. Metall., **22**, 567.

Abriata, J.P. and Bolcich, J.C. (1982) "The Nb-Zr (Niobium-Zirconium) System" Bulletin of Alloy Phase Diagrams **3**, 34.

Amelinckx, S. (1979) "Dislocations in Particular Structures" in Dislocations in Solids Nabarro, F.R.N ed., **2**, 67.

Ashcroft, N.W. and Mermin, N.D., (1976) Solid State Physics, Saunders College, Philadelphia.

Balluffi, R.W., Brokman, A. and King, A.H., (1982) "CSL/DSC Lattice Model for General Crystal Boundaries and Their Line Defects", Acta Metall., **30**, 1453.

Banerjee, S. and Krishnan, R., (1971) "Martensitic Transformation in Zirconium-Niobium Alloy", Acta Metall., **19**, 1317.

Bäro, G. and Gleiter, H., (1973) 1405 " On the Structure of Incoherent Interphase Boundaries between fcc/bcc Crystals", Acta Metall. **21**, 1405.

Bilby, B.A., Boullough, R. and de Grinberg, D.R., (1964) "General Theory of Surface Dislocations", Discuss. Faraday Sic., **38**, 61.

Bollmann, W. and Nissen, H.-U., (1968) "A Study of Optimal Phase Boundaries: The Case of Exsolved Alkali Feldspar", Acta Cryst. **A24**, 546.

Bollmann, W., (1970) Crystal Defects and Crystalline Interfaces, Springer, Berlin.

Bollmann, W., (1974, a) "O-Lattice Calculation of an fcc-bcc Interface", Phys. Stat. Sol., **A21**, 543.

Bollmann, W., (1974, b) "Classification of Crystalline Interfaces by Means of the O-Lattice Method", J. Micro., **102**, 233.

Bonnet, R. and Durand, F., (1975) "Study of Intercrystalline Boundaries in Terms of the Coincidence Lattice Concept", Phil. Mag., **32**, 997.

Bowles, J.S. and Mackenzie, J.K., (1954) "The Crystallography of Martensite Transformations I", Acta Metall., **2**, 129.

Burgers, W.G., (1934) "On the Process of Transition of the Cubic-Body-Centred Modification into the Hexagonal-Closed Packed Modification of Zirconium", Physica, **1**, 561.

Burgers, W.G. (1939) "Some Considerations on the Fields of Stress Connected with Dislocations in a Regular Crystal Lattice I", Proc. of the Section of Sciences., **42**, 293.

Chang, A.L.J. and Saas, S.L. (1976) " A High Resolution Electron Microscope Study of the Omega Transformation in Zr-Nb Alloys" Acta Metall. **24**, 19.

Christian, J.W., (1975) The Theory of Transformation in Metals and Alloys. Oxford, Pergamon Press

Cometto, D.J., Houze, L.G.Jr., and Hehemenn, R.F., (1965) "The Omega Transformation in Zirconium-Niobium Alloys", Trans. of AIME, **233**, 30.

Dahmen, U. and Westmacott, K.H., (1981) "The Role of the Invariant Line in the Nucleation", Proc. Int. Conf. on Solid-Solid Phase Transformation, Aaronson, H.I., et al., eds., Pittsburgh, 433.

Dahmen, U., (1982) "Orientation Relationships in Precipitation Systems", Acta Metall., **30**, 63.

Dahmen, U., (1987) "Surface Relief and the Mechanism of a Phase Transformation", Scripta. Metall., **21**, 1029

Ecob, R.C. and Ralph, B., (1981) "A Model of the Equilibrium Structure of F.C.C./B.B.B Interfaces", Acta Metall., **29**, 1037.

Ecob, R.C., (1985), "Models and Observations of fcc/bcc interfaces", J. Micros. **137**, 313.

Edington, J.W. (1974) Monographs in Practical Electron Microscopy in Materials Science, Philips.

Fisher, E.S. and Alfred, L.C.R., (1968) "Effects of Elastic Anisotropy on Dislocations in HCP Metals", Trans Met. AIME, **242**, 1575

Forwood, C.T. and Clarebrough, L.M., (1989) "The Dislocation Structure of f.c.c-b.c.c Interfaces in a Cu-Fe Alloy", Phil. Mag., **B59**, 637.

Frank, F.C., (1950) "The Resultant Content of Dislocations in an Arbitrary Intercrystalline Boundary", Symposium on the Plastic Deformation of Crystalline Solids, Office of Naval Research, Pittsburgh, Pennsylvania, 150.

Furuhara, T. (1989) "Crystallography and Interphase Boundary Structures of Proeutectoid α Plates and Grain Boundary Allotriomorphs in a Hypoeutectoid Ti-Cr Alloy" Ph.D. Thesis, Carnegie-Mellon University, Pittsburgh

Gaunt, P. and Christian, J.W., (1959) "The Crystallography of the ß-α Transformation in Zirconium and in Two Titanium-Molybolenum Alloy", Acta Metall., **7**, 534.

Gleiter, H., (1983) "Microstructure", Physical Metallurgy, Cahn, R.W. and Haasen,P., eds., North-Holland Physics Publishing, 649.

Head, A.K., Humble, P., Clarebrough, L.M., Morton, A.J. and Forwood, C.T., (1973) "Computed Electron Micrographs and Defect Identification" Amelinckx, S, Gevers, R. and Nihoul, J. eds, Amsterdam, 31.

Hall, M.G., Aaronson, H.I., and Kinsman, K.R., (1972) "The Structure of Nearly Coherent fcc:bcc Boundaries in a Cu-Cr Alloy", Surf. Sci., **31**, 257.

Hall, M.G.and Rigsbee, J.M. and Aaronson H.I., (1986) "Application of the "O" Lattice Calculation to F.C.C./ B.C.C Interfaces", Acta Metall., **34**, 1419.

Hehemann, R.F., (1972) "Transformations in Zirconium-Niobium Alloys", Can. Metall. Q., **11**, 201.

Hirsch, P., Howie, A., Nicholson, R., Pashley, D.W., and Whelan, M.J. (1977) Electron Microscopy of Thin Crystals Malabar, Florida

Krakow W. and Smith D.A., (1987) "A High-Resolution Electron Microscopy Investigation of Some Low-Angle and Twin Boundary Structures", Ultramicroscopy, **22**, 47.

Knowles, K.M. and Smith, D.A. (1982) "The Application of Surface Dislocation Theory to the fcc-bcc Interface", Acta Cryst., **A38**, 34.

Knowles, K.M. (1982) "The Dislocation Geometry of Interphase Boundaries", Phil. Mag. **A46**, 951.

Knowles, K.M. and Goodhew, P.J. (1983) "The Structure of Interphase Boundaries in an Al-Al_3Ni Directionally Solidified Eutectic Alloy I. Experimental Observations and II. Geometrical Modelling", Phil. Mag. **A48**, 527, 555.

Luo, C.P. and Weatherly, G.C., (1987) "The Invariant Line and Precipitation in a Ni-45Wt% Cr Alloy", Acta Metall., **35**, 1963.

Luo, C.P. and Weatherly, G.C., (1988) "The Interphase Boundary Structure of Precipitates in a Ni-Cr Alloy", Phil. Mag., **58A**, 445.

Mader, W., Necker, G., Babcock, S.E., and Balluffi, R.W., (1987) "Lattice Imaging Study of Grain Boundaries at Normal Incidence to the Boundary Plane", Scripta. Metall., **21**, 555.

Menon, E.S.K. and Aaronson, H.I., (1986) "Interfacial Structure of Widmanstätten Plates in Ti-Cr Alloy", Acta Metall., **34**, 1975.

Perovic, V. and Weatherly, G.C., (1988) "The ß to α Transformation in a Zr-2.5 Wt% Nb Alloy ", Acta Metall., **37**, 813.

Pond, R.C., and Vitek, V., (1977) "Periodic Grain Boundary Structures in Aluminium, I. A combined Experimental and Theoretical Investigation of Coincidence Grain Boundary Structure in Aluminium", Proc. R. Soc. Lond., **A357**, 453.

Pond, R.C., (1984), " Review of the Principal Contrast Effects Observed at Interphase Boundaries Using Transmission Electron Microscopy", J. Microscopy, **135**, 213.

Potter, D.I., (1973) "The Structure , Morphology and Orientation Relationship of V_3 N in α Vanadium", J. Lees-Common Metals, **31**, 299.

Pumphrey, P.H., (1972) "A Plane Matching Theory of High Angle Grain Boundary Structure", Scripta Metall., **6**, 107.

Rigsbee, J.M. and Aaronson, H.I., (1979) "A Computer Modelling Study of Partially Coherent fcc-bcc Boundary", Acta Metall., **27**, 351.

Ryder, P.L. and Pitsch, W., (1966) "The Crystallographic Analysis of Grain-Boundary Precipitation", Acta Metall., **14**, 1437

Sargent, C.M. and Purdy, G.R., (1975), "Epitaxial Dislocations", Phil. Mag., **32**, 27.

Schindler, R, Clemans E.J., and Balluffi, R.W., (1979) "On Grain Boundary Dislocations in Plane Matching Grain Boundaries", Phys. Stat. Sol. **56a**, 749.

Solenthaler, c., (1989) "Reactions between Crystal Dislocations and Grain Boundary Dislocations in Near-coincidence Boundaries", Materials Sci. and Eng. **A115**, 95

Sutton, A.P. and Balluffi, R.W., (1987) "On Geometric Criteria for Low Interfacial Energy", Acta Metall., **35**, 2177.

APPENDIX 1

OBTAINING THE RATIOS OF LATTICE PARAMETERS

Figure A1. 1 is a Kikuchi pattern taken from an α plate. The Kikuchi line pairs of interest in Figure A1.1 are come from $(0\ 0\ 0\ 8)_\alpha$ (a-a pair), $(-4\ 1\ 3\ 0)_\alpha$ (b-b pair), and $(-5\ 1\ 4\ 0)_\alpha$ (c-c pair). If the Bragg angle corresponding to each pair of lines is known, then the c/a of the HCP lattice could be calculated easily from standard crystallographic

Figure A1.1 A Kikuchi pattern taken from the α phase.

formulae. The details of this calculation will not be given here. However, the method to obtain the Bragg angles with a correction for the effect in beam tilt will be provided briefly.

The main zone axes in the Figure A1.1 are indexed as $[-2\ 7\ -5\ 0\ ]_\alpha$ (O_1) and $[-1\ 3\ -2\ 0]_\alpha$ (O_2). The angle between them (3.0045°), independent of c/a, can be used to calibrate the camera length of TEM. A ray diagram is given in Figure A1.2, where different sets of lines are used to show the corresponding features in the plate. The following equations could be obtained from the trigonometric relationships between lines and angles:

$$L^2 + a^2 = (a + b)^2\sin^2\beta/\sin^2\alpha,$$
$$L^2 + b^2 = (a + b)^2\sin^2(\beta + \alpha)/\sin^2\alpha. \qquad \text{(A1.1)}$$

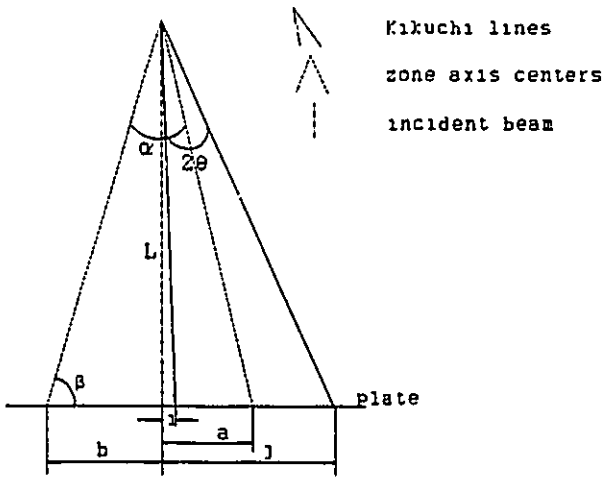

Figure A1.2 An illustration of the trigonometric relationship between lines and angles used in evaluating the beam tilt effect on the Bragg angle calculation.

In the above equations the values of a, b, i, and j could be measured directly from the plate, and $\alpha = 3.0045°$. The two unknowns, L and ß, could be solved from the equations. Then the Bragg angle, θ, is obtained from relation:

$$\theta = (\arctan(j/L) - \arctan(i/L))/2 \qquad (A1.2)$$

Three photographic plates, each from different regions of the α phase, have been taken. Two values of a and one value of c could be obtained from each plate. The parameter of the BCC phase is acquired in a similar way. The results are:

$$c/a = 1.588 \pm 0.003,$$
$$a_{\beta}/a_{\alpha} = 1.091 \pm 0.002,$$

and assuming a high tension of 120kV is applied,

$$a_{\beta} = 0.3528 \pm 0.0004 \text{ nm},$$
$$a_{\alpha} = 0.3233 \pm 0.0002 \text{ nm}.$$

In order to study the orientation relationship and the geometry of the interface formed during the phase transformation, the lattice parameters at the transformation temperature (650°C) must be used in any calculation. These parameters are obtained by considering the thermal expansion

effect. Because the α phase contains very low Nb, the thermal expansion data for pure Zr are used. They are 5.65μm/(m.K) in the direction of the a-axis, and 6.96μm/(m.K) in the direction of the c-axis. The ß phase contains about 15%Nb, and this composition effect is also taken into account. The thermal expansion coefficient for BCC Nb is

$$\Delta l/l = 6.892*10^{-6}\ T + 8.17\ *10^{-10}\ T^2\ (/°K),$$

where T is temperature, Δl/l is the relative linear change. The thermal expansion coefficient for BCC Zr (ß phase) is 9.7 x 10^{-6} (/°C). * After correction for the effect of thermal expansion the ratios to be used in further calculation are: c/a = 1.589, $a_ß/a_α$ = 1.094. The value of $a_ß$, without thermal effect correction, is still used in calculation of dislocation spacing.

---

* All data are from Metals Handbook (1979) 9th ed. v.2, except the one for BCC Zr, which is from 'Zirconium'- Metallurgy of the Rarer Metals 2 by G. L. Miller (London, 1957).

APPENDIX 2

RELATIONSHIP BETWEEN THE SUPERPOSITION OF MOIRÉ FRINGES AND THE SINGLE-SET-DISLOCATION CONFIGURATION

The properties of the invariant lines presented in section 3.6 can be used to understand the relationship between the superposition of moiré fringes and the single-set-dislocation configuration. As menticned Section 3.8, the habit plane is $\mathbf{OP}_4^*$, which is related to the $(1\ 0\ 1)_\beta$ lattice plane. The spacing of the lines of intersection of the habit plane, $\mathbf{OP}_4^*$, with a set of planes determined by $\mathbf{OP}_i^*$ is: (refer to Figure 3.1))

$$\text{ints}_i = 1/|\mathbf{OP}_i^* \times \mathbf{OP}_4^*/|\mathbf{OP}_4^*||$$

or

$$1/\text{ints}_i = |\mathbf{OP}_i^* \times \mathbf{OP}_4^*/|\mathbf{OP}_4^*|| \qquad \text{(A2.1)}$$

Since all $\mathbf{OP}_i^*$ are coplanar (the second property of invariant lines), all of vectors determined by $\mathbf{OP}_i^* \times \mathbf{OP}_4^*/|\mathbf{OP}_4^*|$ are either parallel or anti-parallel. If $\mathbf{OP}_j^* \times \mathbf{OP}_4^*/|\mathbf{OP}_4^*|$ and $\mathbf{OP}_k^* \times \mathbf{OP}_4^*/|\mathbf{OP}_4^*|$ are parallel, the following relation holds:

$$|OP_j^* \times OP_4^*/|OP_4^*|| - |OP_k^* \times OP_4^*/|OP_4^*|| = |(OP_j^* \times OP_4^*/|OP_4^*|) - (OP_k^* \times OP_4^*/|OP_4^*|)|. \quad (A2.2)$$

If they are anti-parallel then the minus sign in the right side of (A2.2) should be replaced by a plus sign. Hence the condition for

$$1/ints_j = 1/ints_k, \quad (A2.3)$$

is that one side of (A2.2) should be equal to zero. This condition can be guaranteed if

$$OP_4^* \;/\!/\; (OP_j^* +/- OP_k^*). \quad (A2.4)$$

From the definition in (3.12) we know

$$b_{\beta 4}^* = b_{\beta 1}^* - b_{\beta 6}^*$$

and

$$b_{\beta 4}^* = b_{\beta 2}^* + b_{\beta 5}^*, \quad (A2.5)$$

and these linear relationships still hold after the transformation defined by (3.16). Therefore the following relations always hold:

$$OP_4^* = OP_1^* - OP_6^*$$
$$OP_4^* = OP_2^* + OP_5^*, \quad (A2.6)$$

so we have

$$1/\text{ints}_1 = 1/\text{ints}_6,$$
$$1/\text{ints}_2 = 1/\text{ints}_5.$$

This explains why the points of intersection planes $\mathbf{OP}_1^*$ and $\mathbf{OP}_6^*$ with the habit plane, and those of planes $\mathbf{OP}_2^*$ and $\mathbf{OP}_5^*$ in both Figures 3.4 (a) and (b) are common.

It is also possible to bring the intersection points of planes $\mathbf{OP}_1^*$ and $\mathbf{OP}_2^*$ with the habit plane coincident with each other. This requires

$$\mathbf{OP}_4^* \;/\!/\; \mathbf{OP}_7^*, \qquad \text{(A2.7)}$$

where

$$\mathbf{OP}_7^* = \mathbf{OP}_1^* + \mathbf{OP}_2^*, \qquad \text{(A2.8)}$$

and $\mathbf{OP}_7^*$ is transformed from $(2\ 0\ 0)_\beta$. The plus sign in (A2.8) is used because the calculations show that $\mathbf{OP}_1^* \times \mathbf{OP}_4^*/|\mathbf{OP}_4^*|$ and $\mathbf{OP}_2^* \times \mathbf{OP}_4^*/|\mathbf{OP}_4^*|$ are antiparallel. According to the fifth property of the invariant lines, (A2.7) will hold if $\mathbf{b}_{\beta 4}^*$ and $\mathbf{b}_{\beta 7}^*$ are in the same zone axis as the invariant normal $\mathbf{x}^*$. The zone axis of these planes can be written as: (refer to equations (3.4) and (3.7))

$$\mathbf{b}_{\beta 6} = \frac{\mathbf{b}_{\beta 4}^* \times \mathbf{b}_{\beta 7}^*}{\mathbf{b}_{\beta 1}^* \cdot \mathbf{b}_{\beta 4}^* \times \mathbf{b}_{\beta 7}^*}, \qquad \text{(A2.9)}$$

which is $[0\ 1\ 0]_\beta$. In other words, in order to meet the

condition of (A2.7), $\mathbf{b}_{\beta 6}$ must lie in the plane with invariant normal $\mathbf{x}^*$. Remember that $\mathbf{b}_{\beta 3}^*$, $\mathbf{b}_{\beta 9}^*$ are also contained in zone axis $\mathbf{b}_{\beta 6}$. The moiré planes corresponding to them should be also parallel to $\mathbf{OP}_4^*$. Given that this is true, it can be shown that the intersection points of planes $\mathbf{OP}_2^*$, $\mathbf{OP}_{10}^*$ and $\mathbf{OP}_{11}^*$ with the habit plane must also coincide. The result in Figure (3.4, b) is thus explained.

The relationship between $\mathbf{b}_{\beta 6}$ and $\mathbf{x}^*$ indicates that $\mathbf{b}_{\beta 6}$ is the displacement vector of all vectors in a plane containing the invariant line, because of the third property of the invariant lines. Therefore, the equation

$$\mathbf{T}\ \mathbf{X}^0_6 = \mathbf{b}_{\beta 6}, \qquad \text{(A2.10)}$$

is solvable when the rank of $\mathbf{T}$ is two. If we multiply (A2.10) with $(\mathbf{b}_{\beta 4}^*)^T$ and use the relationship (3.16), we get

$$\begin{aligned} (\mathbf{b}_{\beta 4}^*)^T \cdot \mathbf{b}_{\beta 6} &= (\mathbf{b}_{\beta 4}^*)^T\ \mathbf{T}\ \mathbf{X}^0_6 \\ &= (\mathbf{OP}_4^*)^T \cdot \mathbf{X}^0_6 \\ &= 0, \end{aligned} \qquad \text{(A2.11)}$$

because $\mathbf{b}_{\beta 6}$ is in the plane $\mathbf{b}_{\beta 4}^*$. Thus, at least one solution of (A2.10), $\mathbf{X}^0_6$, lies in the habit plane, $\mathbf{OP}_4^*$. The displacement along the $\mathbf{X}^0_6$ direction is in the $\mathbf{b}_{\beta 6} = [0\ 1\ 0]_\beta$ direction. We know from the fourth property of the invariant lines that the displacements of all vectors in an interface containing the invariant line are in one direction. It follows that the

displacement in the habit plane is in the $\mathbf{b}_{\beta 6}$ direction as the plane contains the invariant line. This is important because the mismatch in the plane can be completely accommodated by a single set of dislocations with the Burgers vector $[0\ 1\ 0]_{\beta}$.

The spacing of the dislocations is determined by using formulae (3.9-10)

$$ds_6 = 1/|\mathbf{D}_6|$$

or

$$1/ds_6 = |\mathbf{OC}_6^* \times \mathbf{OP}_4^*/|\mathbf{OP}_4^*|| \qquad \text{(A2.12)}$$

It can be shown that due to all the vectors $\mathbf{OC}_i^*$ are contained in a plane with an invariant line as its normal, the relationship (A2.2) is also applicable to $\mathbf{OC}_i^*$. Because

$$\mathbf{WS}_6^* = \mathbf{b}_{\beta\beta}^*/2 = (\mathbf{b}_{\beta 1}^* - \mathbf{b}_{\beta 2}^*)/2 \qquad \text{(A2.13)}$$

and

$$\begin{aligned} &1/ints_1 - 1/ints_2 \\ &= |\mathbf{OP}_1^* \times \mathbf{OP}_4^*/|\mathbf{OP}_4^*|| - |\mathbf{OP}_2^* \times \mathbf{OP}_4^*/|\mathbf{OP}_4^*|| \\ &= |(\mathbf{OP}_1^* \times \mathbf{OP}_4^*/|\mathbf{OP}_4^*|) + (\mathbf{OP}_2^* \times \mathbf{OP}_4^*/|\mathbf{OP}_4^*|)| \\ &= 0, \end{aligned}$$

the spacing of the dislocations ds_6 will be

$$\begin{aligned} ds_6 &= 1/|\mathbf{OP}_8^*/2 \times \mathbf{OP}_4^*/|\mathbf{OP}_4^*|| \\ &= 2/|(\mathbf{OP}_1^* - \mathbf{OP}_2^*) \times \mathbf{OP}_4^*/|\mathbf{OP}_4^*|| \\ &= 2/|(\mathbf{OP}_1^* \times \mathbf{OP}_4^*/|\mathbf{OP}_4^*|) - (\mathbf{OP}_2^* \times \mathbf{OP}_4^*/|\mathbf{OP}_4^*|)| \\ &= 2/(2|\mathbf{OP}_1^* \times \mathbf{OP}_4^*/|\mathbf{OP}_4^*|) \\ &= ints_1, \end{aligned} \qquad \text{(A2.14)}$$

which is the same as the spacing of the lines of intersection of many "moiré planes" with the habit plane. As a result, the mismatch in the habit plane is highly localized around the dislocation lines.

APPENDIX 3

HABIT PLANE ATOMIC STRUCTURE PLOTTING

The calculated habit plane corresponding to the orientation relationship denoted by the arrow 2 in Figure 3.7 is

$$OP_{\beta 4}^{*} = (3\ -2.1626\ -3.0521)$$

referred to the BCC lattice, or

$$OP_{\alpha 4}^{*} = (-3\ 4.0543\ -1.0543\ 0.7172)$$

referred to the HCP lattice. The atomic structure in the habit plane is generated by the following method. It is possible to plot the atomic positions in a crystal with di3000 graphic software (installed in the VAX on campus). A slice of crystal, slightly thinner than the diameter of an atom, is cut out with the broad face of the slice parallel to the habit plane. This slice is then projected in the direction normal to the habit plane and plotted as shown in Figure A3.1a. Due to resolution of the plotter, the atomic positions in the plots of Figure A3.1a cannot be precisely located. However, the plots serve as

a useful demonstration of the atomic structure of a habit plane.

It may be seen from the indices of the habit plane that the habit plane is very close to the rational plane $(3\ -2\ -3)_\beta$ in the BCC lattice, or $(-3\ 4\ -1\ 1)_\alpha$ in the HCP lattice. Three vectors: $[1\ 3\ -1]_\beta/2$, $[-3\ 3\ -5]_\beta/2$, and $[-1\ 0\ -1]_\beta$, in the $(3\ -2\ -3)_\beta$ plane are indexed in Figure A3.1 a. If one connects the atomic positions by repeating these vectors, one would be able to define a large area of $(3\ -2\ -3)_\beta$ plane. Other layers of $(3\ -2\ -3)_\beta$ could be found in a similar way. As a result, the habit plane consists of layers of $(3\ -2\ -3)_\beta$. The stacking of these layers can be constructed based on the BCC structure. The $(3\ -2\ -3)_\beta$ plane is oriented nearly edge-on in Figure A3.1b, which shows the atomic structure projected in the $[1\ 1\ 0]_\beta$ direction. Due to the structure of the BCC lattice, there is another atomic plane parallel to the $(3\ -2\ -3)_\beta$ plane lying between each pair of $(3\ -2\ -3)_\beta$ planes. The actual plane index should be $2 \times (3\ -2\ -3)_\beta = (6\ -4\ -6)_\beta$, as shown by the parallel lines in Figure A3.1b. It can be seen that the close packed direction $[-1\ 1\ -1]_\beta$ actually lies in the habit plane on an atomic scale. Because $[-1\ 1\ -1]_\beta$ and $[1\ 3\ -1]_\beta$ define the $(1\ -1\ -2)_\beta$ plane, the habit plane is composed of steps of $(1\ -1\ -2)_\beta$ planes. A narrow region (about four atomic spacings in width) of $(1\ -1\ -2)_\beta$ planes has been determined by structure analysis. For example, any atoms

defined with the same symbol should not lie in the same $(3\ -2\ -3)_\beta$ plane. A few of these planes is indicated with different symbols in Figure A3.1a. There are steps between different layers of (1 -1 -2), as is demonstrated in Figure A3.1c. This result is also consistent with the stacking of $(3\ -2\ -3)_\beta$ planes shown in Figure A3.1b. The same argument can be applied using the HCP lattice as a reference. Corresponding to the vectors: $[1\ 3\ -1]_\beta/2$, $[-3\ 3\ -5]_\beta/2$, and $[-1\ 0\ -1]_\beta$, in the BCC $(3\ -2\ -3)_\beta$ plane, the vectors with reference to the HCP lattice are $[-1\ -1\ 2\ 3]_\alpha/3$, $[-5\ -2\ 7\ 0]_\alpha/3$, and $[-4\ -1\ 5\ -3]_\alpha/6$ in $(-3\ 4\ -1\ 1)_\alpha$ respectively. The habit plane consists of many layers of $(-3\ 4\ -1\ 1)_\alpha$ planes over a large area. On the atomic scale it contains $[-1\ -1\ 2\ 0]_\alpha/3$, and is hence composed of steps along $(-1\ 1\ 0\ 0)_\alpha$ planes, also about four atomic spacings in width. It should be emphasized that the actual step face (terrace) is not four atomic spacings in width. There is a in-plane shift between a pair of $(1\ -1\ -2)_\beta$ or $(-2\ 2\ 0\ 0)_\alpha$, as can be seen in Figure A3.1a (between the triangles and the circles or the squares). Due to the position of this layer, as displayed in Figure A3.1b, the step face could be only about two atomic spacings in width.

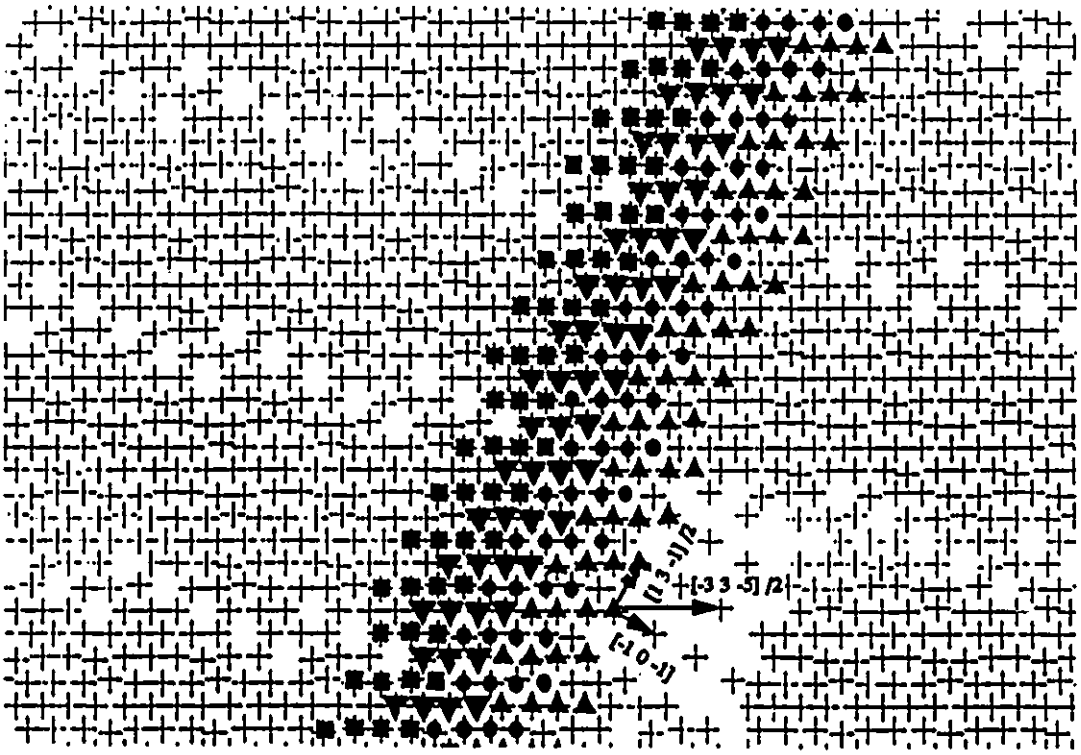

(a)

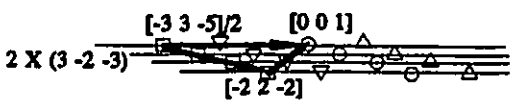

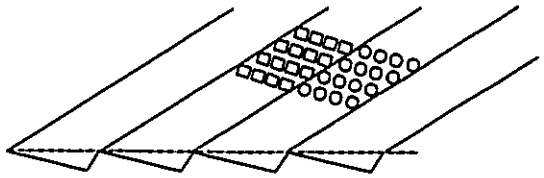

(b) (c)

Figure A3.1 (a) The atomic structures in the habit plane referred to BCC lattice; (b) projection of atoms viewed along the $[1\ 1\ 0]_\beta$ direction, a direction lying in the habit plane in the atomic scale, i.e. the upright direction in (a); (c) an illustration of the steps between the planes defined by different type of symbols.